

DEVELOPMENT OF NEAR REAL TIME AND CUMULATIVE GIC PROXY INDICES

by

ABU-BAKR ESSOP

A thesis submitted in partial fulfilment of the
academic requirements for the degree of
Master of Science
in the School of Chemistry and Physics,
University of KwaZulu-Natal
Durban

20 August 2021

As the candidate's supervisor I have/have not approved this thesis for submission.

Signed: Name: Date:

As the candidate's co-supervisor I have/have not approved this thesis for submission.

Signed: Name: Date:

Abstract

Geomagnetic storms are phenomena which can give rise to geomagnetically induced currents (GICs), which have an adverse effect on technology in that they can cause anomalous low frequency currents that damage critical infrastructure. The problems with quantifying the damage in the absence of accurate GIC data (which can show the level of damage) are twofold, namely, for near real-time applications and the other for long-term applications respectively. Since GIC data is not easily available due to power utilities either not having measuring devices or not allowing its dissemination readily, other methods of quantifying damage as unambiguously as possible using data from more attainable sources such as local magnetometer stations, are necessary improvements that can be made. Attempts are made in this work, using an algorithm similar to that of Wintoft et al. [1], to address these problems via the creation of two GIC proxies to, in the case of near-real time applications, track damage, and in the long-term case, by combining ideas from Yu and Ridley [2] as well as Lotz and Danskin [3], to indicate damage incurred during storms. Using these algorithms, results are acquired by making use of Pearson's correlation and graphical methods, although the data set is too small to draw statistically significant conclusions. The results from the short-term index show that the index works well with the best indicators of short-term behaviour available as well as GIC data from power stations in South Africa. The results from the long-term index corroborates with the literature, in that damage done in long, yet less intense events can be as significant as damage done by short-term, yet highly intense events, as reported by Lotz and Danskin [3].

PREFACE

The experimental work described in this dissertation was carried out in the School of Chemistry and Physics, University of KwaZulu-Natal, Durban, from July 2018 to December 2020, under the supervision of Dr. Zolile Mtumela (UKZN) and Dr. Stefan Lotz (SANSA Space Science).

These studies represent original work by the author and have not otherwise been submitted in any form for any degree or diploma to any tertiary institution. Where use has been made of the work of others, it is duly acknowledged in the text.

DECLARATION - PLAGIARISM

I, Abu-Bakr Essop declare that

1. The research reported in this thesis, except where otherwise indicated, is my original research.
2. This thesis has not been submitted for any degree or examination at any other university.
3. This thesis does not contain other persons' data, pictures, graphs or other information, unless specifically acknowledged as being sourced from other persons.
4. This thesis does not contain other persons' writing, unless specifically acknowledged as being sourced from other researchers. Where other written sources have been quoted, then:(a) Their words have been rewritten but the general information attributed to them has been referenced(b) Where their exact words have been used, then their writing has been placed in italics and inside quotation marks, and referenced.
5. This thesis does not contain text, graphics or tables copied and pasted from the Internet, unless specifically acknowledged, and the source being detailed in the thesis and in the References section.

Signed: 

ACKNOWLEDGEMENTS

A special gratitude is owed to the following individuals and organisations:

1. Dr. Stefan Lotz without whose co-supervision this study would have been impossible.
2. Dr. Zolile Mtumela for his supervision.
3. Prof. Sivakumar Venkataraman whose efforts enabled this work to be done with SANSa Space Science.
4. NASSP UKZN and SANSa Space Science.

Contents

1	Introduction	1
1.1	Scientific motivation	1
1.2	Goals of this thesis	2
1.3	Outline	2
2	Scientific background	3
2.1	Geomagnetic phenomena	3
2.2	Solar structure	4
2.3	Solar behaviour	5
2.4	Solar terrestrial interaction	9
2.5	Solar wind-magnetosphere interaction	9
2.6	Description of currents	13
2.7	Geomagnetic storms	15
2.8	Theoretical background related to GICs	18
2.8.1	Earth's magnetic field	18
2.8.2	Mechanism of induced currents	18
2.9	GIC related damage	19
2.10	GIC mitigation	20
2.11	Existent proxies and indices	22
3	Algorithms and data	24
3.1	Software Algorithm: Short term-index	24
3.2	Software Algorithm: Cumulative index	28
3.3	Horizontal magnetic field data	30
3.4	Indices data	30
3.5	Measured GIC data	30
4	Analysis of results and discussion	32
4.1	Methodology	32
4.2	Correlation: Indices	34
4.3	Correlation of e_h with the Hermanus K-index vs. Storm Duration	36
4.4	Correlation: Measured GIC	38
4.4.1	e_h vs. measured GIC	43

4.5	Cumulative index	45
4.5.1	Threshold selection	45
4.5.2	The cumulative index	51
4.5.3	Active time and long-term index	53
4.5.4	Cumulative index and storm duration	55
4.5.5	Events with similar Cumulative index	56
4.5.6	Measured GIC: Events with similar Cumulative index	57
4.6	False warnings	58
4.6.1	Short-term index	58
4.6.2	Long-term index	63
5	Conclusion	65
5.1	Conclusion	65
5.2	Future work	66
A	Appendix: Figure Permissions and Proofreading certificates	74

Glossary

GIC (A) Geomagnetically induced current.

SYM-H (nT) Symmetric H index. An index used to give information about geomagnetic storms using the component of the magnetic field parallel to the dipole axis.

Dst (nT) Disturbance Storm-Time index. An index used to give information about geomagnetic storms using the component of the magnetic field perpendicular to the dipole axis.

e_h (nT/min) The short term index based on the work of Wintoft et al. [1] which uses the 30 minute means of the horizontal component of the magnetic field magnitude.

Threshold (nT/min) The e_h value beyond which damage causing GIC is assumed to occur.

C (nT/min) The cumulative index which sums all the values of e_h that are above the e_h threshold value of 0.5 nT/min.

$\frac{dB}{dt}$ (nT/min) The rate of change of the magnetic field.

$\left| \frac{dB_x}{dt} \right|$ (nT/min) The magnitude of the rate of change of the x-component of the magnetic field.

$\left| \frac{dB_y}{dt} \right|$ (nT/min) The magnitude of the rate of change of the y-component of the magnetic field.

$\left| \frac{dB_h}{dt} \right|$ (nT/min) The magnitude of the x and y-components of the magnetic field.

List of Figures

2.1	Essential components pertaining to solar structure copied from Kivelson and Russell with permission from the publishers [4].	4
2.2	Solar magnetic field modes \mathbf{B}_{tor} (toroidal) and \mathbf{B}_{pol} (poloidal) from Figure 2 of [5] copied according to figure reuse permissions of RAS journals.	6
2.3	Timeseries of sunspot latitude (a) and average daily sunspot area (b) adapted (by labelling panels) under creative commons licence from [6] with permission from the journal. (a) shows the coverage distribution of the sunspots based on their solar location (which appear as a butterfly) against. The size of the butterfly in (a) is closely related to the amplitude of the sunspot area curve in (b).	8
2.4	Localised magnetic field events copied from from Aschwanden [7]. From left to right, (A) a coronal helmet streamer, (B) a loop arcade, and (C) an x-ray jet. Image used under open access permissions courtesy of Yohkoh Team.	9
2.5	Interaction between solar wind plasma and magnetosphere (closed model) copied from Moldwin with permission from the publishers [8].	11
2.6	Interaction between solar wind plasma and magnetosphere (open(ed) model). Copied from Howard with permission from the publishers [9].	12
2.7	Models of different current topologies. Copied from Olsen with permission from the publishers [10].	13
2.8	Visible spectrum solar disk image, EUV solar disk image, and coronagraph (both images below are coronagraphs) imaging of a solar event which caused a large-scale geomagnetic storm in 2003. Copied from SOHO (ESA & NASA) [11].	15
2.9	Dst (nT) against time (days). Copied verbatim from Moldwin [8] with the permission of the publishers (“Reco ery” should read “Recovery”).	17
3.1	SYM-H data for the storm spanning 2011-09-26 to 2011-09-27. Note the noticeable drop to below -100 nT, indicating an intense geomagnetic storm [12].	26

3.2	From top panel: X-component of the magnetic field B_x (blue), time rate of change of X-component of magnetic field $\frac{dB_x}{dt}$ (orange), Y-component of magnetic field B_y (blue), time rate of change of Y-component of magnetic field $\frac{dB_y}{dt}$ (orange), time rate of change of H-field $\left \frac{dB_H}{dt}\right $ (green), and e_h (red) using the Hermanus station magnetometer data for the storm spanning 2011-09-26 to 2011-09-27.	26
3.3	e_h calculated from geomagnetic data recorded at the Hermanus station for the storm spanning 2011-09-26 to 2011-09-27. The red line denotes the fixed threshold magnetic value (chosen as 1 nT/min on the y-axis for clarity here), which, whenever crossed the values of e_h are added together to calculate an index showing cumulative damage post an event.	29
4.1	Map indicating locations of: 1. Matimba power station, 2. SANSA Space Science and 3. the Grassridge power station within South Africa. It can be seen that the locations of 2 and 3 are coastal while that of 1 is inland. Map data 2021 AfriGIS Pty Ltd.	34
4.2	e_h (blue) $\left \frac{dB_x}{dt}\right $ (black), $\left \frac{dB_y}{dt}\right $ (green), SYM-H (red), Hermanus K-index (purple) and Kp (orange) against storm duration for the event dating from 2013-06-28 to 2013-06-30.	36
4.3	Correlation between interpolated the Hermanus K-index data and e_h vs. storm duration in minutes. The correlation between K-index and e_h was performed for the duration of each storm using SYM-H classification for storm duration [12].	37
4.4	e_h and Hermanus K-index vs. time for the event dated 2011-09-26 to 2011-09-27. Observe how the K-index outlines general features of e_h yet lacks the resolution for finer details.	38
4.5	SYM-H (blue), measured GIC (black) and Hermanus K-index (orange) vs. time for a measured GIC event during the period 16 to 23 March 2013. The GIC was measured at the Matimba power station. The red box represents a 10 minute period during which there was a site calibration check (this was provided in the data).	39
4.6	SYM-H (blue), measured GIC (black) and Hermanus K-index (orange) vs. time for a measured GIC event during the period 16 to 24 March 2015. The GIC was measured at the Matimba power station.	40
4.7	SYM-H (blue), measured GIC (black) and Hermanus K-index (orange) vs. time for a measured GIC event during the period 29 to 31 October 2003 (Halloween storm). The GIC was measured at the Grassridge power station.	41
4.8	e_h (blue), the magnitude of measured GIC (black), $\left \frac{dB_x}{dt}\right $ (green), $\left \frac{dB_y}{dt}\right $ (purple), and Hermanus K-index (orange) vs. time for a measured GIC event during the period 2013-03-16 to 2013-03-23 at the Matimba power station.	43

4.9	e_h (blue), the magnitude of measured GIC (black), $\left \frac{dB_x}{dt}\right $ (green), $\left \frac{dB_y}{dt}\right $ (purple), and Hermanus K-index (orange) vs. time for a measured GIC event during the period 2015-03-16 to 2015-03-24 at the Matimba power station.	44
4.10	e_h (blue), the magnitude of measured GIC (black), $\left \frac{dB_x}{dt}\right $ (green), $\left \frac{dB_y}{dt}\right $ (purple), and Hermanus K-index (orange) vs. time for a measured GIC event during the period 2003-10-29 to 2003-10-31 at the Grassridge power station.	45
4.11	Interpolated Hermanus K-index (right) and e_h (left) against time. The threshold of 0.5 nT/min is plotted in green. This event took place as a result of a CME [13].	46
4.12	Interpolated Hermanus K-index data against e_h data of 21 storm events. The threshold of 0.5 nT/min is plotted in blue while a K unit of 1 is plotted in red. Region A has $K > 1$ and $e_h \leq 0.5$ nT/min, region B has $K \leq 1$ and $e_h \leq 0.5$ nT/min, region C has $K \leq 1$ and $e_h > 0.5$ nT/min and region D has $K > 1$ and $e_h > 0.5$ nT/min.	47
4.13	Interpolated Hermanus K-index data against e_h data of 21 storm events. The new threshold of 1.8 nT/min is plotted in blue while a K unit of 4 is plotted in red. Region A has $K > 4$ and $e_h \leq 1.8$ nT/min, region B has $K \leq 4$ and $e_h \leq 1.8$ nT/min, region C has $K \leq 4$ and $e_h > 1.8$ nT/min and region D has $K > 4$ and $e_h > 1.8$ nT/min.	49
4.14	Cumulative result vs. duration (Active time) in integer hours for the Hermanus data (columns 7 and 5 of Table 4.6 respectively). The band bounded by the green horizontal line and x-axis shows the where most of the data lies. The black line shows the line of best fit indicating the positive correlation between C and storm duration.	54
4.15	Cumulative index frequency vs. duration (Active time) in hours for event 16 (blue) and event 1 (orange). The vertical green line shows where the shorter event stops. The horizontal purple and red lines show the cumulative values for both events quoted in rows 16 and 21 of Table 4.6 respectively.	55
4.16	Cumulative index frequency vs. duration (Active time) in hours for events 6 (blue), 19 (orange) and 21 (green), where event numbers denote row events in Table 4.6 respectively. The vertical blue and green dashed lines show where events 6 and 21 stop respectively. The horizontal blue and green dashed lines show the cumulative index values for both events quoted in rows 6 and 21 of Table 4.6 respectively, while the horizontal orange dashed line shows the cumulative index value of event 19 of Table 4.6	56

4.17	Cumulative index frequency vs. duration (Active time) in hours for measured GIC events 1 (blue), 11 (red) and 22 (green), where event numbers denote row events in Table 4.6 respectively. The vertical blue and red dashed lines show where events 1 and 11 stop respectively. The horizontal blue, red and green dashed lines show the cumulative index values for the three events quoted in rows 1, 11 and 22 of Table 4.6 respectively.	57
4.18	(a) ‘Storm’ event Hermanus-K during the period 2015-03-17 to 2015-03-22, (b) ‘quiet’ event Hermanus-K against time during the period 2011-03-14 to 2011-03-19 (b) and (c) differences between (a) and (b). Each label on the x-axis refers to midnight for the ‘storm’ event in panel (a) and ‘quiet’ event in panel (b).	58
4.19	(a) ‘Storm’ event e_h during the period 2015-03-17 to 2015-03-22, (b) ‘quiet’ event e_h against time during the period 2011-03-14 to 2011-03-19 and (c) differences between (a) and (b). The red line denotes the e_h threshold of activity where $e_h = 0.5$ nT/min.	59
4.20	Histograms for Day 1 of ‘Quiet’ event during the period 2011-03-14 to 2011-03-19 (left) and storm event e_h against time during the period 2015-03-17 to 2015-03-22 (right). The red line denotes the mean e_h	60
4.21	Histograms for Day 2 of ‘Quiet’ event during the period 2011-03-14 to 2011-03-19 (left) and storm event e_h against time during the period 2015-03-17 to 2015-03-22 (right). The red line denotes the mean e_h	60
4.22	Histograms for Day 3 of ‘Quiet’ event during the period 2011-03-14 to 2011-03-19 (left) and storm event e_h against time during the period 2015-03-17 to 2015-03-22 (right). The red line denotes the mean e_h	61
4.23	Histograms for Day 4 of ‘Quiet’ event during the period 2011-03-14 to 2011-03-19 (left) and storm event e_h against time during the period 2015-03-17 to 2015-03-22 (right). The red line denotes the mean e_h	61
4.24	Histograms for Day 5 of ‘Quiet’ event during the period 2011-03-14 to 2011-03-19 (left) and storm event e_h against time during the period 2015-03-17 to 2015-03-22 (right). The red line denotes the mean e_h	62
4.25	Histograms for Day of ‘Quiet’ event during the period 2011-03-14 to 2011-03-19 (left) and storm event e_h against time during the period 2015-03-17 to 2015-03-22 (right). The red line denotes the mean e_h	62

List of Tables

4.1	Storm start and end dates.	33
4.2	Correlations between e_h with local and global indices done by bringing the indices to the 30 minute cadence of e_h . Here ‘Storm Number’ indicates the same event number as in Table 4.1 above, ‘Duration’ the days for which the event took place over, ‘Storm Duration’ the time for which SYM-H storm activity took place using the classification system of [12] (where a geomagnetic storm is defined using a time-interval in minutes not based on the total number of integer days), K the Hermanus K-index, Kp the planetary K-index, $\left \frac{dB_x}{dt}\right $, $\left \frac{dB_y}{dt}\right $ and SYM-H the global symmetric H-index.	35
4.3	Correlations of the indices $\left \frac{dB_x}{dt}\right $, $\left \frac{dB_y}{dt}\right $, K and e_h against the magnitude of measured GIC. Here the first and second columns indicate the start and stop dates for an event recorded, and the third, fourth, fifth and sixth columns give the correlation of the magnitude of GIC data with the X-component of the rate of change of the magnetic field magnitude, Y-component of the rate of change of the magnetic field magnitude, the Hermanus K-index, and e_h respectively.	42
4.4	Percentages of data based on the values of the Hermanus K-index and e_h from Figure 4.12 with an e_h threshold of damage assumed to be 0.5 nT/min. The first column gives the constraints on either K, e_h or both K and e_h , the second column gives the approximate percentage of data rounded to 2 decimal places in the region of Figure 4.12 subjected to those constraints and the third column gives the type of storm activity according to the K-classification for storm activity set out in [13].	48
4.5	Percentages of data based on the values of the Hermanus K-index and e_h from Figure 4.12 with an e_h threshold of damage assumed to be 1.8 nT/min. The first column gives the constraints on K and e_h , the second column gives the approximate percentage of data rounded to 2 decimal places in the region of Figure 4.12 subjected to those constraints and the third column gives the type of storm activity according to the K-classification for storm activity set out in [13].	50

4.6	‘Start date’ denotes the date a storm began, ‘Peak e_h ’ the noticeable maximum e_h of an event, ‘Sunspot number’ the American cumulative daily totals from NOAA (National Oceanic and Atmospheric Administration) website of sunspot number for the span of the event, ‘Storm duration’ of the storm in days, ‘ C ’ the cumulative index value, ‘Active time’ the cumulative time in days when the threshold was exceeded and the final column denoting the ratio of the active time to the duration of the storm as a percentage respectively.	52
4.7	Mean e_h for each day of the quiet (row 1) and storm (row 2) events plotted in Figures 4.20-4.25 above as well as the percentage of the fraction (row 3) of the quiet day mean to storm day mean for each day i. e. taking the ratio of the value in row 1 over row 2 as a percentage.	63
4.8	Cumulative index (C) value categories in the first column, the computed value for C based on its requisite number of computed days in the second column, and the estimated 10-day value for C in the second column adjusted for 10 days, all based on Table 4.6 (columns 6 and 5).	63

Chapter 1

Introduction

This chapter will introduce briefly the problems this study aims to address, how the problems will be solved, as well as the general outline of the study.

1.1 Scientific motivation

The K-index is a proxy derived from variations in the magnetic field and is dependent on the geographic location of a given magnetometer station. It yields one value per 3 hours (8 values per day). This scaled index is represented by integer values between 0 and 9 (inclusive of both endpoints) in ascending order of activity [13]. The prediction of geomagnetic storms is difficult [14] and as such, the minimum required is near real time monitoring of them via proxies. The conventional K-index is one such proxy but it is too coarse in time and amplitude [13]. The problems with the way this index is derived are that substorms, which occur on the order of hours, are not identified and that magnetometer measurements are bounded based on a maximum magnetic field value that correlates to the highest value of K, namely 9 (the K-9 limit). Thus the magnetic field values beyond this K-9 limit are not represented accurately by the derivation of the K-index which is a serious matter [15]. Geomagnetically induced currents (GICs), as defined in this study are currents which flow into grounded electrical conductors and may result in damage to important infrastructure as a result of their accumulation beyond a certain level [16]. At middle latitudes which do not incur intense storms frequently, sudden storm commencement is more relevant for studying GIC as it causes short, yet intense storms over shorter periods [17]. A global system for GIC monitoring is required as GICs pose threats to systems involving large conductors such as power grids and oil pipelines, essential systems for life on the planet. The issues with nowcasting arise out of not being able to give a sufficient indicator of the current condition [1]. Short and-long term measurement of the effects which are objective without having to check infrastructure physically [18] and which looks at possible effects of extreme events from data [3], is needed. Effective measurement of GICs is needed to minimize their impact to ensure planning, modelling and prediction, all in order to mitigate the negative effects they incur. Using a proxy is an efficient way to

monitor geomagnetic storms and, thus, possible GICs which may occur and cause a lot of damage. This proxy will be used to track storms and inform the relevant parties of possible threats to their infrastructure via GICs. Another reason for the development of this proxy is that most research on GICs has been done in high latitude regions where geomagnetic storm activity is most prevalent. This study will allow development of research into these phenomena from a mid-latitude perspective which is essential. GICs have been responsible for damage to the South African power grid and the effects on mid-latitude nations needs to be monitored as these are developing nations with economies that will suffer from the consequences of not having systems in place to protect against GIC threats [19].

1.2 Goals of this thesis

This study proposes to develop two proxies for GIC activity, based on local geology and availability of conductivity or surface impedance information. Consideration will also be given to the time resolution of these proxies. This study suggests two proxies that differ in time scale. The goals of this study are twofold, namely,

1. To develop an index that gives information of the near-real time activity of geomagnetic activity (hours) i.e. an indication of the current condition - up to the last minute (magnetometer sampling time) - necessary to track the development of an ongoing event.
2. To develop an index that gives cumulative information of the geomagnetic activity that took place over a specified period (days) i.e. an indication of cumulative damage is likely to track the exposure of the system throughout the event.

The developed proxy would assist in the prediction of geomagnetically induced current (GIC) activity which poses threats to power grids in South African [20] and greater global networks [21]. The indices must be reliable and where possible, scale as well as or be better than those found in the literature, as well as giving information as unambiguously as possible.

1.3 Outline

This thesis is outlined as follows:

Chapter 2 will give the necessary theoretical background, review the literature, and elucidate this study's purpose.

Chapter 3 outlines the methodology used in attempting to solve the problem and describes the data used.

Chapter 4 gives an analysis of the results and discusses them. It includes the reasoning behind the interpretation of the results and their significance.

Chapter 5 concludes this study. Some possible future work is described in relation to what may be done to improve and extend this study.

Chapter 2

Scientific background

2.1 Geomagnetic phenomena

Geomagnetic activity is known to play a significant role in affecting grounded conducting networks, including, albeit not restricted to: power network and oil pipeline infrastructures (henceforth *quasi-antennas*) [22]. Geomagnetically induced currents (GICs) are significant enough in their impact on the aforementioned critical network infrastructures to warrant careful study of their genesis, development, and long and short-term effects on the terrestrial environment of the Earth.

With regard to a theoretical framework on which to base experimental procedures, an application of the Faraday's law of induction, which explains that the sum of a spatially changing electric field and its associated temporally changing magnetic field is zero, can be found in GICs. Elucidation of GICs as a process is as follows:

1. Abnormal solar wind conditions, such as during CMEs (coronal mass ejections), elicit abnormal behavioural responses in the terrestrial ionospheric and magnetospheric current systems (located in the terrestrial atmosphere, via intimately coupled interactions, known as geomagnetic storms).
2. These current systems in turn induce, via Faraday's law of induction, abnormal responses in the geomagnetic field.
3. The abnormal, fluctuating field induces via Faraday's law of induction, abnormal responses in the geoelectric field, which, being intimately linked to surface-GICs, effects abnormal electrical responses in quasi-antennas (the natural locus of such infrastructures, by conventional architecture, being *in situ* with GICs).

The Sun emits high energy particles through an abnormal event known as a CME, which causes a rapidly fluctuating magnetic field on Earth, which in turn interacts with Earth's magnetic field, inducing an electric field on the surface of the Earth, causing GICs. Note that the power transformers need to be grounded for the accumulation of GICs to

cause damage to them [16]. The problems with GICs are found in quantifying them meaningfully at different timescales, as well as when there is a lack of meaningful GIC data. For the short-term, near real time tracking of abnormal geomagnetic activity requires a method that is as unambiguous as possible. This will give an indicator as to the current condition of the geomagnetic activity. For the long-term, after abnormal geomagnetic storm events have happened, they need to be assessed and meaningful conclusions need to be drawn. This requires another means of quantification that looks at the overall storm profile.

To solve these problems, the work set out in this thesis aims to create two proxies that work in the short-term, as well as in the long-term. In the short-term, the index aims to work as a proxy in the absence of GIC data. This will enable stakeholders to be informed of the current geomagnetic situation so that they can take steps to minimize damage to their critical infrastructure. The long-term proxy aims to indicate the severity of a storm post-event. This will enable recommendations to necessary stakeholders as to the possible damage their infrastructure has undergone.

2.2 Solar structure

The main driver of abnormal solar activity, namely the Sun, must first be viewed from a structural viewpoint before it's behaviour spatially, temporally, and terrestrially, can be explained.

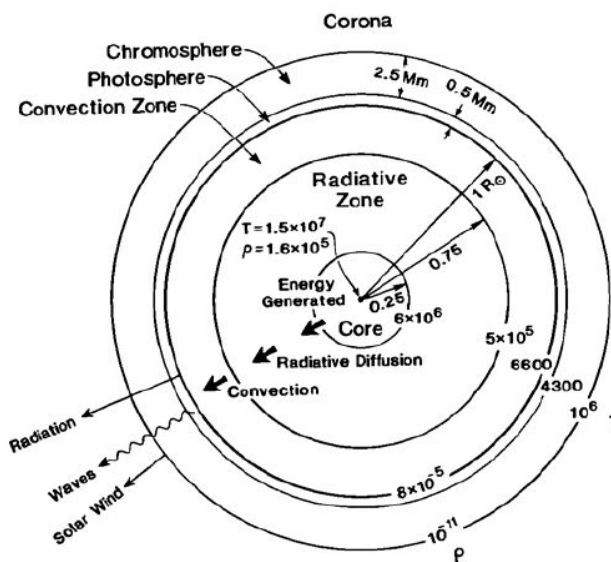


Figure 2.1: Essential components pertaining to solar structure copied from Kivelson and Russell with permission from the publishers [4].

Solar structure presents anatomically inwards *ordo essendi* as [23]: The corona, tran-

sition region, chromosphere, and photosphere, which collectively make up the Solar atmosphere. The solar wind consists of plasma, which, when disturbed (such as by a CME) and focused towards the Earth, can cause geomagnetic storms which may lead to GICs.

2.3 Solar behaviour

For all intents and purposes of this study, a discussion of the behaviour of the solar core, transition region and chromosphere, beyond what has already been mentioned, will be omitted for the study of the propagation of Earth-bound solar wind.

The behaviour of the convection and radiation zones, given by the inequalities in (2.1) and (2.2) below respectively, are intimately coupled mathematically by the Schwarzschild adiabatic criteria [24], both given and briefly discussed respectively, as:

$$\left| \frac{dT}{dr} \right| < \left| \left(\frac{dT}{dr} \right)_{ad} \right| \quad (2.1)$$

For the radiation zone, the converse is true, yielding (2.1), where the adiabatic lapse rate, $\left| \left(\frac{dT}{dr} \right)_{ad} \right|$, is greater than the radial temperature gradient, $\left| \frac{dT}{dr} \right|$. Convective stability within the plasma of the convection zone occurs.

$$\left| \frac{dT}{dr} \right| > \left| \left(\frac{dT}{dr} \right)_{ad} \right| \quad (2.2)$$

For the convection zone, the assumption of negative temperature gradients yields (2.2), where the adiabatic lapse rate, $\left| \left(\frac{dT}{dr} \right)_{ad} \right|$, is less than the radial temperature gradient, $\left| \frac{dT}{dr} \right|$. Convective instability within the plasma of the convection zone occurs, and the buoyancy force which results creates fluctuating harmonic motion.

The photosphere is where the aforementioned harmonic motions result in *granules* (convection cells), spatially observable phenomena (observed with high magnification telescopes) ranging in diametric size classified as (1) granule ~ 1000 km, (2) Supergranule ~ 10000 km, and (3) giant cell $\sim \frac{1}{3}$ (third of the) solar radius.

From the definition of plasmas in the classical sense, being in possession of charged ions, and due to the fact that the Sun rotates, a discussion of the solar magnetic field(s) from such motions is pertinent. A brief discussion of the general solar magnetic field will be presented [25] and then the drivers of the solar magnetic field based on the work researched in [26], [27], [28], [29], [9] will be presented.

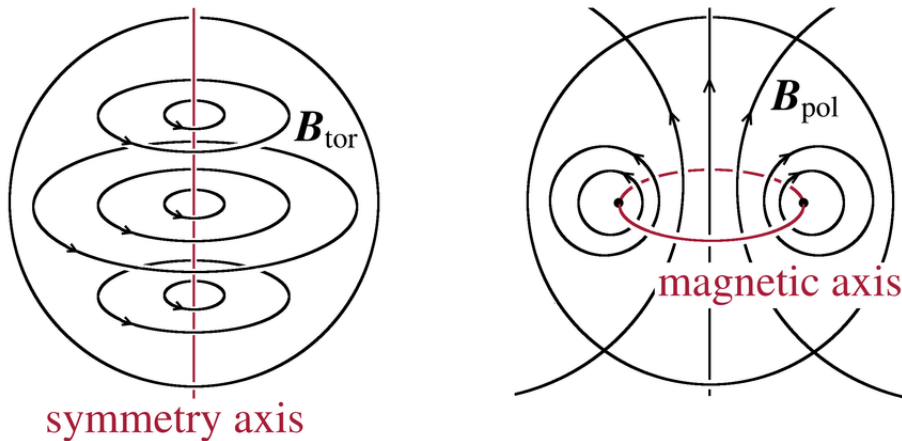


Figure 2.2: Solar magnetic field modes \mathbf{B}_{tor} (toroidal) and \mathbf{B}_{pol} (poloidal) from Figure 2 of [5] copied according to figure reuse permissions of RAS journals.

Differential rotation between the poles and equator of a well approximated spherical plasma wherein a frozen magnetic field (seed field) lines, yields the following magnetic field observations [25]: (1) Assuming the rotational equatorial motion dominates the magnetic behaviour of the sphere and the axis is that of the vertical direction, the magnetic field is toroidal as the seed field is stretched azimuthally. The toroidal mode is shown in Figure 2.2 (\mathbf{B}_{tor}), and (2) due to the convective instability of the plasma causing harmonic motion, coupled with the deflective Coriolis force, the field would to some extent, preserve the azimuthal loops, and eventually stretch out to become poloidal. The poloidal mode is shown in Figure 2.2 (\mathbf{B}_{pol}).

Granulation, due to the aforementioned convective instabilities and their resultant harmonic motions, present photospherically with characteristic time and diametric duration of approximately 10 minutes and 1000 km respectively.

Supergranulation does not present with the visibly observable photospheric prominence of it's underlying counterpart (granulation), but is observable magnetically via field lines or visibly observable chromospherically as spicules, and presents with characteristic time and diametric length of approximately 1-3 days and 20000 km respectively.

The Sun undergoes periodic behaviour, including two extremes known as the solar maximum and minimum respectively, with the approximate period between successive maxima being 11 years. The period between two minima is known as the solar cycle. Solar maximum and minimum are defined in terms of the sunspot number which is derived from the number of sunspots and the number and sizes of sunspot groups. Sunspots can be observed because they present as clearly visible structures on the solar surface.

Sunspots can be described magnetically, temperature-wise, diametrically and cardinally, as approximately 0.1 T (a strong field), approximately 3000 K (thus observable as dark spots on the solar surface), as far as 20 000 km (comparable to supergranulation above),

and as countable within groups over time (plotted on butterfly diagrams and time series), respectively.

The magnetic field associated with sunspot groups taken together can exhibit collective or individual behaviour, such that the fields can be stretched over the group, or be found singularly, both in a unipolar or in a bipolar sense. Sunspot groups tend to be located in opposite hemispheres with magnetic fields of opposing parity. Each sunspot group comprises of regions of opposite magnetic polarity. The magnetic field lines between these poles can be observed via the hot plasma moving along these magnetic lines.

The temperature associated with sunspots as well as their characteristic development times (from appearance to disappearance being 1-4 days respectively, depending on a spectrum of small-large size), allows them to be observed since their temperature is much less than their surrounding environment, due to the adiabatic cooling via upward harmonic motion of plasma with associated magnetic field lines from the convection zone.

The spatial characteristics (roughly circular) across large diametric lengths (20 000 km) are the main reason that visible observation of the magnetic field motion of sunspots is possible, along with their characteristic development times, which renders accurate accounting of their cardinality possible as well.

Sunspots have been counted and recorded, and found to follow certain patterns, such as the solar cycle, with time. Sunspot patterns are usually represented graphically in the form of two types of graphs: 1) Sunspot number vs. time, and 2) Sunspot location and size vs. time. The first type is shown in Figure 2.3 (b) and the second type, known as a butterfly diagram, is shown in Figure 2.3 (a).

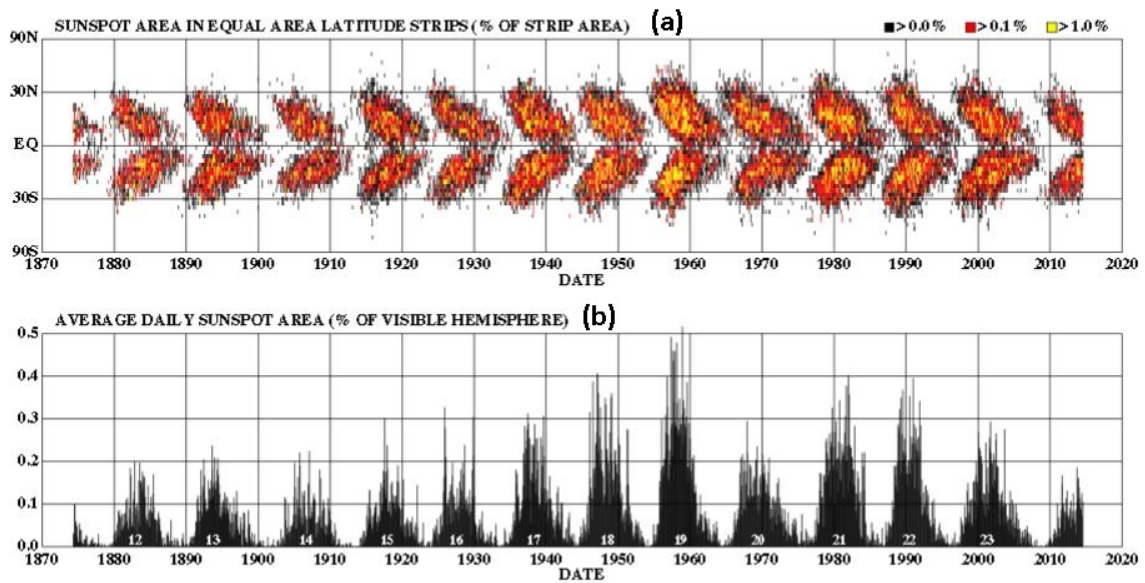


Figure 2.3: Timeseries of sunspot latitude (a) and average daily sunspot area (b) adapted (by labelling panels) under creative commons licence from [6] with permission from the journal. (a) shows the coverage distribution of the sunspots based on their solar location (which appear as a butterfly) against. The size of the butterfly in (a) is closely related to the amplitude of the sunspot area curve in (b).

Figure 2.4 shows three events: A- coronal helmet streamers, B- loop arcades, and C- x-ray jets; these events contribute to the formation of the solar magnetic field. The discussion of these phenomena is primarily focused on work done by Skoug et al. [30]. Coronal helmet streamers are radially oriented structures that extend many solar radii into the heliosphere (the solar sphere of influence). They are highly observable due to electron transport taking place along the magnetic field lines and can be seen during eclipses on the outer form of the Sun. Loop arcades are regions of opposite magnetic polarity occurring over a large solar surface area. The arcade appears when a bundle of loops come together after solar flares have taken place. X-ray jets are optically observable linear structures found when plasma follows a magnetic field line's trajectory, that can be observed with x-ray detectors.

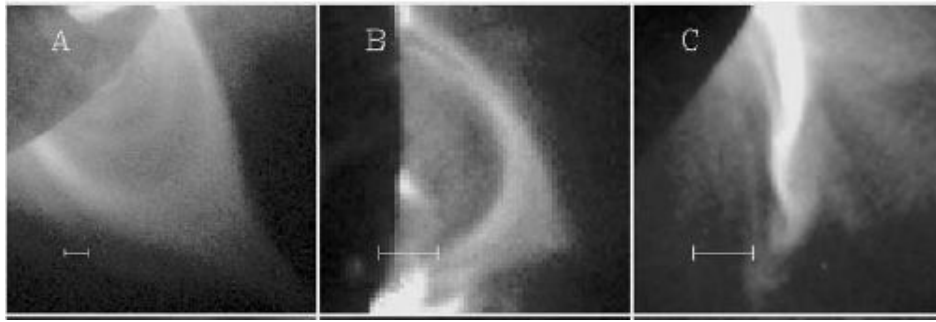


Figure 2.4: Localised magnetic field events copied from from Aschwanden [7]. From left to right, (A) a coronal helmet streamer, (B) a loop arcade, and (C) an x-ray jet. Image used under open access permissions courtesy of Yohkoh Team.

The solar sphere of influence, namely the heliosphere, is a region encapsulating all the planets, and extending beyond them to form a three dimensional region. The Earth, which is shielded by the magnetosphere, atmosphere and interplanetary magnetic field, is found within the heliosphere. Next, the solar terrestrial interaction will be discussed with a focus on geomagnetic storms.

2.4 Solar terrestrial interaction

The solar wind, essentially the chief distribution mechanism of solar matter within the heliosphere, has been recorded at maximum speeds in excess of 1850 km/s [30]. The propagation of such high energy charged particles toward the Earth's surface does not occur due to the atmosphere and the magnetosphere. The former is less important than the latter for the purposes of this study, and will be mentioned *ad hoc* from this point forward.

At such extreme propagation speeds, charged matter will penetrate the atmosphere and be stopped at approximately 100km above the Earth's surface. Current which enters the conductors of transformers via neutral ground points due to the interaction of the Earth's electric field and abnormal magnetic field conditions can cause damage. The rapid transfer of energy into the magnetosphere can occur typically due to a southward IMF (from a CME) which reconnects with Earth's northward field and can cause the ring current to expand, which indicates geomagnetic field perturbations (observed as a drop in Dst) [8]. A description of the magnetosphere under the closed and open(ed) magnetic field line models is essential [8], [31], [32], [33]. It is amidst this backdrop that geomagnetic storms will be elucidated in section 2.5.

2.5 Solar wind-magnetosphere interaction

For a more detailed description of the solar wind, magnetosphere and their coupling, see [34] and [8] upon which the following is based.

The solar wind is essentially an extension of the Sun which, for all intents and purposes of this study, extends to the Earth environment, interacting with the magnetosphere and atmosphere of the planet. The solar wind travels in the form of a plasma at supersonic speeds and can be modelled as such.

Geophysically, the Earth behaves as a magnet and can be approximated by a dipole, although this can lead to errors at middle and low latitudes when compared to the International Geomagnetic Reference Field (IGRF) model, which is a better adjusted dipole approximation model that can be preferred for the internal field of the Earth [35]. The region in space where the predominant magnetic field is that of the Earth (as opposed to the prevailing magnetic fields in space), is known as the magnetosphere which couples to the solar wind in a special manner. This serves as a pathway for the transfer of energy from high energy solar material into the magnetosphere resulting in phenomena known as geomagnetic storms.

This can occur due to activities on the surface of the Sun such as coronal mass ejections (CMEs). CMEs are unpredictable phenomena which result in plasma being ejected from the Sun towards Earth, or solar flares. CMEs also result in spontaneous bursts of electromagnetic energy travelling at the speed of light. Both of the aforementioned phenomena, namely coronal mass ejections and solar flares, can occur independently or together. Upon reaching the magnetosphere, they will perturb the magnetosphere and cause geomagnetic storms which can occur due to magnetic reconnection. This phenomenon in the dayside sense occurs when the z-component of the interplanetary magnetic field (IMF) becomes negative i.e. opposite orientation to the geomagnetic field .

Interplanetary coronal mass ejections (ICMEs) are phenomena driven by the solar wind which cause a magnetospheric response, and are the key drivers of “intense geomagnetic storms and large GIC” [36].

Figure 2.5 below shows the interaction between the solar wind and the Earth's magnetosphere in the two dimensional sense at an instant.

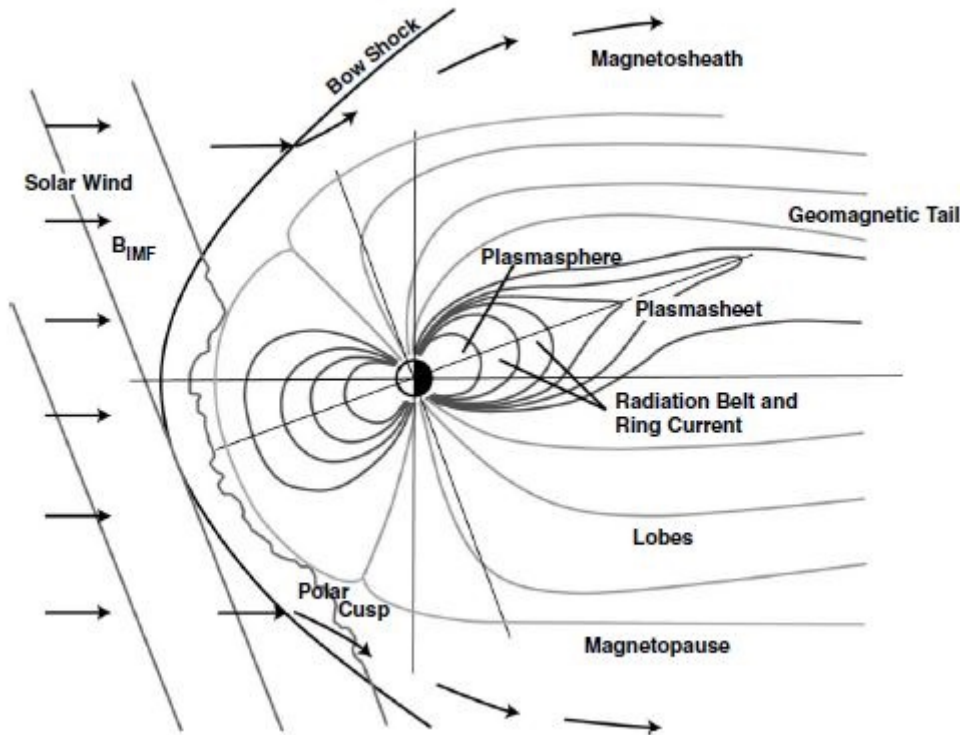


Figure 2.5: Interaction between solar wind plasma and magnetosphere (closed model) copied from Moldwin with permission from the publishers [8].

Figure 2.5 presents a simple illustration of the closed model. The discussion that follows is based on [8], [31], [32], [33].

The distorted dipole occurs as a result of flow pressure from the solar wind compressing the dayside and elongating the nightside of the magnetosphere. This is due to the "frozen-in flux" condition which says that there is an interplay between magnetic field and plasma particle dynamics. The significance of the plasma sheet in the derivation of GIC proxies will be explained in section 2.6.

The sheet currents associated with flow along the magnetopause are called Chapman-Ferraro currents [8]. These currents are responsible for the external cancellation and the internal doubling, respectively, of the magnetic dipole either side of the magnetopause [31]. This dipolar doubling (from the shock) is detected terrestrially by abnormal changes in the magnetic field, classified as the onset of a geomagnetic storm [8].

The confluence of the open and closed field lines into the dipolar geographic regions, namely

North and South Poles, causes the emergence of the auroral oval, a region of highly charged particles visibly observed at certain terrestrial latitudes as the aurora borealis and australis variants in the northern and southern poles respectively [33].

The preceding model makes oversimplifying assumptions that have allowed, via theoretical and experimental findings, the need for the succeeding model such as: (1) There is *in situ* particle evidence [37] for open field lines even though magnetospheric magnetic reconnection (joining of open field lines) takes place [38], (2) The magnetopause is not electrically equipotential and not susceptible to magnetic reconnection [39], and (3) The assumption of collisionless plasma leaves a vacuum to be filled by effective viscosity [40] to bridge the transfer of the momentum of charged particles.

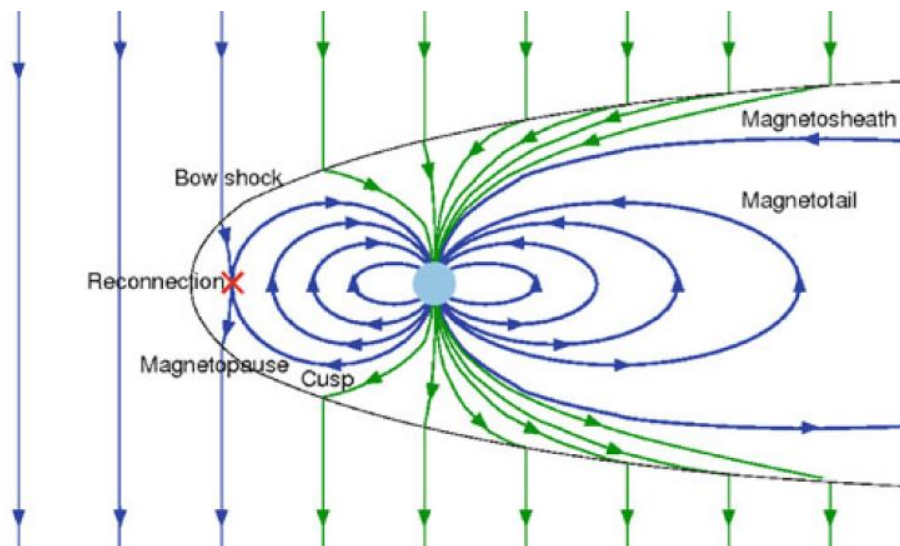


Figure 2.6: Interaction between solar wind plasma and magnetosphere (open(ed) model). Copied from Howard with permission from the publishers [9].

Figure 2.6 presents a simple illustration of the open(ed) model. The discussion which follows is based on [31], [32], [33].

Magnetic reconnection, a phenomenon in which the geometrical nature of the magnetic field re-orient, due to which kinetic energy outflows in groups, is proposed to be responsible for the connection between the magnetosphere and the interplanetary magnetic field (IMF). Energy is transferred from the solar wind via magnetic reconnection and the highly charged plasma acts as a vector to propagate this energy, perceived as geomagnetic storms and substorms. When magnetic reconnection is factored into the interaction between the solar wind and the magnetosphere, the model is preferred. Thus, during times of intense geomagnetic activity, the model is without comparison. As direct measurements, coupled with stronger computing power and advanced magnetohydrodynamics becomes more ac-

cessible, better models can be developed.

2.6 Description of currents

Due to the outflow of Earth bound energetic particles travelling to different latitudes (where their effects are different), a discussion of the main currents coupled between the terrestrial and the magnetospheric environments will be presented. Figure 2.7 [(a)-(c)], and subsequent discussions of current systems are based on [10] and [41], [42] respectively.

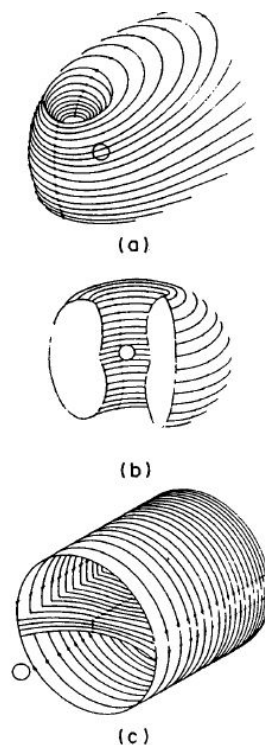


Figure 2.7: Models of different current topologies. Copied from Olsen with permission from the publishers [10].

The explanation of the main currents is as follows:

Figure 2.7 (a) shows a topological model of the Chapman-Ferraro current (magnetopause current). The Biot-Savart law links electrical currents and magnetic fields. The current flowing along the magnetopause and magnetic field outside it effectively cancel one another. Within the inner, more dipolar magnetosphere, the current is much smaller than that of the terrestrial dipolar current.

Figure 2.7 (b) shows a topological model of the magnetospheric ring current. This

current is located within approximately 5 Earth radii and is the reason for the decrease in the geomagnetic field after magnetospheric compression due to geomagnetic storm activity. The current flows clockwise (as observed from the North pole), and its geomagnetic field acts in direct opposition to the geomagnetic field caused by currents in the Earth's core.

Figure 2.7 (c) shows a topological model of the tail current. This current appears as doubly solenoidal. That the magnetosphere tapers off into a bounded tail on the nightside and allows for the flow of a tail current across the plasma sheet from the dayside. This current has associated power comparable to thousands of gigawatts.

The final current system to be mentioned will be that of Birkeland (field-aligned) currents. Independent satellite observations (ISIS-2 and TRIAD) confirm their existence as related to the propagation of the auroral oval from the polar sense (region 1) to the equatorial sense (region 2) with increasing disturbance activity. Current density in region 1 and 2 respectively depends on the time in the day and coincides with roughly equal intensity around midnight. Of note is the fact that current density varies linearly with the K_p index, a proxy used to show the amount of the magnetic activity taking place.

Next, geomagnetic storms will be discussed, as what has been presented about the solar-terrestrial interaction is sufficient to proceed.

2.7 Geomagnetic storms

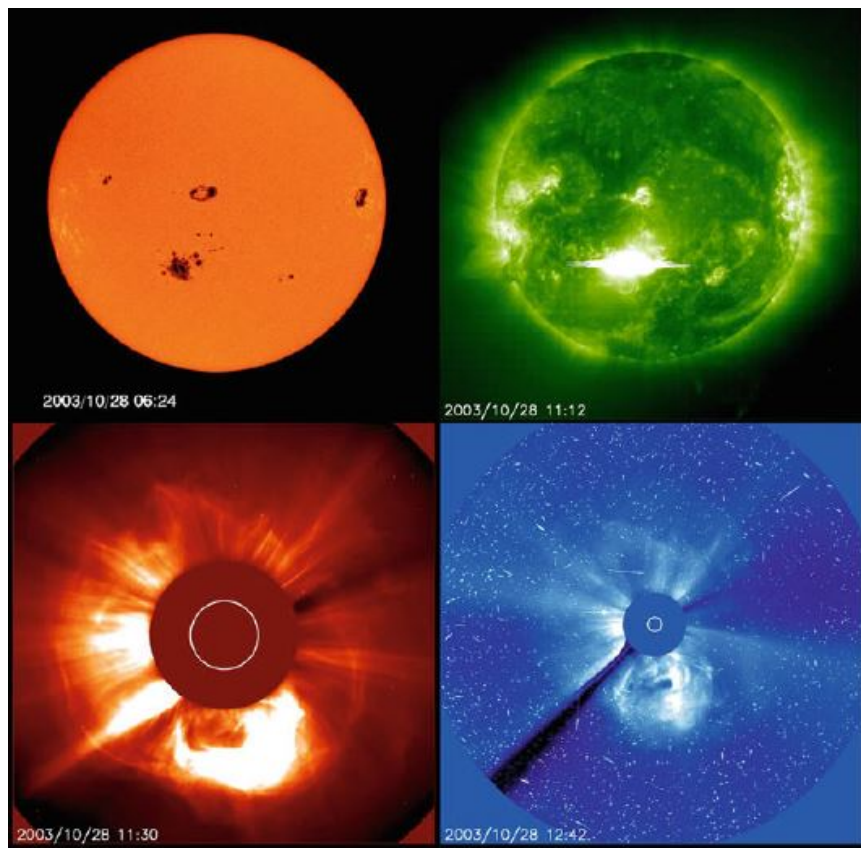


Figure 2.8: Visible spectrum solar disk image, EUV solar disk image, and coronagraph (both images below are coronagraphs) imaging of a solar event which caused a large-scale geomagnetic storm in 2003. Copied from SOHO (ESA & NASA) [11].

Figure 2.8 shows solar flares as well as solar wind activity. These images are taken at different frequencies. They all show the same event, in this case a CME, which erupted causing the well noted ‘Halloween’ storm of 2003 [43]. What can be observed from the figures (clockwise) are, respectively, a large concentration of sunspot groupings, an EUV flash associated with a CME eruption, and abnormal extensions of coronal matter into the heliosphere. The storm was responsible for a power outage in Sweden and the failure of at least one Japanese spacecraft [43], [44].

A geomagnetic storm is an interval of time during which abnormal changes in the magnitude and orientation of the Earth’s magnetic field occurs for discernible periods on the order of days [12].

This occurs due to abnormal activities on the surface of the Sun as previously discussed, such as coronal mass ejections and solar flares perturbing the terrestrial magnetosphere via the solar wind.

The storm phases presented below are largely based on [45] and [46].

The onset of geomagnetic storms are detected via instruments known as magnetometers. Geomagnetic storms are identified and classified by a number of indices (such as K-index, SYMH, Dst, etc.) [47]. The Disturbance Storm-Time index is an index used to give information about geomagnetic storms using the component of the magnetic field perpendicular to the dipole axis. Thus, a moderate geomagnetic storm may be defined as a phenomenon wherein the Dst index records a drop between -50 nT and -100 nT and intense storms below -100 nT for a given storm [12].

The encounter between the magnetosphere and leading shock front of the solar wind causes a sudden commencement (SC) or sudden storm commencement (SSC) [46]. SSC exists when there is a “change of rhythm” in the magnetic activity post a sudden impulse [48], [49] while SC occurs when there is “a sudden increase of the solarwind dynamic pressure” [50], [49]. Commonly found after a SC, due to magnetospheric compression, is an increase in northward component of the geomagnetic field, which lasts on the order of hours.

The main component of the storm thereafter is known as the growth phase, which presents as rapidly fluctuating geomagnetic field values, varying with higher absolute amplitudes than those within the initial phase, with most terrestrial auroral phenomena (borealis in the north, australis in the south) occurring.

The final phase of a storm, known as the recovery phase, is when geomagnetic order approaches terrestrial quiet time levels, and lasts longer than both previous phases.

The graph below (Figure 2.9) shows the Dst index against time for a geomagnetic storm with initial, main, and recovery phases during an event on the temporal order of days.

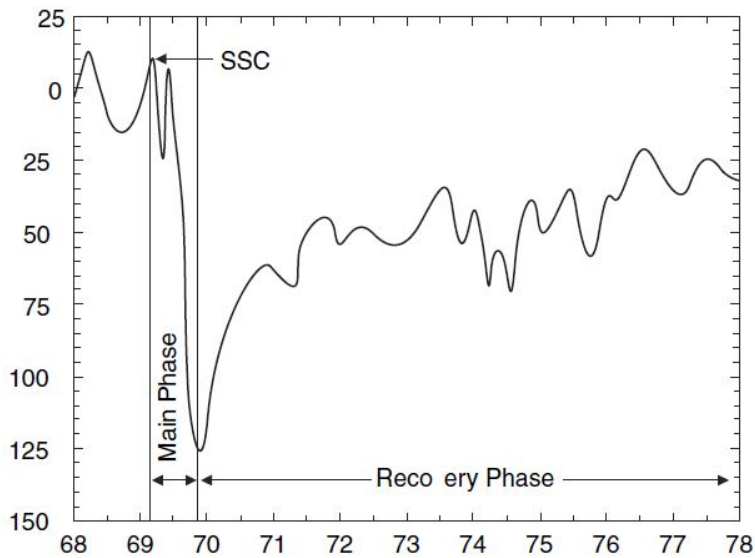


Figure 2.9: Dst (nT) against time (days). Copied verbatim from Moldwin [8] with the permission of the publishers (“Recovery” should read “Recovery”).

The sudden storm commencement (SSC) is a sudden positive deviation of the horizontal component of the geomagnetic field which lasts on a relative scale of minutes to hours. The SSC is followed by a drop in the horizontal component of the geomagnetic field, indicating the main phase of the storm which lasts on the scale of hours, and finally the approach toward the recovery phase which takes place on a relative scale of a few days, reestablishing a dynamic equilibrium that does not deviate far from the quiet-time behaviour [8].

It is pertinent that each phase of the storm is well noted, as the SSC may lead to transients that cause tripping of protection relays [51], and the main phase of the storm is when the transformer damage can occur and continues to occur over a period of days, which is detrimental to critical infrastructures on a local, and possible global, scale. Phase identification is important for stakeholders to assess the potential power interruptions and damage that could be done during the onset, progress and restoration of the magnetic field when geomagnetic storms take their course.

Although they are events which occur with low probability at mid-latitudes, GICs in South Africa may have caused significant damage to transformers within the power network (and to oil pipelines in other parts of the world) and thus the prediction of GICs is vital to the country and those parts of world at which they are likely to occur [19], [52]. Geomagnetic storms which occur during peak usage of electricity can cause surges in the system grid in the form of GIC induced increases in the currents, voltages and harmonics [8].

2.8 Theoretical background related to GICs

This section seeks to explain GIC formation, resultant damage to infrastructure, methods of GIC mitigation as well as direct damage mitigation. Furthermore the necessity for indices to be derived from geomagnetic field data, the proxies which exist, and the purpose of this study are explained in this section.

2.8.1 Earth's magnetic field

In this section, the x and y components of the magnetic field B_x and B_y respectively are discussed. These components are two strength quantities in the x and y directions of Cartesian coordinates respectively, that are necessary in describing the horizontal components of Earth's magnetic field. These Cartesian coordinates are incident onto the geomagnetic north and east directions respectively. This study uses the H-component as a requirement to understand induced fields in the x and y directions of the magnetic field (i.e. the geomagnetic locus of infrastructure susceptible to the internal propagation of induced currents of great magnitudes and their potentially harmful effects). The H-component is defined as equation (2.3) i.e.

$$B_h = \sqrt{(B_x)^2 + (B_y)^2} \quad (2.3)$$

2.8.2 Mechanism of induced currents

The mathematical description of the relationship between a time changing magnetic field and a position changing electric field (and hence induced an electric current) is accurately described by Faraday's law of induction as:

$$\nabla \times \vec{E} = -\frac{\partial \vec{B}}{\partial t} \quad (2.4)$$

With respect to currents induced in the geomagnetic sense, for long enough conductors such as power grids and oil pipelines [53], equation (2.4) holds accurately.

The following paragraph is based on a paper by Oliviera and Ngwira [54]:

Magnetospheric perturbations which present as a compression of its three dimensional field which causes the z-component of the field to interact with the north-facing geomagnetic field causing magnetic reconnection. This causes a release of energy, which through ionospheric interaction induces electrical currents in the ground which in turn result in a secondary magnetic field and hence due to equation (2.4), an electric field at the surface of the Earth is induced. The electric field in the Earth causes a voltage difference between the grounded ends of a power line, which in turn induces a surge in current in transformers. It must also be noted that the Earth's magnetic field varies in time and place without fixed poles which has ramifications for the variance of the Earth's electric field variations that

are associated with phases of geomagnetic storms [55]. The ground conductivity structure of the Earth thus varies as has been studied at various different locations such as Canada and India [56], [57] and South Africa [58]. A review by Dong et al. [59] showed that Earth conductivity structure has a key role in the determination of the geoelectric field. This is especially relevant in the case of GICs in terms of geographical location as parameters such as rock type and depth [59], location near the coast [56], as well as soil type [57] have to be considered. Thus it can be seen that different places on the planet will have local features unique to its ground conductivity.

2.9 GIC related damage

GICs cause damages to multiple infrastructures [22]. The damage that will be discussed below will be based on that occurring in power systems as this is of particular importance globally as well as locally in South Africa.

The current surges encountered by power transformers can be broadly grouped into two categories, namely events of the short term with high magnitude (such as the Carrington event of 1859 or Halloween storm of 2003), and events of medium to long term of lower intensity magnitudes, where both groups cause damage [3]. A concise understanding of the damage caused in South Africa as well as globally will be discussed.

Gaunt and Coetzee [60] identify and discuss the relationship between damage (thought to be geographically irrelevant) in South African transformers and 3 variables, namely theoretical GIC calculations, practical GIC measurements, and dissolved gas analysis (DGA) records, respectively.

Pertinent to power systems is the thermal damage caused by GICs during the Halloween storm of 2003 in 18 transformers (a set of 12 and a set of 6 of 2 different types respectively), some of which were equipped with active DGA instruments. Throughout 2004, some transformers from the above set as well as others had to be replaced. Gas ratio results in the aftermath of the Halloween event were found to be consistent with thermal degradation of transformers that began during the Halloween storm. To understand the various types of damage in power systems, Gaunt et al. [14] give a concise understanding of the various classes of GIC related damage in the power system chain, namely “thermal damage to transformers, voltage instability and protection maloperation”. The authors used tested magnetic effects on transformers, using finite element method (FEM), which can reveal areas of damage, as well as DGA, which can indicate the relative time of damage. In the presence of GICs, it was shown using FEM that the 3P3L transformer (3-phase 3-limb, a type of transformer), thought previously to be less susceptible to such currents than the 3P5L transformer, was in fact at risk [14]. Furthermore, it was shown that thermal damage due to heating within transformers arising out

of GICs manifests after different time periods based on the geographical location of the transformers, as is revealed by DGA. A case in point was the replacement after 2 days apropos the 1989 event in Quebec versus replacement after weeks to months apropos the 2003 event in South Africa by Eskom. DGA results also show that in the short term, damage occurs at a specific transformer by the evolution of gases which cause heating due to the decreased thermal conductance of the cooling oil, as well as in the long term via accumulated damage that did not manifest clearly but leads to a cascading system failure when the system is either in use, or another GIC event occurs.

Two important causes of power interruptions resulting from GICs are voltage instabilities and power imbalances that are mismatched with the range of operational capabilities that the transformers are designed for, leading to eventual system collapse and tripping of protection relays in response to overvoltage conditions or increased levels of harmonics or accumulated transformer damage.

2.10 GIC mitigation

This section will give a broad understanding of the ways that have been attempted to mitigate GIC related damage via indices/proxies as well as various other means, as well the need for indices/proxies to be derived from geomagnetic field data.

The types of GIC mitigation strategies depend mainly on which part of the GIC chain the focus is placed and where data is captured.

Methods of mitigation with site specific geomagnetic data in real time are those which monitor or track the evolution of GICs and analyse their trends, while seeking to predict whether or not damage will occur. On a larger scale of time, a clear result of a total event may be analysed from geomagnetic data, and its cumulative features taken into account. In both of these cases, data may be compared with direct GIC recordings from power utilities and from global measurements taken to cross correlate both the local features of the event as well the global features. Both of these methods, namely indicators of the current condition (near real-time) and cumulative conditions assessed with geomagnetic data, are the focus of this study.

The key features in estimating the relative level of GIC damage that can occur were reported by Boteler and Pirjola [61]. They are power system characteristics, geomagnetic source fields, and Earth conductivity structure [61] work in an interconnected manner to produce the unique GICs that enter a conductor at a specific location. The fact that these features are important have been verified at different geographical locations such as in Ireland by Blake et al. [62], Italy by Tozzi [63] and Greece by Zois [18]. This shows that geomagnetic field data is key at the local level. It can also be reasoned from the fact that since each geographical location has a unique geomagnetic profile [61], [62], [18], [63],

that any index-based system for a specific place must take that place's geomagnetic data into account. Global indices can be used as an indicator to verify the level of activity in the sense of large coherent structures, but obstruct the local features [64]. Thus they are important in damage mitigation in the sense that their data can be used to interpolate models for verification that an event was in fact encountered.

In an effort to mitigate damage by looking at near real time monitoring, Stankov et al. [65] has presented a detection method, now in use at Dourbes, for alerting users to possible geomagnetic storms though the method has limitations such as overestimating low geomagnetic activity and requiring data sets that are 'clean' (complete without anomalies or date gaps). Assessing data from the historical record has been important in seeking to understand whether or not damage can occur and the relative level of damage which can occur. It has been estimated via extreme value analysis on magnetic field data of storm events spanning 41 years what the maximum magnetic disturbance levels could be for the 1 in 100 year and 1 in 200 year extrapolated extreme events by Lotz and Danskin [3]. It was also shown that long-term events where cumulative exposure to a moderate accumulation of magnetic field fluctuations took place could cause the same amount of damage as shorter, though much more pronounced events [3], by deriving a cumulative exposure index using the induced electric field data.

In another study by Winter et al. [66] a new method to model an electric field was set out based on the Carrington event (the largest observed geomagnetic storm, often used as a worse case scenario for planning for GICs), where it was calculated that electric field values of 10 volts per kilometre can be expected for the UK during an extreme event, thus capable of producing substantial GICs. An important study for Greece was carried out by Zois [18] who showed that the national power grid of Greece was not protected from GIC events (as had been previously assumed), using technician reports of transformer malfunction consistent with GIC transformer damage seen in Scandinavian countries. The paper also mentions that no direct GIC recording devices are used in Greece similar to those used in South Africa. This also serves to explain the lack of data available for direct GIC measurements. Direct GIC measurements do take place in South African infrastructure as will be shown in this study. These measurements are extremely important to check models and are not widely available due to their sensitive nature for each nation. Furthermore, such continuous direct recording devices are not currently in use in South Africa. This further shows the necessity of using geomagnetic data for index/proxy derivation since utilities are not often willing to release GIC and damage results to the wider scientific community.

Finally, more motivation for the use of geomagnetic data, in addition what has already been mentioned, can be seen in the use of the data from INTERMAGNET (see URL: <https://intermagnet.org/>) (an organisation which provides data from a global network of geomagnetic stations at different geographic latitudes) by Winter et al. [66] in creating a

model for the UK by making use of data from various stations at different latitudes. This data is more readily available, objective, accessible across the planet openly, is independently verified, accounts for the geographical location of each station on the planet, and spans stretches of time for which lengthy historical analyses may be carried out [67].

Other methods are those that use data from the affected infrastructure (such as power utilities) and seek to understand what happened during a geomagnetic storm.

Proxies for damage such as Dissolved Gas Analysis (DGA) can be used after the events to show when GIC activity caused damage, as is presented by Gaunt and Coetzee [60], who show that damage is of geographical relevance, and that equipping transformers with active DGA instruments can help understand damage conditions by allowing stakeholders to cross correlate the time of damage with geomagnetic activity data.

Furthermore, models are formulated and tested which show the simulation of GICs in power networks and transformers. This was done by Gaunt et al. [14] to find problem areas in actual transformers by simulating GICs flowing within them, as well as in coastal infrastructures by Boteler and Pirjola [61] who showed that an adjustment factor needs to be considered at coastlines when considering the damage GICs can cause.

2.11 Existent proxies and indices

This section will elucidate existent proxies and indices in more detail. Generally the distinctions of proxies fall into spatial and temporal categories. Temporally, the distinction may be drawn between near real-time tracking (within minutes to hours) or cumulatively (day(s)) while spatially, the distinction takes place either locally or globally with at least one combination of spatial-temporal fields combined to look at geomagnetic activity [68]. Furthermore, a cumulative index for damage may be used to look at possible accumulated damage as has been mentioned by Lotz and Danskin [3].

Indices derived from magnetometer data indicate geomagnetic storm activity and can thus act as proxies for possible GIC activity. Such indices include the disturbance storm time, or Dst (hourly and global type) [69] and symmetric disturbance in H-field indices, or SYM-H (at 1-minute cadence and global type), respectively [47]. Geomagnetic storms are classified by Gonzalez et al. [12] based on Dst values.

Recorded Dst observations from Kyoto University of large storms (1998-2012), as opposed to Kp (see description below), were used, because Dst has a better resolution and can accommodate extreme events. As shown by Cid [70], the global Dst (or other global indices) cannot be used to calculate large H-spikes by taking averages, due to the large asymmetry in H-records.

Kp or planetary K-index is a scaled global index which produces one value per 3 hours (8 values per day). This scaled index is represented by integer values between 0 and 9 (inclusive of both endpoints) in ascending order of activity. Kp, SYM-H, and Dst use data

from various magnetic observatories and provide global features of geomagnetic activity. In terms of Kp and Dst, it has been shown by Rostoker [71] that the choice of observatories chosen in deriving the indices is fundamental to their results in different degrees, as well as that they tend to exclusively reveal the “lower activity limit at any given time”.

The time variation of the magnetic field $\frac{d\mathbf{B}}{dt}$ is derived from the geomagnetic data at a specific station. Yu and Ridley [2] highlight the various uses of this variation by defining a threshold over which a storm may be defined, as well as a window of activity. The local K-index is one similar to the Kp index in terms of scale, yet it is station specific, which has to be taken into account when deriving this index. Of these methods, that of Takahashi et al. [72] was used in the Honours study [73] to derive an unbounded K-index for the Hermanus data in South Africa. Stankov et al. [65] present an algorithm for real time K-index calculation as part of a detection method that is now in use at Dourbes, Belgium for alerting users to possible geomagnetic storms.

The index used in this work is called e_h , is the one where the method uses 30 minute maximum values of geomagnetic data from the specific station under investigation, as defined by Wintoft et al. [1], and shown to work in strong agreement with the literature. Long-term indices, in an effort to indicate accumulated damage, are scant due to the difficulty of putting a single number to a cumulative event [3]. The motivation for them can be found by Tozzi [63], Marshall [74] and Zois [18]. An attempt made by Lotz and Danskin [3] using a “Cumulative Exposure Index”, is used to look at the long-term distribution of events.

In context of what has been described in this chapter, this study aims to create two indices, namely one that describes near real time tracking that is based on the work of Wintoft et al. [1], and a longer term index to indicate possible accumulated damage by GIC activity over the course of events. For both purposes, a list of about 20 events taken from the list studied by Lotz and Danskin [3] will be used. The short-term index will use data from INTERMAGNET for South Africa (Hermanus magnetometer data) and will be compared with multiple indices as well as with GIC measurements provided by a power utility from specific stations in South Africa in an effort to establish an efficient near real time tracking device. With regard to the second purpose, a cumulative index spanning the totality of geomagnetic storm events will be created using the short-term index itself, in an effort to determine the relative level of cumulative damage incurred by infrastructures in South Africa to inform stakeholders of the risk posed by GICs.

Chapter 3

Algorithms and data

This chapter outlines the algorithms for both the short and long-term indices used in this study.

3.1 Software Algorithm: Short term-index

The methods employed here use the mathematical tools built into the Python programming language. Version 3.6.3 was used with the libraries Pandas (used to sort data into a dataframe for ease of access), Scipy (used to calculate statistics such as Pearson R coefficient and confidence intervals of error), Numpy (used to carry out numerical calculations) and Matplotlib (used for plotting graphs), proving invaluable [75], [76].

The short-term index derived is similar to that of Wintoft et al. [1], where the paper aimed to model solar plasma (magnetic field) data into a predictive quantity to make an accurate comparison with ground electric field data. e_h used in this study differs from the definition of Wintoft et al. [1] in that it is the mean value of every 30 minute period, and not the maximum 30 minute period value.

The rate of change of the magnetic field ($\frac{d\mathbf{B}}{dt}$) scales well with the electric field data as can be seen from Faraday's law of induction (2.4). Cadences of \mathbf{B} equal to or greater than 1-minute are sufficient to show the dominant features of the time rate of change of the magnetic field [77]. It is also not sufficient for the estimation of GIC peak amplitudes to "predict the detailed variation of $\frac{d\mathbf{B}}{dt}$ at 1-minute resolution" [1]. Previously it was shown by Wintoft et al. [77] that the 10 minute root mean square of the rate of change of the horizontal magnetic field B_h (see equation (2.3)) was comparable to a proxy of noticeable utility. Also Trichtchenko and Boteler [68] showed that the geomagnetic data at 1-hour and 3-hour resolution times showed better results than data at 1-minute cadence when comparing rate of change of the magnetic field and measured GIC, indicating that general features of both data sets correlate better than at finer details with respect to time periods chosen for comparison. The use of a 30 minute window is also a good choice because the study by Wintoft et al. [1] (which used a 30-minute window with the maximum from each window) showed that though this metric does not predict the geoelectric field well, it is a

good proxy of the geoelectric field. Thus, the group behaviour at 30 minute cadence makes for relevant use of tracking/nowcasting trends in **B**-field behaviour [1]. This is the reason why the temporal filtering window of 30 minutes was used in the algorithm in this study. Another study conducted by Schrijver and Mitchell [78] validated the use of a 30 minute window. Weigel et al. express as an index the fluctuation amplitude D with 30 minute intervals (48 local values per day) in terms of a 30 minute block average over the period centered on the time of D [79]. The index used in this study differs in that it uses north-south as well as east-west components; it is also mentioned by Wintoft et al. that the average as it is used in this study will result in signal damping that will be more pronounced for sudden impulses (SI) [1]. SI are phenomena that present with unique geomagnetic morphology due to global variations in the geomagnetic field [80]. The key motivations for the use of the 30-minute window are: (1) that it is efficient to compare general behaviour of **B**-field variation in terms of features over higher cadence, rather than specific variation in behaviour at 1 minute cadence, and (2) that the method has been verified [1], [78], [68], [77].

The equation (3.1) to get the index:

$$e_h(k) = \frac{1}{30} \sum_{n=30(k-1)+1}^{30(k-1)+30} \sqrt{\left(\frac{dB_x(n)}{dt}\right)^2 + \left(\frac{dB_y(n)}{dt}\right)^2} \quad (3.1)$$

where k indexes e_h data values at time $t_k = 30*k$ minutes, $\frac{dB_x(n)}{dt}$ and $\frac{dB_y(n)}{dt}$ are the rates of change of the **B**-field components B_x and B_y at time $t_n = n$ minutes since the beginning of the storm. This equation is a special case of the index when it has not been scaled, namely 30-minute averages of $\left|\frac{dB_h}{dt}\right|$.

Figure 3.1 shows the SYM-H data plotted pertaining to an CME-event [13] which took place from 2011-09-26 to 2011-09-27 so that it can be placed in context of other events, since SYM-H provides a universal way of interpreting geomagnetic storms. Thereafter, the algorithm is presented with the aid of relevant graphs in Figures 3.2-3.3 and is developed here using storm 3 from Table 4.1 (likewise for the SYM-H graph):

SYM-H against time.

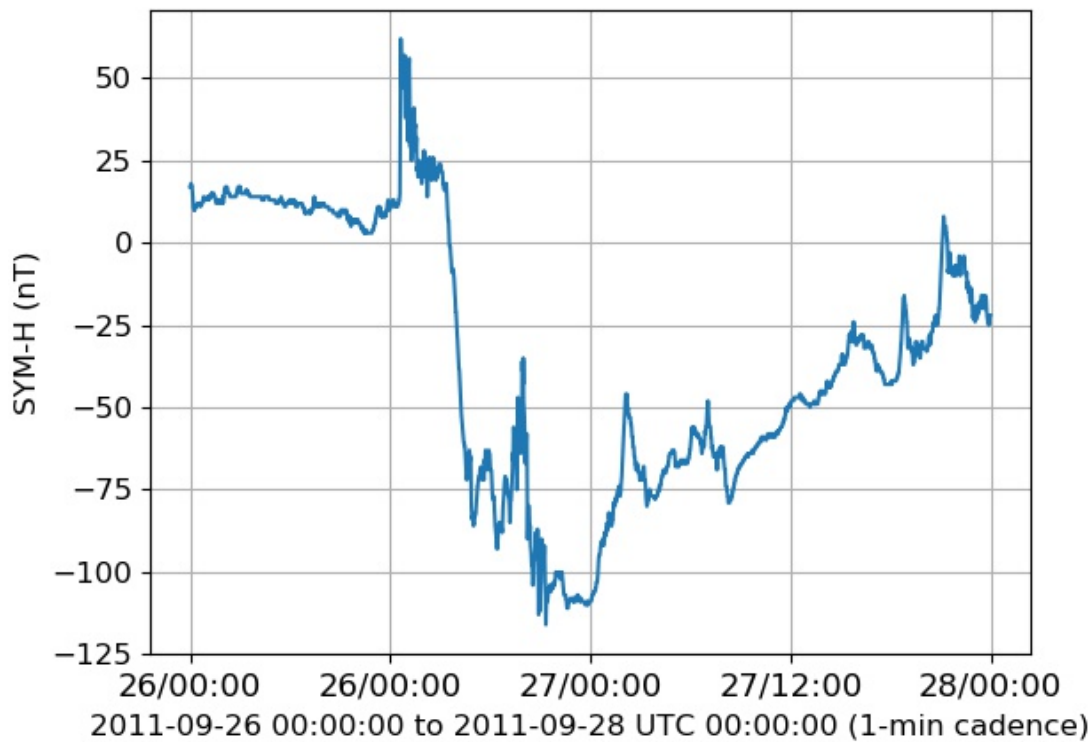


Figure 3.1: SYM-H data for the storm spanning 2011-09-26 to 2011-09-27. Note the noticeable drop to below -100 nT, indicating an intense geomagnetic storm [12].

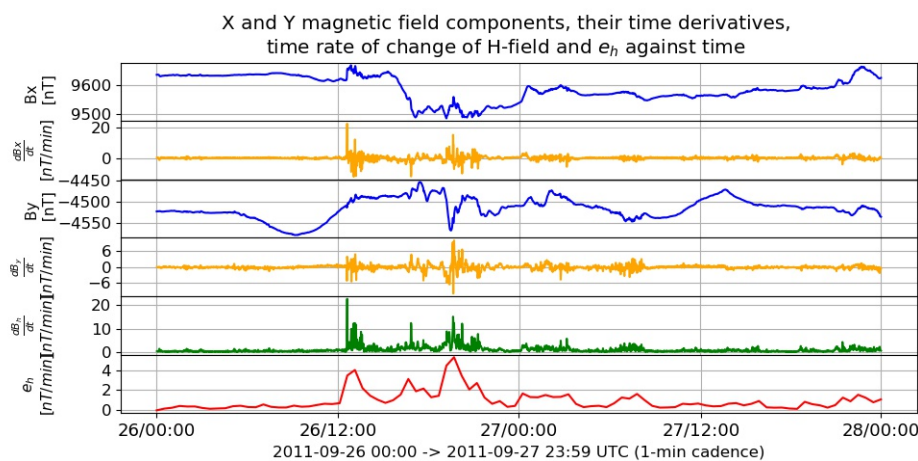


Figure 3.2: From top panel: X-component of the magnetic field B_x (blue), time rate of change of X-component of magnetic field $\frac{dB_x}{dt}$ (orange), Y-component of magnetic field B_y (blue), time rate of change of Y-component of magnetic field $\frac{dB_y}{dt}$ (orange), time rate of change of H-field $\left| \frac{dB_h}{dt} \right|$ (green), and e_h (red) using the Hermanus station magnetometer data for the storm spanning 2011-09-26 to 2011-09-27.

1. The X and Y component values B_x and B_y respectively of the magnetic field per event are separated (see blue graphs in 1st and 3rd panels from top in Figure 3.2 respectively).
2. The difference between consecutive values of B_x and B_y are computed yielding the quantities $\frac{dB_x}{dt}$ and $\frac{dB_y}{dt}$ respectively (see orange graphs in 2nd and 4th panels from top in Figure 3.2 respectively). This causes Python to recognise the first value of the data set as not being a number. To treat this, this study replaces this value with a zero. This is also done when comparing e_h with $\left|\frac{dB_x}{dt}\right|$ and $\left|\frac{dB_y}{dt}\right|$ i.e., the first value of the latter two quantities is replaced by a zero. A further explanation is given in step 4.
3. The square of the sum of the rate of change of B_x and B_y gives (see green graph in 5th panel from top in Figure 3.2 respectively):

$$\left|\frac{dB_h}{dt}\right| = \sqrt{\left(\frac{dB_x}{dt}\right)^2 + \left(\frac{dB_y}{dt}\right)^2} \quad (3.2)$$

4. A mean over a period of 30 minutes is then taken for all the values. This is e_h used in this project with a scale factor of $a = 1$ [1] which is shown for each 30 minute interval in Equation 3.1. In the case of missing data, the next value in the data which is not problematic is used to calculate the means as missing data is deleted. Deleting values results in averages being taken with non-consecutive values i.e. a longer average time increments than is necessary. If interpolation is performed over those values, this could result in underestimation of real storm behaviour over those data gaps. These are methods to handle date gaps in an attempt to account for missing real world data. It may also be possible to take averages for the exact amount of consecutive data involved, for example if in a 30 minute interval, there were only j values, then take a j minute average over existent values, and create a graph that is discontinuous yet realistic but can be compared at the exact same intervals with other available indices such as K, K_p and SYM-H. This would be problematic in a study that required 30 minute means. Although these are 3 possible ways the algorithm may be handled, it was not necessary to implement any of them as data in this study had no missing gaps. Note that the first e_h value is taken as zero i.e. the previous day is not used to calculate the first value of e_h . This does not present with a problem as the previous days are not storm days.
5. e_h is then ready to use for comparison with indices such as K, K_p and SYM-H as well as to calculate statistically relevant quantities such as the maximum and percentiles.

3.2 Software Algorithm: Cumulative index

The cumulative index equation (3.3) is presented as follows:

$$C = \sum_{j=1}^m e_h(t_j) \quad (3.3)$$

where each t_j is an instance for which $e_h(t_j)$ i.e. the instantaneous e_h value at t_j is greater than the threshold of 0.5 nT/min on the y -axis. Note that each $e_h(t_j)$ is not necessarily consecutive as the condition of crossing the threshold needs to be met i.e. the index values can only be consecutive for intervals when the threshold is exceeded in that intervals. C is thus the discrete sum used as an approximation of the integral of the e_h function over a certain interval. Consider Figure 3.3 below as a generic example. Clearly there is a single threshold (denoted by the red line). Assume this threshold is 1 nT/min (chosen for clarity of representation and to illustrate the method). The process of choosing a specific threshold will be discussed later. Whenever e_h intersects the threshold, increases to a peak, and then decreases back down to the threshold, the sum is performed for each timestamp over this interval or if necessary at discrete points that exceed the threshold. The total sums over each interval for a single event are added and this gives C . This method of threshold selection is similar to one used by Yu and Ridley [2] who compared geomagnetic field perturbations to $\left| \frac{dB_h}{dt} \right|$, which recorded events based on $\left| \frac{dB_h}{dt} \right|$ exceeding 0.5 nT/s [2]. This study uses 30 minute means for e_h , which is itself used for C , namely when e_h exceeds 0.5 nT/min. Thus the cumulative index differs from Wintoft et al. [1] in that they do not create a long-term index based on threshold selection. It also differs from Yu and Ridley [2] who selected a threshold but did not derive a cumulative index. The method is similar to Lotz and Danskin in that it uses a time discrete sum but differs in that it uses magnetometer data instead of the induced electric field data [3].

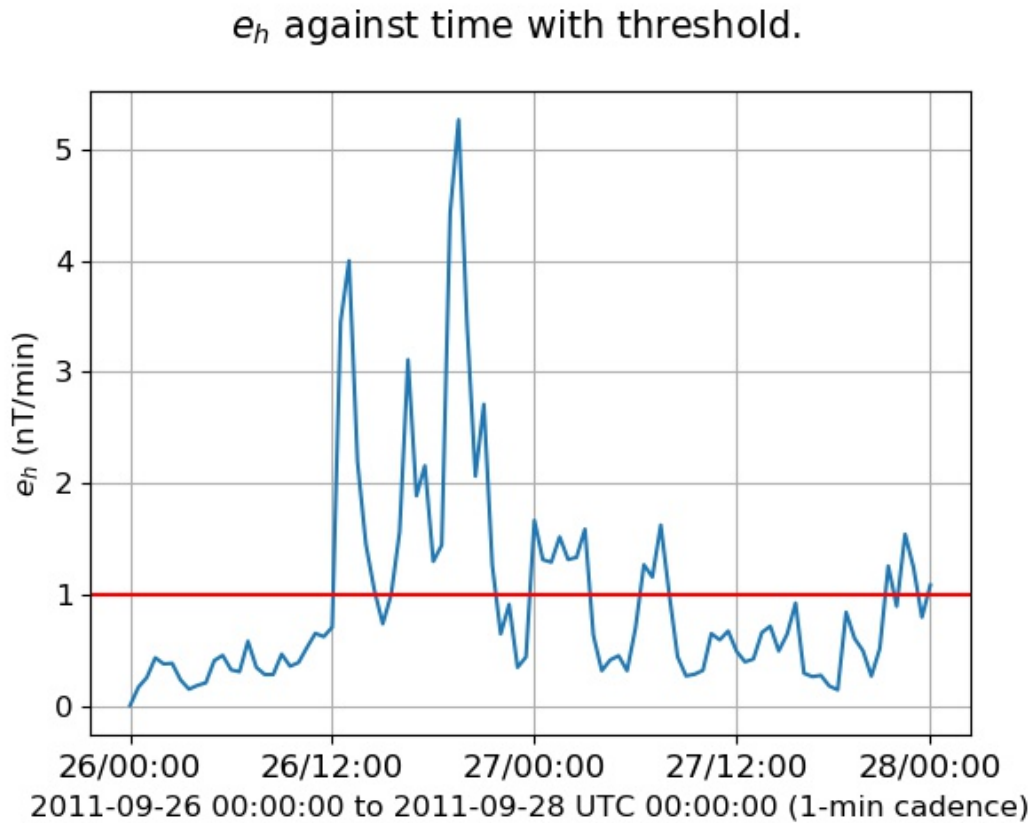


Figure 3.3: e_h calculated from geomagnetic data recorded at the Hermanus station for the storm spanning 2011-09-26 to 2011-09-27. The red line denotes the fixed threshold magnetic value (chosen as 1 nT/min on the y-axis for clarity here), which, whenever crossed the values of e_h are added together to calculate an index showing cumulative damage post an event.

The method to calculate the cumulative index is as follows:

1. The events in this work were selected from an event data set used by Lotz and Danskin [3], in accordance with available data. The criteria for the start of a geomagnetically intense event (commencement of the active period) is the instance before SYM-H falls -50 nT when SYM-H is larger than -20 nT [12].
2. The threshold(s) is (are) fixed as 0.5 nT/min on the y-axis, similar to a method used by Yu and Ridley [2]. This was verified by comparison of the calculated e_h data with the K-index for quiet times (see chapter 4). Abnormal behaviour is said to be occurring at specific points or for each set of values contained in intervals (there can be many intervals or points for each event) at (in the case of points) or over (in the case of intervals) which the threshold is crossed respectively. The threshold is demarcated (and chosen as 1 nT/min units for graphical clarity) by a red horizontal line on Figure 3.3.
3. Values of the graph above the threshold are isolated from the data set.
4. Using the values which exceed the threshold, a sum is performed. To account for false warnings, a quiet event of days was assessed and compared to a storm. These results with

the full justification will be shown in the next chapter (see section 4.5.1).

3.3 Horizontal magnetic field data

This was obtained from the INTERMAGNET website. The data for calculating e_h as well as the rate of change in the magnetic field in this study is based on the horizontal magnetic field data namely the X and Y components of the magnetic field. This data is the best available of its kind (minimal gaps in data sets, curated and vetted for) and is recorded every minute in nanoteslas and is available in yearly files, where the years that were analysed spanned 2011-2016. These years incorporated events in a paper used by Lotz and Danskin who derived a cumulative exposure index using a discrete time sum of the absolute induced electric field magnitude values with relevance to the South African context (middle geomagnetic latitude) to perform an extreme value analysis [3]. The data is measured using magnetometers.

3.4 Indices data

The Hermanus K-index (local index) data was provided by SANSA Space Science. This index is calculated based on measurements of the horizontal (H) component of the geomagnetic field at the Hermanus geomagnetic observatory and is then scaled (unit free) on a logarithmic scale to values between and including 0 and 9, in rank of ascending strength. The K-index is derived using ΔH (northward) and ΔD (eastward) variations, which remain after the removal of secular and diurnal variations [72], [13]. This data is then presented every three hours (from GMT midnight for each day) by following a standardised algorithm that is dependent on the geographical location of a magnetometer station [13].

The Kp-index (global index) data was downloaded from the recognised authority's website in Kyoto, Japan (See <http://wdc.kugi.kyoto-u.ac.jp/>). This data is calculated based on the global reaction to changes in the Earth's magnetic field, incorporating a global network of active magnetometer data stations, and is then scaled (unit free) to values between and including 0 and 9, in rank of ascending strength, similar to the aforementioned K-index data [72].

The final index used for comparison was the SYM-H-index (global index), with data downloaded from the recognised authority's website in Kyoto, Japan. This data is calculated based on the secular variation of the geomagnetic field and has a temporal resolution of 1 minute, recorded in nanoteslas [81].

3.5 Measured GIC data

For measured GIC, three events were compared due to the limited nature of access to such data.

The first event was compared with GIC data from the Grassridge station for the ‘Halloween’ storm event of 29-31 October 2003.

This current is recorded every 2 s (seconds) in A (amperes).

The second and third events were compared with GIC data from the Matimba station with one event in 2013 and the other in 2015 respectively.

The GIC data recorded at the Matimba power station is given in terms of the mean, maximum and minimum determined over non-overlapping 5 minutes periods. This GIC data is compared with the 1 minute geomagnetic data that is used in this study.

Chapter 4

Analysis of results and discussion

In this chapter, the rate of change of the magnetic field component magnitudes, namely $\left|\frac{dB_x}{dt}\right|$, $\left|\frac{dB_y}{dt}\right|$, the Hermanus K-index, SYM-H index and Global Kp index will be compared with e_h for 21 storms.

Subsequently, comparisons will be carried out of e_h with GIC for a reduced set of 3 storms for which measured GIC data was available. Thereafter, results of the cumulative index will be presented and discussed.

4.1 Methodology

The 21 storms were selected from the list of 285 storms used by the authors Lotz and Danskin in their paper [3]. The list of storms is given in Table 4.1 below with a † designating the events for which measured GIC data was available:

Table 4.1: Storm start and end dates.

Storm	Start date	End date
1.	2003-10-29	2003-10-31 †
2.	2011-08-05	2011-08-09
3.	2011-09-26	2011-09-27
4.	2011-10-24	2011-10-28
5.	2012-04-23	2012-04-26
6.	2012-07-14	2012-07-18
7.	2012-09-29	2012-10-02
8.	2012-10-07	2012-10-09
9.	2012-10-12	2012-10-15
10.	2012-11-12	2012-11-16
11.	2013-03-17	2013-03-20 †
12.	2013-06-28	2013-06-30
13.	2014-02-18	2014-02-22
14.	2014-02-27	2014-03-01
15.	2015-03-17	2015-03-23 †
16.	2015-06-22	2015-06-25
17.	2015-08-25	2015-08-29
18.	2015-09-08	2015-09-10
19.	2015-10-06	2015-10-09
20.	2015-11-06	2015-11-10
21.	2015-12-19	2015-12-22

The GIC (2 second cadence) data for the first case (storm 1) comes from the Grassridge power station in Eastern Cape province, South Africa (see map below). This event took place in 2003 and is known as the ‘Halloween’ storm of 2003.

The GIC (5 minute cadence) data in the latter two cases (storms 11 and 15 respectively) comes from the Matimba power station in Limpopo province, South Africa (see map below) with the events occurring in 2013 and 2015 respectively.

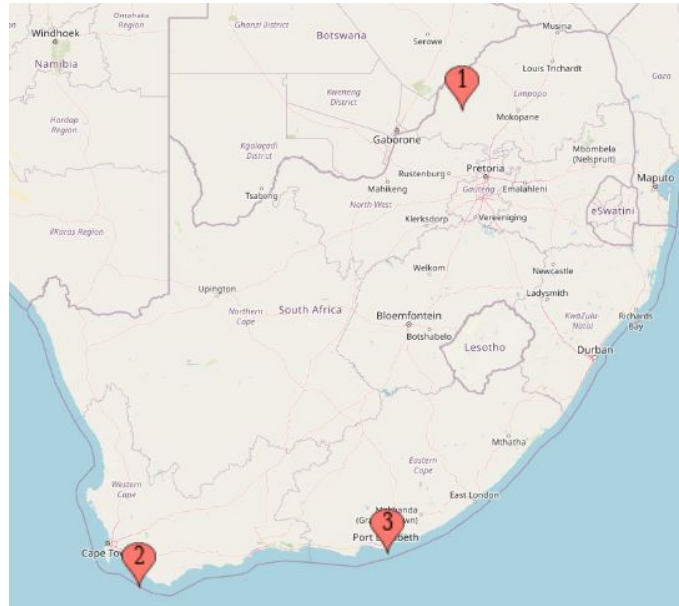


Figure 4.1: Map indicating locations of: 1. Matimba power station, 2. SANSA Space Science and 3. the Grassridge power station within South Africa. It can be seen that the locations of 2 and 3 are coastal while that of 1 is inland. Map data 2021 AfriGIS Pty Ltd.

4.2 Correlation: Indices

For the list of storms in Table 4.1, correlations (Pearson R coefficient) between the e_h and $\left| \frac{dB_x}{dt} \right|$, $\left| \frac{dB_y}{dt} \right|$ as well as indices (K, Kp and SYM-H) are tabulated below. The relationship between two variables (specifically signals in these cases such as (K, Kp) and e_h) which are of differing scales is best measured by the Pearson R coefficient. Due to the mismatch in cadence, (K,Kp) values are repeated to 30-minute intervals to match the cadence of e_h . The Pearson R coefficient is a unitless measure of how well two sets of data vary in the same direction with correlations close to 1 indicating that their variation is in the same direction, correlations close to zero indicating that the variables do not relate in their variation, and correlations close to -1 indicating that variables anti-correlate. This correlation coefficient has an associated probability (p-value) between 0 and 1, indicating how well the variables correlate. A low p-value is generally a very good indicator of the data's behaviour not being based on random influence, given a null hypothesis stating that the data behaves in a certain way is assumed to be true [82].

For each storm the correlation (Pearson's R) between variables (e_h and other indices) was calculated to measure the linear correlation between the parameters. Correlation is a trusted measure of linear co-variance.

The numbering in Table (4.2) will be the same as that of Table (4.1) above with the labels K, Kp, $\left| \frac{dB_x}{dt} \right|$, $\left| \frac{dB_y}{dt} \right|$ and SYM-H denoting the correlations between e_h and those indices respectively.

Table 4.2: Correlations between e_h with local and global indices done by bringing the indices to the 30 minute cadence of e_h . Here ‘Storm Number’ indicates the same event number as in Table 4.1 above, ‘Duration’ the days for which the event took place over, ‘Storm Duration’ the time for which SYM-H storm activity took place using the classification system of [12] (where a geomagnetic storm is defined using a time-interval in minutes not based on the total number of integer days), K the Hermanus K-index, Kp the planetary K-index, $\left|\frac{dB_x}{dt}\right|$, $\left|\frac{dB_y}{dt}\right|$ and SYM-H the global symmetric H-index.

Storm Number	Duration (days)	Storm Duration (minutes)	K [-]	Kp [-]	$\left \frac{dB_x}{dt}\right $ [-]	$\left \frac{dB_y}{dt}\right $ [-]	SYM-H [-]
1.	3	3203	0.65	0.65	0.96	0.85	0.79
2.	5	896	0.72	0.76	0.98	0.95	0.80
3.	2	960	0.65	0.59	0.97	0.91	0.89
4.	5	812	0.78	0.78	0.97	0.91	0.90
5.	4	1700	0.62	0.64	0.89	0.92	0.52
6.	5	1884	0.77	0.78	0.94	0.95	0.73
7.	4	636	0.71	0.73	0.94	0.88	0.69
8.	3	861	0.71	0.75	0.96	0.93	0.74
9.	4	1116	0.53	0.57	0.95	0.881	0.66
10.	5	924	0.63	0.66	0.95	0.89	0.88
11.	4	1166	0.72	0.76	0.97	0.96	0.83
12.	3	1080	0.51	0.54	0.90	0.90	0.57
13.	5	1300	0.72	0.74	0.93	0.88	0.82
14.	3	536	0.76	0.74	0.97	0.94	0.87
15.	7	2999	0.67	0.69	0.96	0.96	0.65
16.	4	1700	0.70	0.67	0.97	0.96	0.58
17.	5	1820	0.57	0.54	0.95	0.95	0.43
18.	3	1208	0.59	0.63	0.89	0.94	0.40
19.	4	1981	0.53	0.55	0.91	0.94	0.50
20.	5	1717	0.60	0.63	0.91	0.91	0.55
21.	4	1470	0.70	0.70	0.93	0.85	0.53

Note that from Storm 15 to Storm 21 of Table 4.2 have an extra zero placed in the beginning of the e_h array to match the size of the K and Kp arrays which results in a loss in correlation but maintains the correct amount of K and Kp data points interpolated correctly. e_h has a positive correlation upwards from 0.5 to about 0.8 with both K and Kp which is a good result as it shows that e_h has a positive correlation, with reliable indices that are both local and global [72].

It can be seen from the Table 4.2 that e_h correlates really well with $\left|\frac{dB_x}{dt}\right|$ and $\left|\frac{dB_y}{dt}\right|$ which is a good result as these are relevant to GICs [21]. This is also the case with H whose deviations are used to make the K-index [13]. It should also be noted that the list of events is not large, and more data will be needed to establish a clear relationship between $\left(\left|\frac{dB_x}{dt}\right|, \left|\frac{dB_y}{dt}\right|\right)$ and e_h .

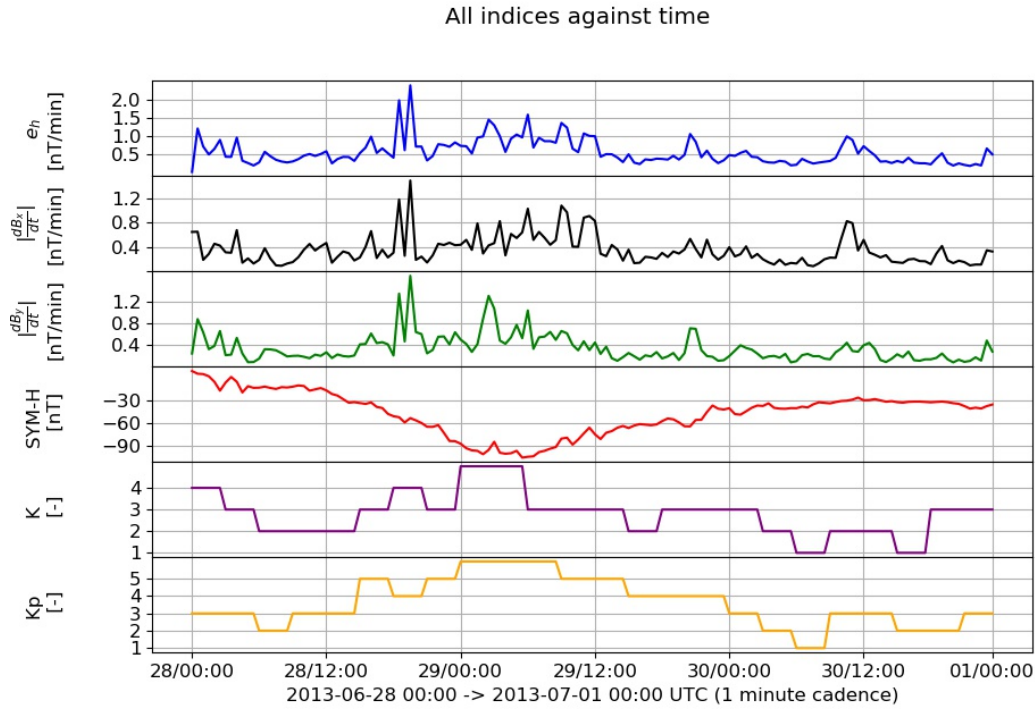


Figure 4.2: e_h (blue) $\left|\frac{dB_x}{dt}\right|$ (black), $\left|\frac{dB_y}{dt}\right|$ (green), SYM-H (red), Hermanus K-index (purple) and Kp (orange) against storm duration for the event dating from 2013-06-28 to 2013-06-30.

Figure 4.2 shows that the SYM-H index is slightly anti-correlated with e_h (their peaks do not line up and as e_h rises, SYM-H falls and vice versa). SYM-H is a global index which is susceptible to losing local features and is not available in near-real time as it requires global collaboration from various stations. While in contrast, e_h can be computed in near real time without the need of global data as it can be computed at a single station as well. Thus, SYM-H seems to be good enough for tracking generalised behaviour and for the identification of the onset, main, and recovery phases of storms generally, but the trade-off incurred is a loss in finer details.

4.3 Correlation of e_h with the Hermanus K-index vs. Storm Duration

Figure 4.3 shows a plot of interpolated correlation coefficient vs. duration of storm for the Hermanus K-index values that have been correlated with e_h . Figure 4.4 shows a typical plot of e_h and interpolated Hermanus K-index values against time for the storm 2011-09-26 to 2011-09-27 (see Table 4.2). This was done to show that duration of an event does not play an important role in the good correlation between e_h and K. e_h tends to have

a correlation with the Hermanus K-index values of about 0.65 regardless of the duration. If there were a duration dependence it would have presented a problem since storms do damage regardless of whether they have short duration or long duration [3].

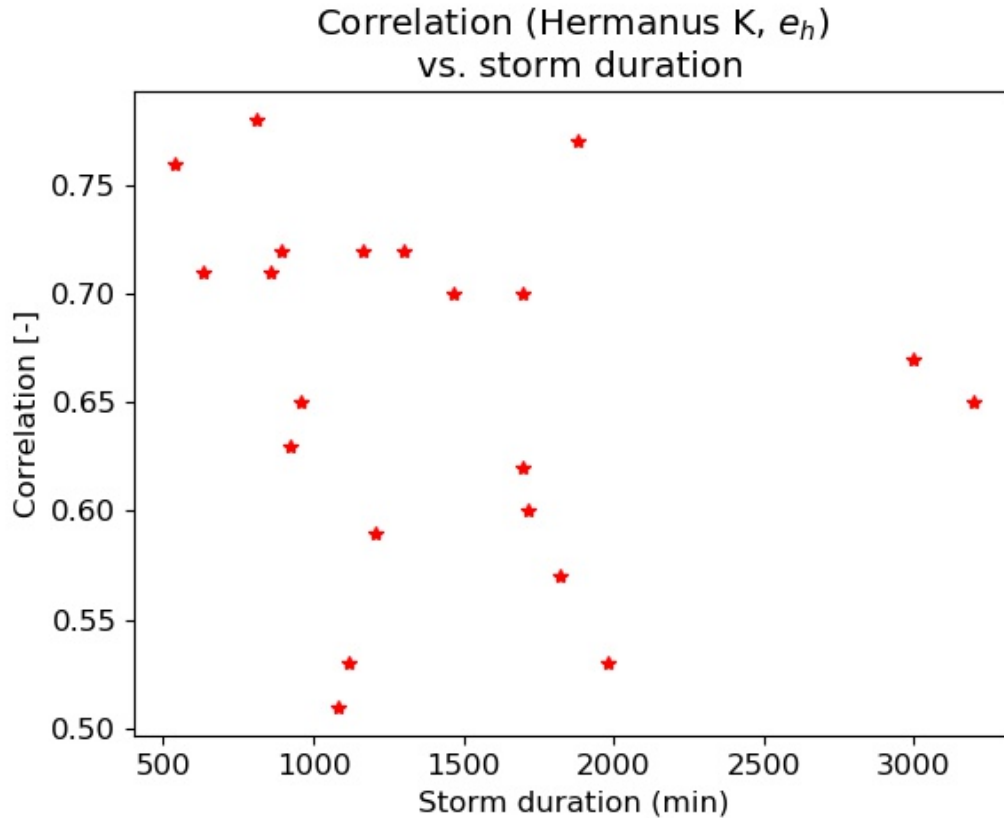


Figure 4.3: Correlation between interpolated the Hermanus K-index data and e_h vs. storm duration in minutes. The correlation between K-index and e_h was performed for the duration of each storm using SYM-H classification for storm duration [12].

The range of the correlation values was 0.27, with a roughly even split of storms above and below the median correlation of 0.67. The amount of time that storm activity is found to be above a selected threshold within a given event is defined as the Active time and will be seen to play a key role later on. The relationship between e_h and the Hermanus K-index against storm duration is not expected to correlate well as both indices are of varying time frames and the K-index data has to be interpolated from 8 values per day to 48 values per day to have a comparison with e_h . Furthermore, during the time period of a storm, K-index data is estimated to show the general trend of a storm and not its precise local behaviour [1], [78]. This was verified when it was found that the correlation between storm duration and Correlation (e_h , Hermanus-K) was found to be -0.1 with a p-value of 0.65, indicating that there is no clear correlation between storm duration and agreement between the two indices. It must also be noted that the number of days over which storm activity takes place is only a rough time indicator. The actual time of the storm taking

place is what is relevant. This is explained further when considering how the data behaves generally in Figure 4.4 below.

Figure 4.4 shows a typical plot of an interpolated index (Hermanus K-index in this case) with e_h .

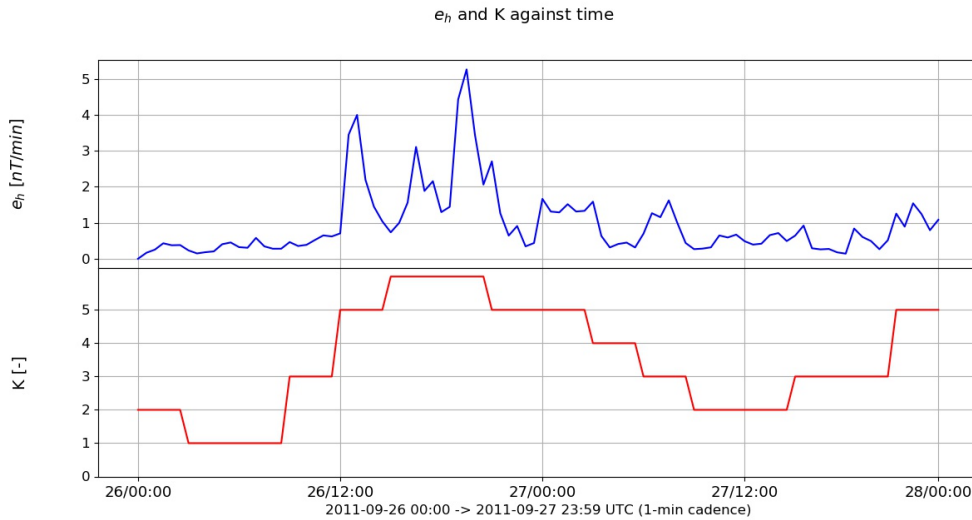


Figure 4.4: e_h and Hermanus K-index vs. time for the event dated 2011-09-26 to 2011-09-27. Observe how the K-index outlines general features of e_h yet lacks the resolution for finer details.

It was observed that the e_h and K-index indicate that storm activity is taking place although their general behaviour does not always coincide. Due to such low resolution of the K and Kp indices, the interpolations yielded low or constant values for periods of 3 hours, where some peaks were not in perfect alignment with e_h . This is attributed to the domination by large coherent structures in the magnetic field by the Kp-index as opposed to e_h which focuses on local station behaviour.

A loss in resolution is the down-side of using decimation to 30 minute cadence of $\left|\frac{dB_x}{dt}\right|$ and $\left|\frac{dB_y}{dt}\right|$ for comparison of e_h with $\left|\frac{dB_x}{dt}\right|$ and $\left|\frac{dB_y}{dt}\right|$. Note that in this study, every index has been brought to the cadence of e_h for comparison, namely SYM-H, $\left|\frac{dB_x}{dt}\right|$ and $\left|\frac{dB_y}{dt}\right|$ have been decimated from 1-minute cadence to 30-minute cadence and K and Kp have been interpolated from 3-hour cadence to 30-minute cadence.

4.4 Correlation: Measured GIC

The GIC data that was available was limited due to power utilities not making such data readily available. The GIC data is recorded in A (amperes) (quasi-direct current) with the

average being captured in files at cadences of either 5 minutes or 10 seconds. The graphs (see Figures 4.5, 4.6 and 4.7) showing SYM-H, the Hermanus K-index and the measured GIC for three events will be discussed first and then a comparison will be made with e_h and the results explained. Note that timestamps are indicative of the data provided i.e. taken from and to the times as they appear in the data files for the GIC data.

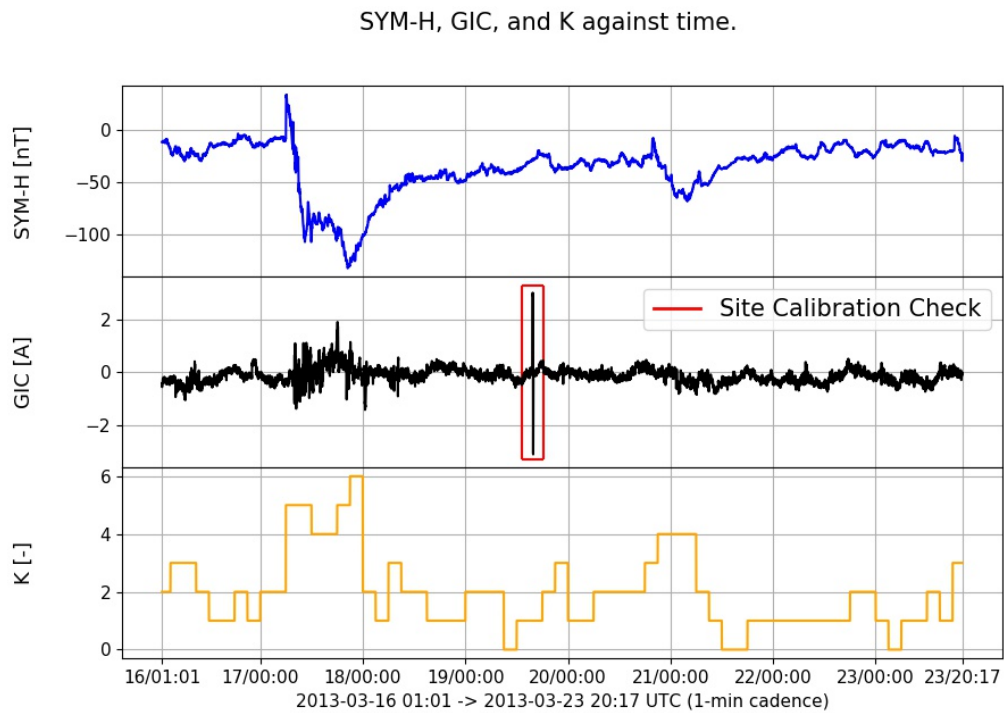


Figure 4.5: SYM-H (blue), measured GIC (black) and Hermanus K-index (orange) vs. time for a measured GIC event during the period 16 to 23 March 2013. The GIC was measured at the Matimba power station. The red box represents a 10 minute period during which there was a site calibration check (this was provided in the data).

SYM-H, GIC, and K against time.

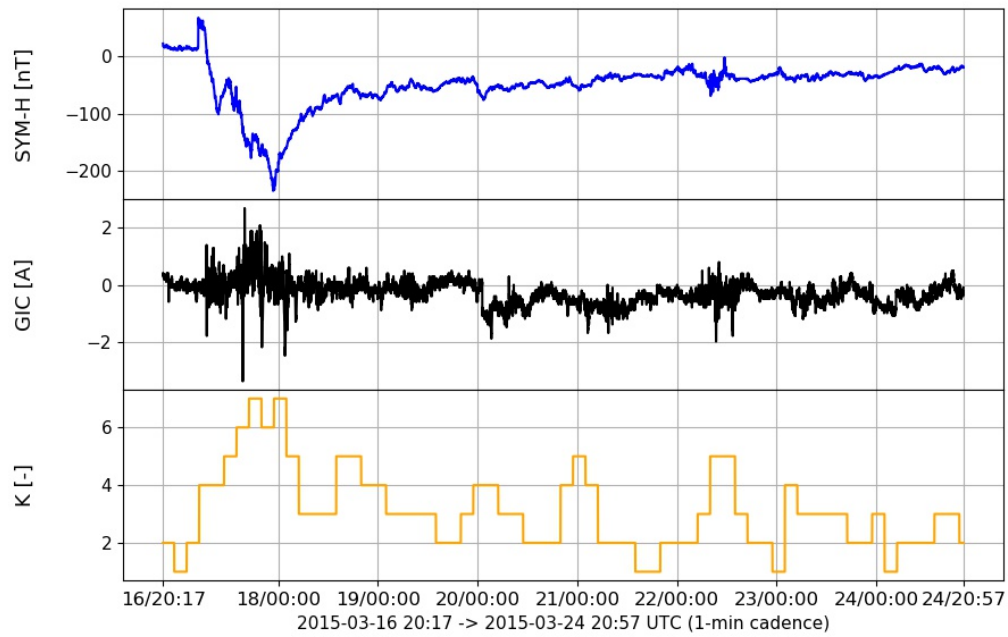


Figure 4.6: SYM-H (blue), measured GIC (black) and Hermanus K-index (orange) vs. time for a measured GIC event during the period 16 to 24 March 2015. The GIC was measured at the Matimba power station.

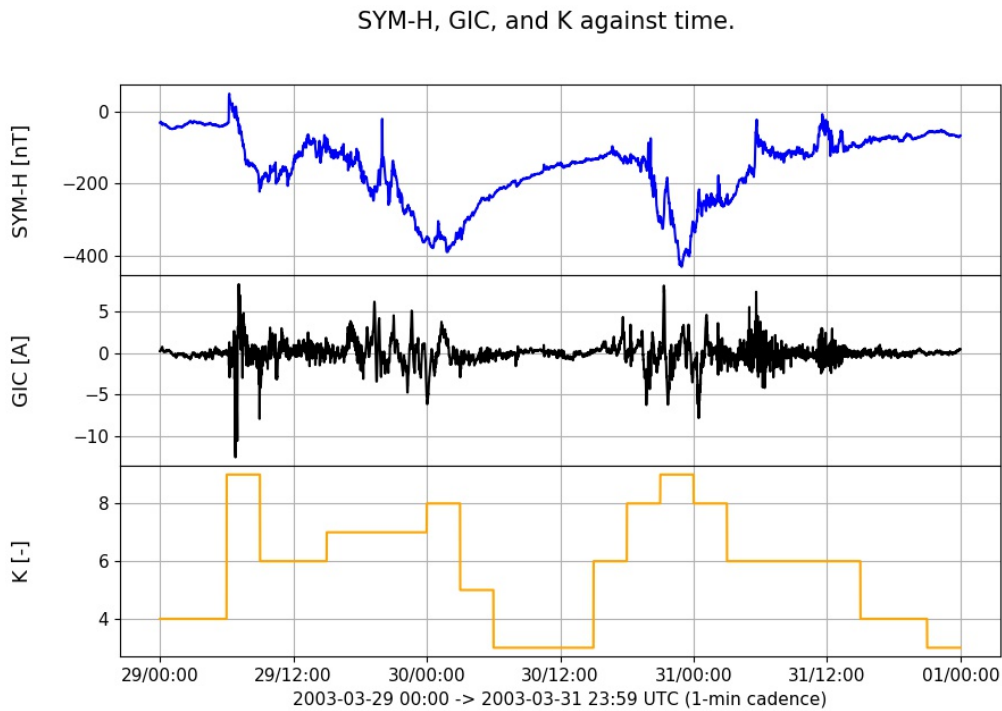


Figure 4.7: SYM-H (blue), measured GIC (black) and Hermanus K-index (orange) vs. time for a measured GIC event during the period 29 to 31 October 2003 (Halloween storm). The GIC was measured at the Grassridge power station.

Figures 4.5, 4.6 and 4.7 show SYM-H, the measured GIC and the Hermanus K-index plotted against universal time. The K-index cannot give enough information as it only has 8 values per day when compared to SYM-H and measured GIC data which are measured in minutes and seconds respectively. Thus interpolation of K-index to 30-minute cadence had to take place. Figures 4.5 and 4.6 (events in 2013 and 2015 respectively) show GIC data from the Matimba power station while Figure 4.7 shows GIC data from the Grassridge power station (2003 Halloween storm). The GIC data from the 2003 storm is quite important as it is the largest geomagnetic storm in recent history [52].

The SYM-H data correlates better with measured GIC but since it is a global index it misses key features of the GIC. The K-index, though local, catches the main phases of the storm well but misses finer details of the GIC variation.

Table 4.3 shows the correlations between the indices ($|\frac{dB_x}{dt}|$ and $|\frac{dB_y}{dt}|$, Hermanus K-index, and e_h) and measured GIC. It is important to mention that GIC is not equally sensitive to the x and y components of the electric field since the induced electric field drives current only in lines that run parallel to the electric field vector [14]. Note that the quantities are converted first to magnitudes, interpolated (or decimated in the case of K) to 30-minute cadence, then correlated. In the case of finding the correlation of the 2013 storm in Table 4.3, the 10 minute site calibration check shown in Figure 4.5 has been

removed and replaced by a window of 10 minute mean behaviour from the data after the calibration check.

Table 4.3: Correlations of the indices $\left|\frac{dB_x}{dt}\right|$, $\left|\frac{dB_y}{dt}\right|$, K and e_h against the magnitude of measured GIC. Here the first and second columns indicate the start and stop dates for an event recorded, and the third, fourth, fifth and sixth columns give the correlation of the magnitude of GIC data with the X-component of the rate of change of the magnetic field magnitude, Y-component of the rate of change of the magnetic field magnitude, the Hermanus K-index, and e_h respectively.

Start date	End date	$\left \frac{dB_x}{dt}\right $	$\left \frac{dB_y}{dt}\right $	K	e_h
2015-03-17	2015-03-23	0.36	0.38	0.17	0.38
2013-03-16	2013-03-24	0.31	0.24	0.24	0.28
2003-10-29	2003-10-31	0.59	0.87	0.01	0.74

For $\left|\frac{dB_x}{dt}\right|$ and $\left|\frac{dB_y}{dt}\right|$, it can be seen that the correlations with the GIC magnitude indicate a weaker positive correlation in all but one case when it is 0.87. Note that comparison is taking place between a quantity measured with 10-second cadence averaged to a cadence of 1 minute (the measured GIC magnitude), as well as quantities $\left|\frac{dB_x}{dt}\right|$ and $\left|\frac{dB_y}{dt}\right|$ derived from the \mathbf{B} -field which is measured with a cadence of 1-min as well as with e_h which is at a 30-minute cadence. For K-index data, weak positive correlations can be seen, even in the case of a strong event such as the ‘Halloween’ storm seen in the third row of Table 4.3. The timescale of the K-index requires interpolation for comparison with the GIC magnitude since the K-index is calculated at 3 hour intervals. Thus, the correlation of the K-index with the measured GIC magnitude is not as strong as the correlation between $\left|\frac{dB_x}{dt}\right|$, $\left|\frac{dB_y}{dt}\right|$, e_h and the measured GIC magnitude.

e_h correlation values with the measured GIC magnitude are close to the mean of the correlation values of $\left|\frac{dB_x}{dt}\right|$ with the GIC magnitude and $\left|\frac{dB_y}{dt}\right|$ with the GIC magnitude. e_h will have both the variations of $\frac{dB_x}{dt}$ and $\frac{dB_y}{dt}$ since it is composed of these indices.

Since e_h has a cadence of 30 minutes (and uses data from the preceding 30 minutes for its derivation), which is a cadence between the cadence of 1-minute (in the case of both $\left|\frac{dB_x}{dt}\right|$ and $\left|\frac{dB_y}{dt}\right|$) and 3 hours (in the case of K), it appears that this could be a possible reason for the correlation observed between e_h and the GIC magnitude when taken relative to the correlations between the GIC magnitude with $\left|\frac{dB_x}{dt}\right|$ and $\left|\frac{dB_y}{dt}\right|$.

The cadence of e_h is between the smaller cadence of $\left|\frac{dB_x}{dt}\right|$ and $\left|\frac{dB_y}{dt}\right|$ and the coarser cadence of K, and thus acquires aspects of both the rapid variations in the magnetic field during the storm and the slow variations tracked by the $\left|\frac{dB_x}{dt}\right|$, $\left|\frac{dB_y}{dt}\right|$ and K-indices respectively.

This seems to indicate an affirmation of the methodology carried out by Wintoft et al. [1], [77] as well as Schrijver and Mitchell [78] in that the general variation of storms with respect to \mathbf{B} -field at 30-minute cadence is easier to observe and more efficient than at 1-minute

cadence. It is also worth mentioning that the results agree with the general behaviour of indices that have 3-hour cadence such as K and Kp, and while there may be gaps in data recorded with a 1-minute cadence, the use of a 30-minute window will resolve these issues by monitoring the general features even in the presence of some gaps in the 1-min data from which it is derived. The physical significance of using a 30-minute window is that an efficient proxy can be developed to measure geoelectric fields and that a real-time forecast system can be implemented, as has been done by Wintoft et al. [1]. Of further physical significance, Schrijver and Mitchell found that a 30-minute window (\mathbf{B} -field) was statistically significant in determining the “impact of the exposure” to the US power grid [78]. Thus it may be said that the use of a 30-minute window is justifiable.

4.4.1 e_h vs. measured GIC

Figure 4.8 shows e_h plotted with other indices from Table 4.2 against time.

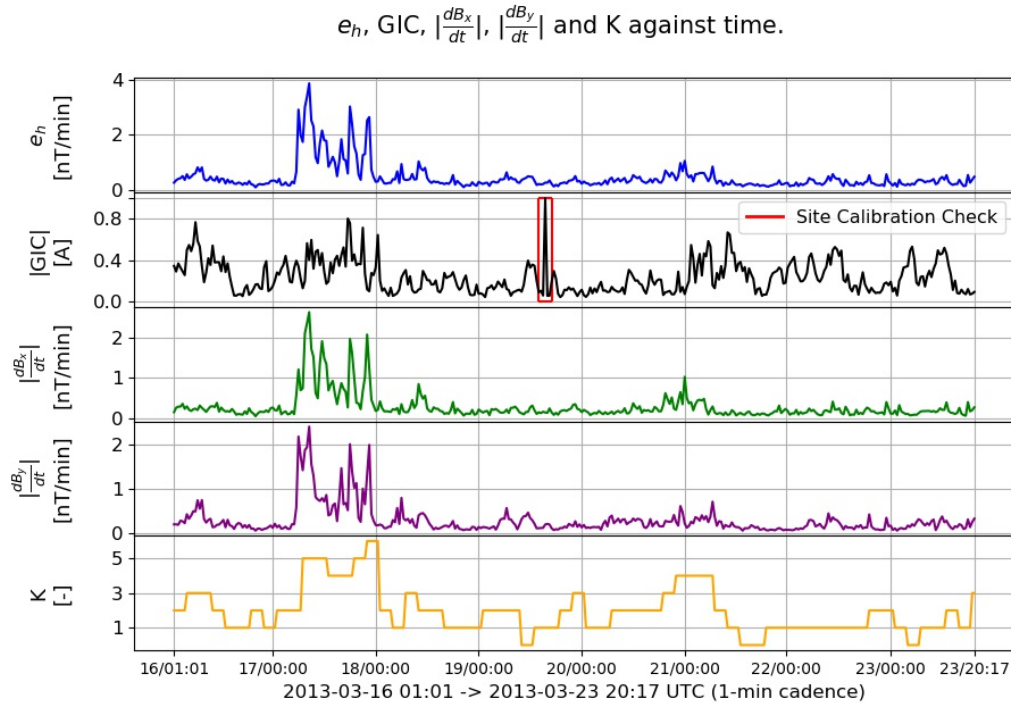


Figure 4.8: e_h (blue), the magnitude of measured GIC (black), $\left|\frac{dB_x}{dt}\right|$ (green), $\left|\frac{dB_y}{dt}\right|$ (purple), and Hermanus K-index (orange) vs. time for a measured GIC event during the period 2013-03-16 to 2013-03-23 at the Matimba power station.

The magnitude of measured GIC values shown in Figure 4.8 are 1-minute interval averages of 10-second samples taken from the Matimba station (the same process was carried out with GIC data from the Grassridge station).

With regard to the 2013 event, the abnormal rise bounded by the red box in Figure 4.8 represents a site calibration check carried out at the Matimba station and is not an anomaly

that was not picked up by e_h . This check causes a loss in correlation (which should be resolved by removing the calibration check from the data and calculating the correlation in the absence of this error) but also reveals the practical realities of instruments, namely they have to be managed and maintained.

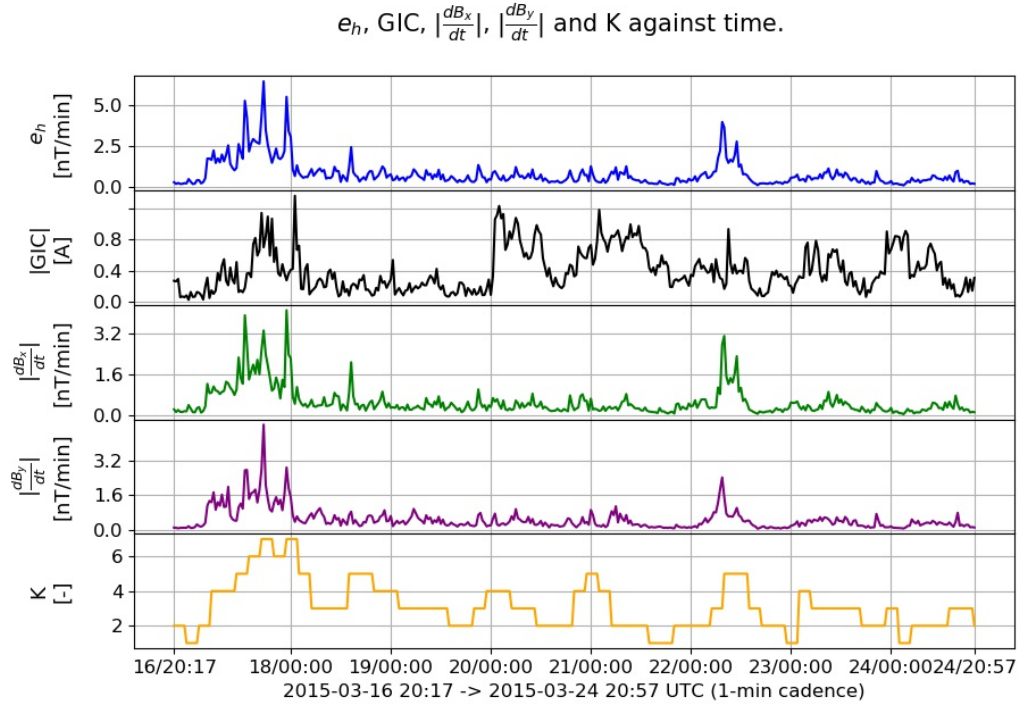


Figure 4.9: e_h (blue), the magnitude of measured GIC (black), $\left|\frac{dB_x}{dt}\right|$ (green), $\left|\frac{dB_y}{dt}\right|$ (purple), and Hermanus K-index (orange) vs. time for a measured GIC event during the period 2015-03-16 to 2015-03-24 at the Matimba power station.

For this 2015 event, it can be seen that the major features in abnormal behaviour are picked up to good resolutions by e_h but that a portion of data, namely 2015-03-20 to 2015-03-22 is not shown in the e_h graph.

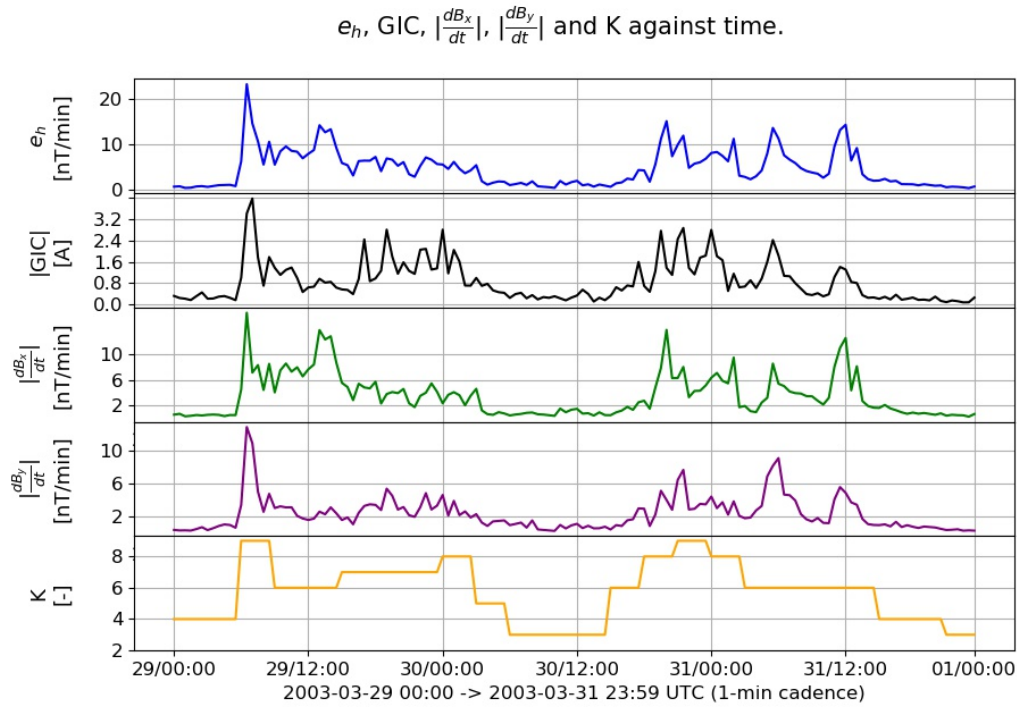


Figure 4.10: e_h (blue), the magnitude of measured GIC (black), $\left|\frac{dB_x}{dt}\right|$ (green), $\left|\frac{dB_y}{dt}\right|$ (purple), and Hermanus K-index (orange) vs. time for a measured GIC event during the period 2003-10-29 to 2003-10-31 at the Grassridge power station.

For the Halloween storm, the duration of the storm was 3 days, which is about half the time as that of the other two events from the Matimba station, resulting in a short, yet intense event. Here the efficacy of e_h can be seen with great clarity, with similar results for the other indices as those discussed for the two Matimba power station events, namely having the best correlations with the magnitude of measured GIC.

4.5 Cumulative index

4.5.1 Threshold selection

At the outset, it must be noted that $K = 0, 1$ is classified as “quiet”, while $K = 2, 3, 4$ are classified as “moderate” [13]. An algorithm integrating over periods (by making use of the Biot-Savart law) where the magnetic field values were found to be higher than an absolute value of 5 nT calculated based on variations from the H-field was used to develop a magnetohydrodynamic (MHD) model for latitudes closer to the North pole in a study by Yu and Ridley, while the same study used 0.5 nT/s as threshold for storm activity [2]. It must be emphasised that this integration algorithm was not implemented in this study, but the idea of a window of activity beyond a certain threshold level of activity deserves

mentioning. Clearly, the threshold used in this study and that by Yu and Ridley [2] differ in both cases of the thresholds used by the authors. The threshold e_h value for quiet time (when it is assumed that there is no destructive activity) validated against a K-index value is required for the calculation of the cumulative index. Furthermore, using a data set composed almost entirely of storm activity presents a possible threshold bias in that data will be skewed in the direction of destructive behaviour. An attempt is made to look at quiet time events near the end of this chapter, but the establishment of a correct threshold, being an important parameter of GIC research, definitely needs further development in absence of clear storm features. A threshold of $e_h = 0.5$ nT/min is used to assess when storm activity becomes pronounced enough to have significance in terms of possible damage to infrastructure that may be occurring. A quantifiable justification for this threshold will be given. Consider Figure 4.11:

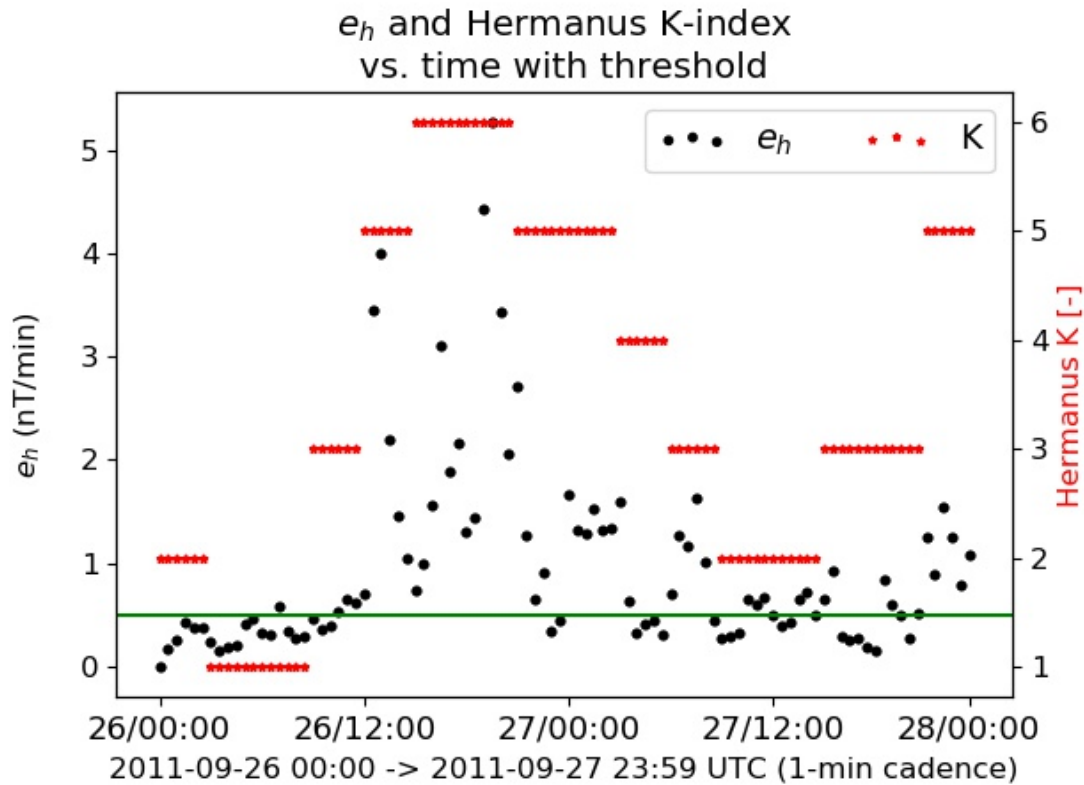


Figure 4.11: Interpolated Hermanus K-index (right) and e_h (left) against time. The threshold of 0.5 nT/min is plotted in green. This event took place as a result of a CME [13].

In the specific case, the choice of the threshold is chosen by comparison of the unscaled K-index values with e_h . Figure 4.11 shows that below $K = 2$ on the K-axis, the e_h axis is intercepted at 0.5 nT/min (This just being used as a case in point to introduce the concept, the case for this choice goes beyond just visual scaling of the plots, see Figure 4.12 below

for a clearer and more general description). Note that $K = 1$ accounts for 12.5 % of K values for this storm. 43% of all e_h data points for this storm lie above this threshold and are assumed to be values which cause damage.

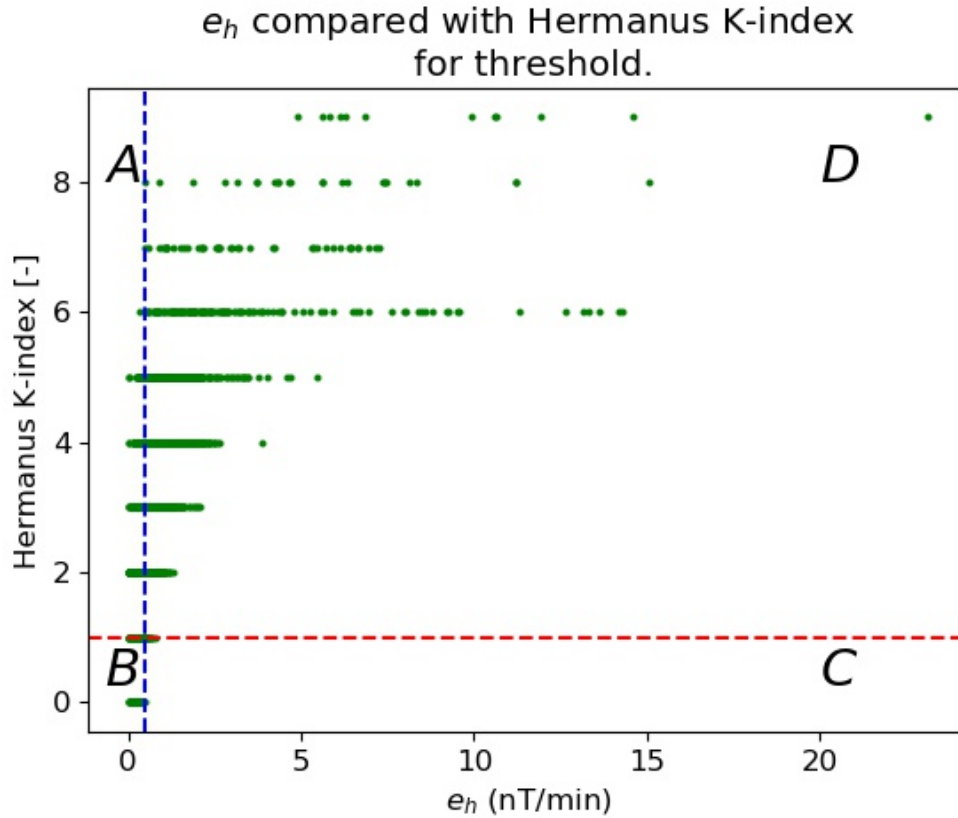


Figure 4.12: Interpolated Hermanus K-index data against e_h data of 21 storm events. The threshold of 0.5 nT/min is plotted in blue while a K unit of 1 is plotted in red. Region A has $K > 1$ and $e_h \leq 0.5$ nT/min, region B has $K \leq 1$ and $e_h \leq 0.5$ nT/min, region C has $K \leq 1$ and $e_h > 0.5$ nT/min and region D has $K > 1$ and $e_h > 0.5$ nT/min.

Table 4.4: Percentages of data based on the values of the Hermanus K-index and e_h from Figure 4.12 with an e_h threshold of damage assumed to be 0.5 nT/min. The first column gives the constraints on either K, e_h or both K and e_h , the second column gives the approximate percentage of data rounded to 2 decimal places in the region of Figure 4.12 subjected to those constraints and the third column gives the type of storm activity according to the K-classification for storm activity set out in [13].

Constraints	Percentage of data	Type of Storm Activity
$K \in [0, 1]$ and $e_h \in [0, 0.5]$ nT/min	23.26%	Quiet
$K \in [2, 4]$ and $e_h \in [0, 0.5]$ nT/min	35.39%	Moderate
$K \in [5, 9]$ and $e_h \in [0, 0.5]$ nT/min	0.68%	Strong
$K \in [0, 1]$ and $e_h > 0.5$ nT/min	0.29%	Quiet
$K \in [2, 4]$ and $e_h > 0.5$ nT/min	28.56%	Moderate
$K \in [5, 9]$ and $e_h > 0.5$ nT/min	11.82%	Strong
$K \in [2, 9]$ and $e_h > 0.5$ nT/min	40.38%	Moderate or Strong
$K \in [0, 1]$	23.55%	Quiet
$K \in [2, 4]$	63.95%	Moderate
$K \in [5, 9]$	12.5%	Strong
$K \in [2, 9]$	76.45%	Moderate or Strong
$e_h \in [0, 0.5]$ nT/min	59.32%	-
$e_h > 0.5$ nT/min	40.68%	-

Analysis using data from the 21 storms was carried out. First, 8 K-index points per day were interpolated to 48, which is the number of e_h values per day. Table 4.4 shows the percentages of the data distributed in Figure 4.12. The region with $K \in [2, 9]$ and $e_h > 0.5$ nT/min includes 40.38% of the data while the region with only $K > 1$ includes 76.45% of the data and the region with only $e_h > 0.5$ nT/min includes 40.68% of the data. The first two of the regions mentioned are where storm activity is said to be “Moderate or Strong” while the last region is where damage causing values of e_h are assumed to be in this study. 59.32% of the data is assumed not to incur damage from the perspective of e_h alone, while “Quiet” activity according to K-classification is less than half this amount at 23.55% of the data. Using just the K classification of “Moderate or Strong” activity, this amount of data (76.45%) is about twice the amount of data that uses e_h only for the amount of values assumed to be indicative of damage causing GICs (40.68%). Thus it is possible that e_h may give a false positive. The amount of data assumed to be “Moderate or Strong” with e_h values assumed to be indicative of damage causing GICs accounts for 40.38% of the data. This number is similar to the total amount of data assumed to be indicative of damage causing GICs when looking at the data from the perspective of e_h only which is 40.68%. This gives a difference of 0.3% when considering the difference between constraining the data based on both e_h and K against constraining the data based solely on the e_h threshold which may indicate that setting the e_h at 0.5 nT/min may be valid since this is only about 6 hours of data that is left out when considering the total number of data

points. A problem with having a threshold that is too high for e_h is that the threshold may become too close to the peak value of a given storm; in the data set of storms used in Figure 4.12, the peak e_h is found to be close to about 3.0 nT/min in 11 out of 21 cases of Table 4.6 [13]. The problem with setting the threshold too low is that the cumulative index would then incorporate features of quiet behaviour into itself, contributing to a stronger numerical cumulative index value than is realistic for storm activity. It can be seen from Figure 4.12 that above a K value of 4, e_h activity becomes far more widely spread, which is in agreement with the literature for the K -classification of strong storm activity [13]. Consider the case made for a new threshold by taking both Figure 4.13 and Table 4.5:

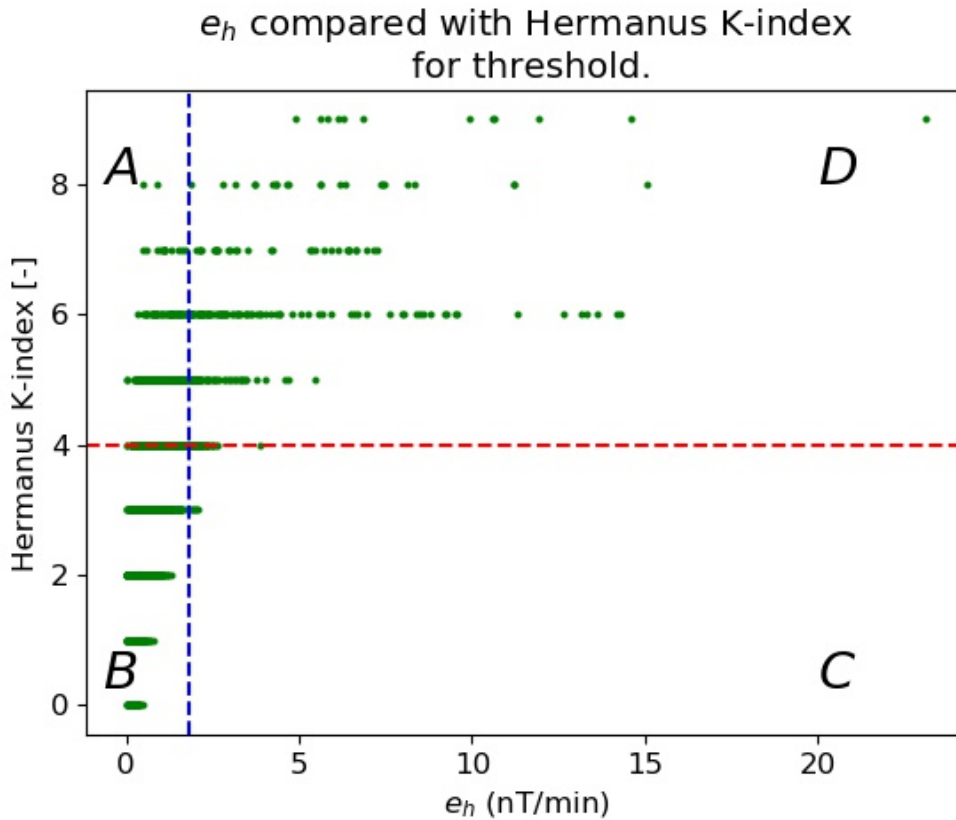


Figure 4.13: Interpolated Hermanus K-index data against e_h data of 21 storm events. The new threshold of 1.8 nT/min is plotted in blue while a K unit of 4 is plotted in red. Region A has $K > 4$ and $e_h \leq 1.8$ nT/min, region B has $K \leq 4$ and $e_h \leq 1.8$ nT/min, region C has $K \leq 4$ and $e_h > 1.8$ nT/min and region D has $K > 4$ and $e_h > 1.8$ nT/min.

Table 4.5: Percentages of data based on the values of the Hermanus K-index and e_h from Figure 4.12 with an e_h threshold of damage assumed to be 1.8 nT/min. The first column gives the constraints on K and e_h , the second column gives the approximate percentage of data rounded to 2 decimal places in the region of Figure 4.12 subjected to those constraints and the third column gives the type of storm activity according to the K-classification for storm activity set out in [13].

Constraints	Percentage of data	Type of Storm Activity
$K \in [0, 1]$ and $e_h \in [0, 1.8]$ nT/min	23.55%	Quiet
$K \in [2, 4]$ and $e_h \in [0, 1.8]$ nT/min	62.81%	Moderate
$K \in [5, 9]$ and $e_h \in [0, 1.8]$ nT/min	7.36%	Strong
$K \in [2, 9]$ and $e_h \in [0, 1.8]$ nT/min	70.17%	Moderate or Strong
$K \in [0, 1]$ and $e_h > 1.8$ nT/min	0%	Quiet
$K \in [2, 4]$ and $e_h > 1.8$ nT/min	1.14%	Moderate
$K \in [5, 9]$ and $e_h > 1.8$ nT/min	5.14%	Strong
$K \in [2, 9]$	76.45%	Moderate or Strong
$e_h \in [0, 1.8]$ nT/min	93.73%	-
$e_h > 1.8$ nT/min	6.27%	-

From Table 4.5 the e_h threshold is raised to 1.8 nT/min, the amount of data that will be discarded due to the assumption that these values are not indicative of damage causing GICs is 93.73% namely almost all the data. When the amount of data assumed to be indicative of damage causing GICs taken from the perspective of the e_h threshold of 1.8 nT/min is compared to the amount of data assumed to be indicative of “Strong” K activity, the numbers are similar namely 6.27% compared to 5.14%. The difference between these two numbers in real terms accounts for about 27 hours of data though which would be much smaller than e_h values assumed to be indicative of damage causing GICs compared to K values assumed to be indicative of “Moderate or Strong” behaviour namely 6.27% compared to 76.45%, which gives a difference of about 70% in the amount of data values when looking at using either of the classification systems by themselves as being indicative of damage causing GICs. Performing a similar comparison using Table 4.4, the corresponding quantities are 40.68% to 12.5% of the data values with a difference of about 30% which is less than half the amount than when setting the threshold to 1.5 nT/min. An inherent assumption being made with the specific threshold of 0.5 nT/min is that storms with peaks as low as approximately 2.0 nT/min (see Table 4.6) should be considered as damaging in roughly the same class as storms for which damage has been known to occur i. e. the available GIC data- giving rise to possible ambiguities. With reference to the GIC data available in this study, consideration of a threshold value of e_h indicative of possible serious damage (damage for which it is known in this case by direct measurements) must be considered apart as a class of storms. The three peaks associated with these events are (see Table 4.6) 20.0 nT/min (event 1, 3 days in duration), 3.6 nT/min (event 11, 4 days in duration), and 6.0 nT/min (event 22, 6 days in duration) respectively.

For these three events, the case could be made to raise the threshold as in Figure 4.13 to 1.8 nT/min, where about 7.36% (see Table 4.5) of the total data was found in high K-high e_h pairs (above K at 4 and e_h at 1.8 nT/min respectively), so that the cumulative index may be recalculated according to strong storm classification for K [13]. For clarity, the selection of a threshold which is verifiable will need many storms whose GIC data is available as well as an analysis of the data of a system where known damage to infrastructure has taken place (verified by dissolved gas analysis etc.), along with the associated continuous GIC data, however these requirements are difficult to achieve due to the proprietary nature of GIC data. Furthermore, it must be stressed that the threshold of 0.5 nT/min used in this study is used according to what e_h values fall above quiet K (0 and 1), and that from the data for GIC, the raising of the threshold might be necessary but this is difficult to say on the basis of three events where the raised threshold might omit the results of other storms' peaks that are comparable to the raised threshold, thereby implying that the entire storm be discarded (as would happen with 50% of the data set in this study) as one which causes damage. The threshold must be chosen in such a way that it includes information that is pertinent to cumulative damage but also excludes information that will cause ambiguities or false warnings.

4.5.2 The cumulative index

The cumulative index C (see equation (3.3)) is created to calculate the sum of e_h values and is supposed to serve as a proxy for the accumulated damage after a geomagnetic storm has taken place. This section will analyse the results of the cumulative index C , and show its relationship with sunspot number, peak e_h value and storm duration.

Table 4.6: ‘Start date’ denotes the date a storm began, ‘Peak e_h ’ the noticeable maximum e_h of an event, ‘Sunspot number’ the American cumulative daily totals from NOAA (National Oceanic and Atmospheric Administration) website of sunspot number for the span of the event, ‘Storm duration’ of the storm in days, ‘ C ’ the cumulative index value, ‘Active time’ the cumulative time in days when the threshold was exceeded and the final column denoting the ratio of the active time to the duration of the storm as a percentage respectively.

No.	Start date	Peak e_h (nT/min)	Sunspot number (total)	Storm duration (L) (days)	C (nT/min)	Active time (A) (days)	%(A/L)
1	2003-10-29	20	494	3	681.615	2.96	98.67
2	2011-08-05	3.5	252	5	56.761	1.02	21.00
3	2011-09-26	5.2	135	2	79.125	1.15	57.50
4	2011-10-24	3.2	348	5	47.869	0.94	18.80
5	2012-04-23	3.9	307	4	94.093	2.27	56.75
6	2012-07-14	3.4	309	5	110.425	2.06	41.20
7	2012-09-29	2.7	203	4	33.280	0.81	20.25
8	2012-10-07	2.4	95	3	49.881	1.15	38.33
9	2012-10-12	1.9	248	4	54.162	1.35	33.75
10	2012-11-12	2.4	474	5	50.317	1.13	22.60
11	2013-03-17	3.6	223	4	70.729	1.06	26.50
12	2013-06-28	2.4	144	3	51.475	1.25	41.67
13	2014-02-18	2.1	427	5	70.184	1.46	29.20
14	2014-02-27	1.8	356	3	24.911	0.52	17.33
15	2015-06-07	1.8	309	4	54.642	1.33	33.25
16	2015-06-22	7.2	123	4	124.329	2.08	52.00
17	2015-08-25	2.2	168	5	93.360	2.06	41.20
18	2015-09-08	2.0	91	3	71.323	1.35	45.00
19	2015-10-06	4.0	60	4	117.983	2.52	63.00
20	2015-11-06	2.6	243	5	96.691	2.27	45.40
21	2015-12-19	3.6	104	4	113.139	1.94	48.50
22	2015-03-17	6.0	186	6	221.640	3.62	60.33

Whether C does/does not show a solar cycle dependence cannot be concluded as a span of events lasting a solar cycle of 11 years has not been assessed. Sunspots tend to persist long after the main abnormal storm activity takes place on Earth and a higher cumulative amount of them is not indicative of higher storm activity [3]. The sunspot number indicates that a certain level of solar activity is taking place, however it cannot give the amount of damage that is to be anticipated. For example, the Halloween storm and a storm with comparable cumulative sunspot number (Row 1 and row 13 in Table 4.6

above respectively), namely 494 and 427 respectively, however the latter falls behind the former in cumulative index value by over 1 order of magnitude.

4.5.3 Active time and long-term index

The ‘active time’ (column 7 in Table 4.6) is defined as the cumulative time over which the threshold (0.5 nT/min) of the cumulative index is exceeded. The significance of this type of metric is twofold, namely to be careful enough so as not to count those e_h values below the threshold, and to ensure that no clustering of data points around integer days or hours for each event occurs. This is then expressed as a percentage over the integer duration of the number of days an event was recorded for in the data (column 8 in Table 4.6) to show more clearly the proportion of time for which the threshold is exceeded for the duration of an event.

To give more clarity for the use of this metric a few points are pertinent. Storms have inherent activity which can be temporally quantified from start to finish using the SYM-H storm classification system as was done in column 3 of Table 4.2. The problem with using this system of temporal classification in context of the cumulative index is that the chosen threshold may not be taken into account and that values within the interval for which data is available may be discarded. It is also important to note that an inherent assumption is that values which fall below the threshold are not considered to cause damage to infrastructure. This is the reason for choosing the threshold as such. In this way, small quantifiable fluctuations in the magnetic field may be rendered negligible.

The important distinction mentioned by Lotz and Danskin [3] was that between short-term events that are more pronounced and long-term events that are not so pronounced, it is possible that both types of events may cause comparable damage. It must be emphasised that a conclusion cannot be drawn due to the small number of events used.

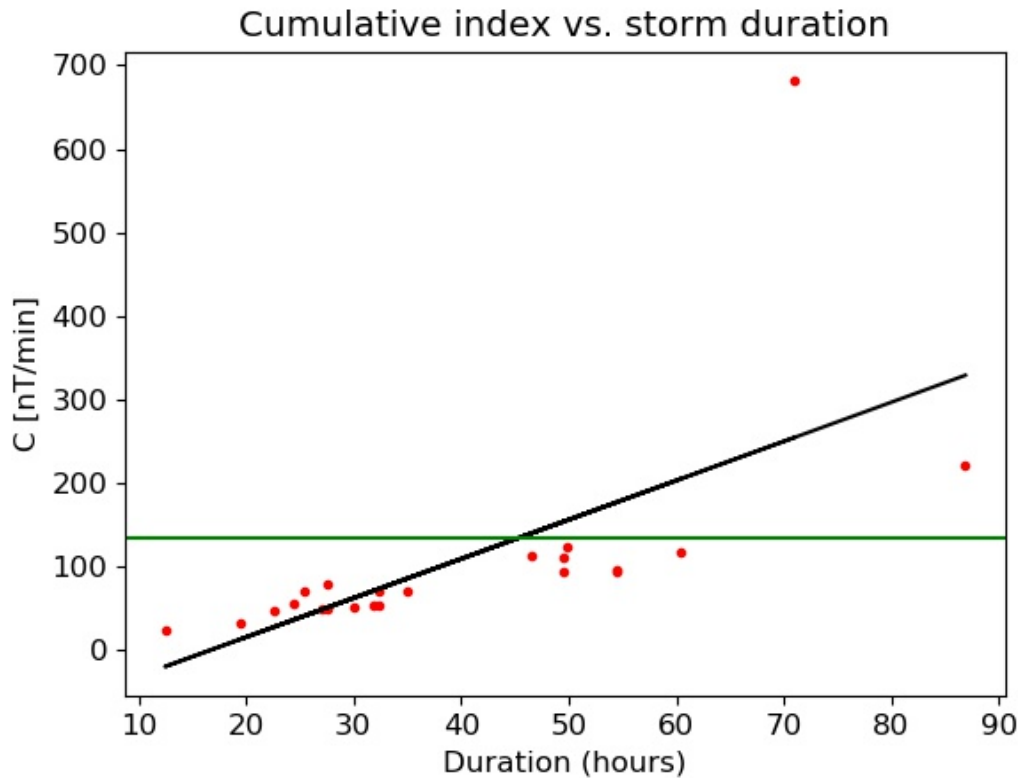


Figure 4.14: Cumulative result vs. duration (Active time) in integer hours for the Hermanus data (columns 7 and 5 of Table 4.6 respectively). The band bounded by the green horizontal line and x-axis shows the where most of the data lies. The black line shows the line of best fit indicating the positive correlation between C and storm duration.

Most of the data in Figure 4.14 lies below the 125.0 nT/min, with two values above this value. The cumulative index in Figure 4.14 above shows that short-term events and long-term events, may do the same amount of damage. One can see a clear linear trend between the cumulative index and storm duration. The Pearson R coefficient was found to be 0.64 using all the events while the removal of the major outliers above the band gave a Pearson R coefficient of 0.72 (even though p-values associated with both these coefficients do not allow for the data to be accepted [82]). The deviation from ‘normal interval damage’ behaviour to ‘abnormal interval damage behaviour’ (threshold being crossed, see Figure 3.3) becomes pronounced when:

1. In the case of the Halloween storm, a short event with values that are skewed by a high peak (for comparison with other storms’ peaks see Table 4.6).
2. For the storm dated 2015-03-17 to 2015-03-23, which lasted about a week, the exposure time is longer than usual for the data set. Here it may be compared with the ‘short and intense’ vs. ‘long yet not so intense’ approach mentioned above [3]. It should be noted that a conclusive conclusion cannot be made as the p-value was

greater than the correlation for this data due to the small number of storms used.

4.5.4 Cumulative index and storm duration

Consider the events numbered 16 and 21 in Table 4.6 respectively. The former event lasts four days with a peak of 7.2 nT/min while the latter event lasts six days with a peak of 6.0 nT/min. The cumulative index of the shorter event is almost half that of the longer event. In seeking to show that an event of a longer time can do the same or more damage, the cumulative frequencies were plotted against the active time as shown in Figure 4.15 below:

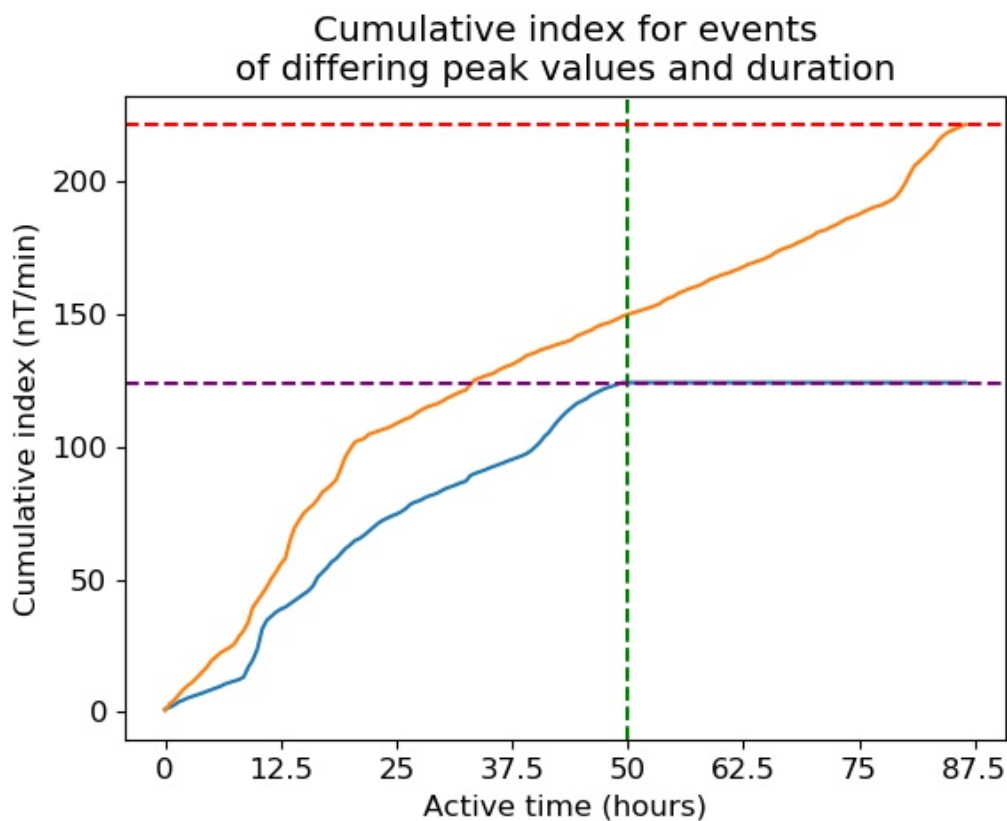


Figure 4.15: Cumulative index frequency vs. duration (Active time) in hours for event 16 (blue) and event 1 (orange). The vertical green line shows where the shorter event stops. The horizontal purple and red lines show the cumulative values for both events quoted in rows 16 and 21 of Table 4.6 respectively.

Figure 4.15 shows how the shorter event with a higher peak (blue curve) is far exceeded by the longer event with a smaller peak as it grows to almost double the cumulative index value of the shorter event. This seems to fit the result shown by Lotz and Danskin where longer, yet less intense events can do more damage than shorter events [3].

4.5.5 Events with similar Cumulative index

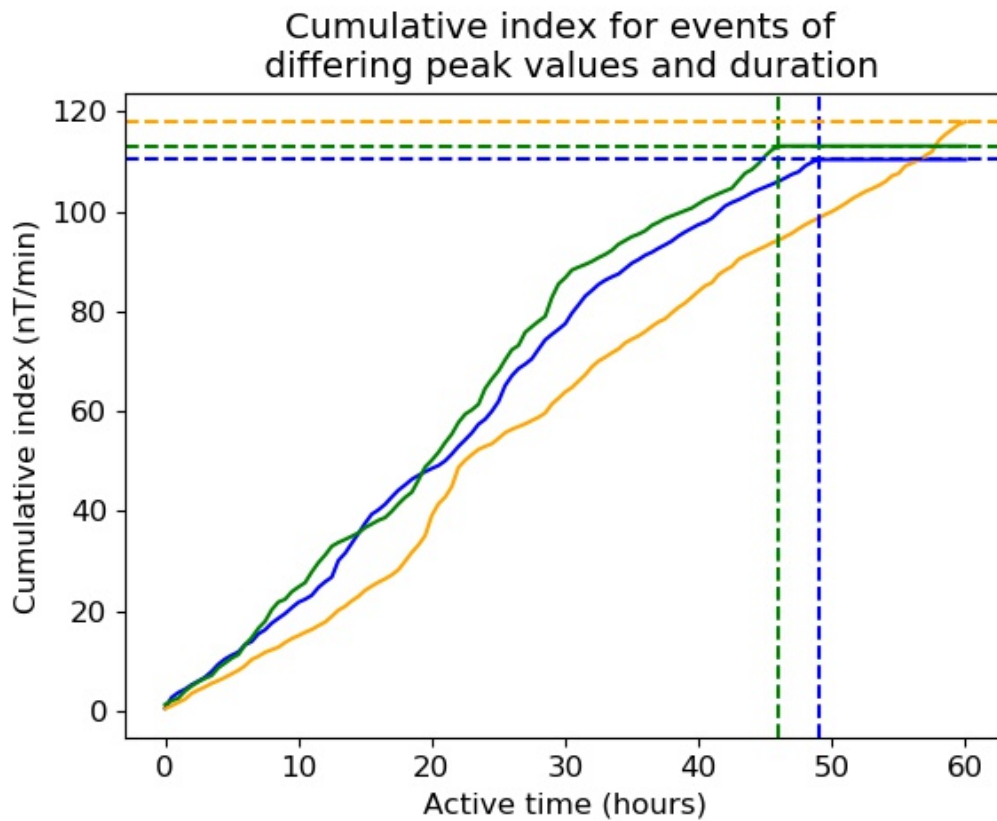


Figure 4.16: Cumulative index frequency vs. duration (Active time) in hours for events 6 (blue), 19 (orange) and 21 (green), where event numbers denote row events in Table 4.6 respectively. The vertical blue and green dashed lines show where events 6 and 21 stop respectively. The horizontal blue and green dashed lines show the cumulative index values for both events quoted in rows 6 and 21 of Table 4.6 respectively, while the horizontal orange dashed line shows the cumulative index value of event 19 of Table 4.6

Figure 4.16 shows 3 events that approach a comparable cumulative maximum value. These events are comparable in that their cumulative index value is close to about 110 nT/min. Event 6 lasted 5 days and had a cumulative index value of 110.425 nT/min, while events 19 and 21 which both lasted 4 days had cumulative index values of 117.983 nT/min and 113.139 nT/min respectively. 4 to 5 days is a 25% increase in time, for which the cumulative percentage change is 15.90% when comparing event 19 to event 6, and 11.51% when comparing event 21 to event 6.

4.5.6 Measured GIC: Events with similar Cumulative index

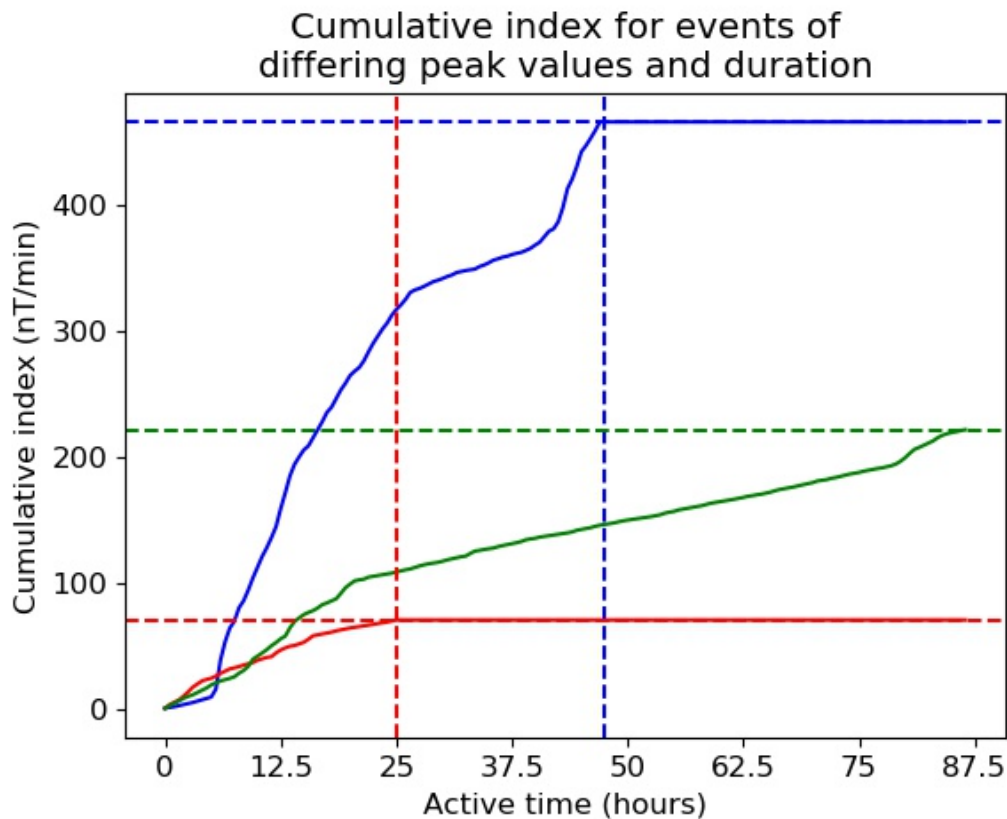


Figure 4.17: Cumulative index frequency vs. duration (Active time) in hours for measured GIC events 1 (blue), 11 (red) and 22 (green), where event numbers denote row events in Table 4.6 respectively. The vertical blue and red dashed lines show where events 1 and 11 stop respectively. The horizontal blue, red and green dashed lines show the cumulative index values for the three events quoted in rows 1, 11 and 22 of Table 4.6 respectively.

Figure 4.17 shows the cumulative frequency curves for the measured GIC events. The blue curve is that of the Halloween storm, which has the largest cumulative index value in the Table 4.6. All three events were ones for which measured GIC was available.

A cumulative damage index should inform the necessary stakeholders of the damage incurred to infrastructure for a given geomagnetic storm, post this geomagnetic storm, in an unambiguous and quantifiable sense. This is no simple task as it remains an open problem in the field of GICs. A cumulative index is good for assessing damage after a storm has passed. For near real time tracking, a short-term index is more useful. The cumulative index may be computed while a storm is being tracked in near-real time, but the full scale impact can only be known after the storm is over. In seeking to understand the manifestations of comparable damage via two alternative pathways, namely short-term and long-term events, a distinction between damage was made in the grouped probabilistic analysis of GICs to assess peak and cumulative exposures to power networks by Heyns et

al. [83]

4.6 False warnings

4.6.1 Short-term index

A false warning is generally defined in this study as a false positive of storm activity- results showing that a possibly damaging storm is happening when it is not. A more specific and quantitative definition will follow after the presentation of the appropriate graphs and calculations.

A baseline level of activity outside storms, known henceforth as a ‘quiet event’, was selected by looking at the Hermanus K-index values where over a period of 6 days, the K-index values oscillated between 0 and 1 with values on both ends of this 6 day period having a K-index value of 2. When taking into account how the e_h index would look when some geomagnetic activity was present, the expectation was for the threshold to be crossed. This is why the K-index values at both ends of the interval were chosen such that they were higher than 0 or 1. Indeed this is what occurred. First, the K-index for this quiet day event is plotted in Figure 4.18.

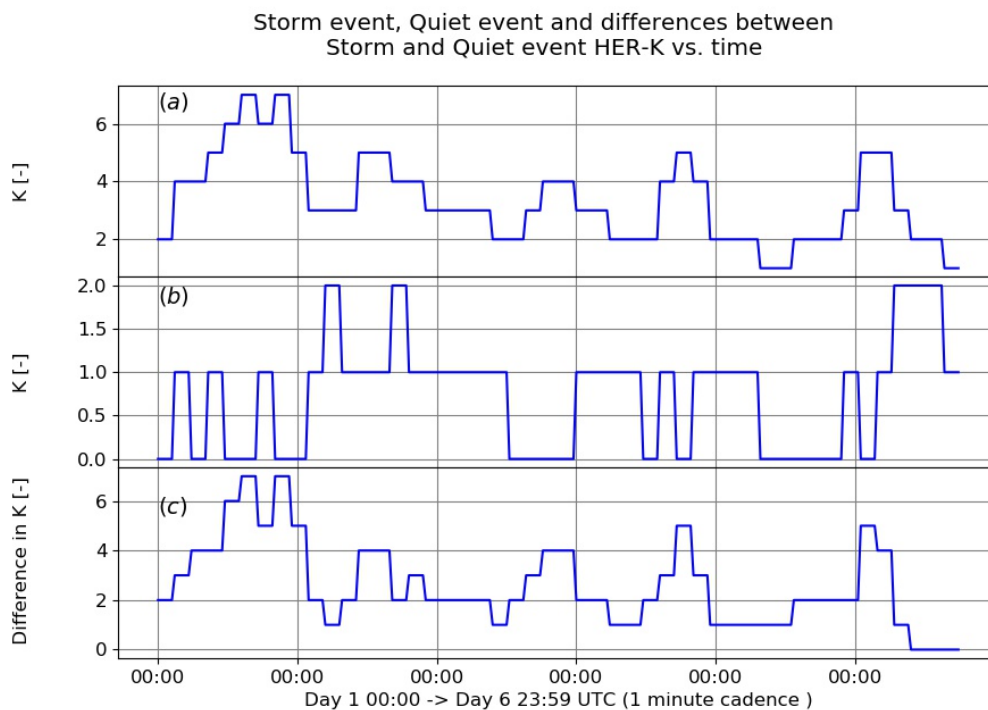


Figure 4.18: (a) ‘Storm’ event Hermanus-K during the period 2015-03-17 to 2015-03-22, (b) ‘quiet’ event Hermanus-K against time during the period 2011-03-14 to 2011-03-19 (b) and (c) differences between (a) and (b). Each label on the x-axis refers to midnight for the ‘storm’ event in panel (a) and ‘quiet’ event in panel (b).

Consider Figure 4.19 showing quiet event e_h vs. time during the period 2011-03-14 to 2011-03-19 contrasted immediately thereafter with e_h for the event spanning 2015-03-17 to 2015-03-22 (used in this study). Each of these days will be called Day 1 to Day 6 respectively 2011-03-14 is Quiet Day 1 and 2015-03-17 is Storm Day 1 and so on.

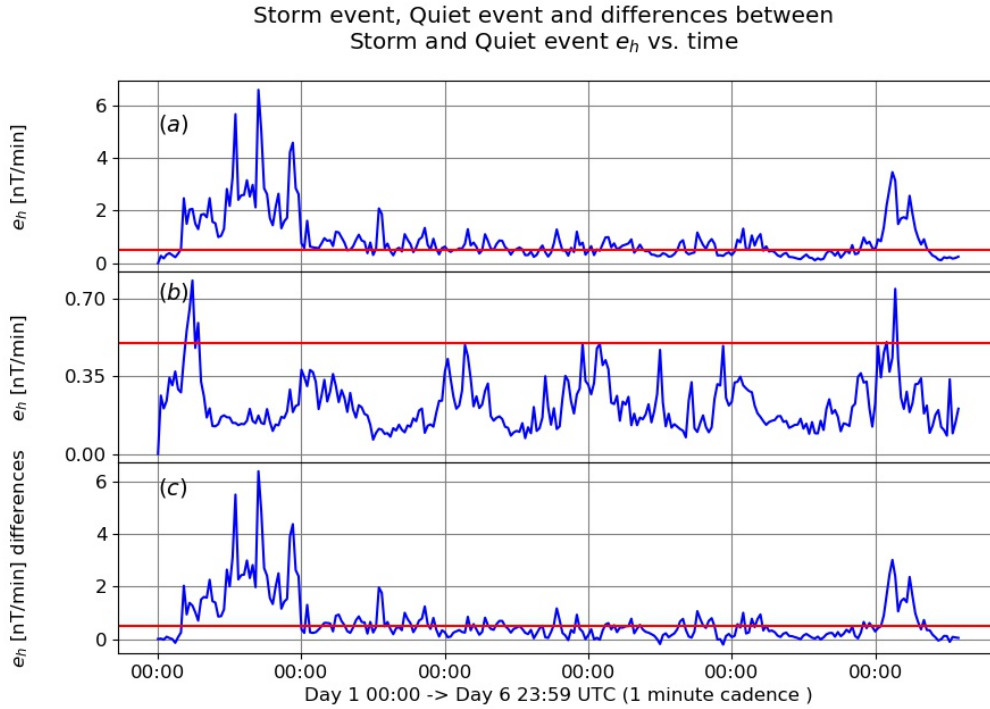


Figure 4.19: (a) ‘Storm’ event e_h during the period 2015-03-17 to 2015-03-22, (b) ‘quiet’ event e_h against time during the period 2011-03-14 to 2011-03-19 and (c) differences between (a) and (b). The red line denotes the e_h threshold of activity where $e_h = 0.5$ nT/min.

Note that the peak values differ greatly in these two events, however this does not give enough information. In order to assess the false warnings that could be given by e_h , the e_h for each day during a typical storm period needs to be compared with the e_h for each day of a quiet period of the same duration. The e_h distributions for each day of these storm and quiet periods are needed. These are plotted in Figures 4.20-4.25.

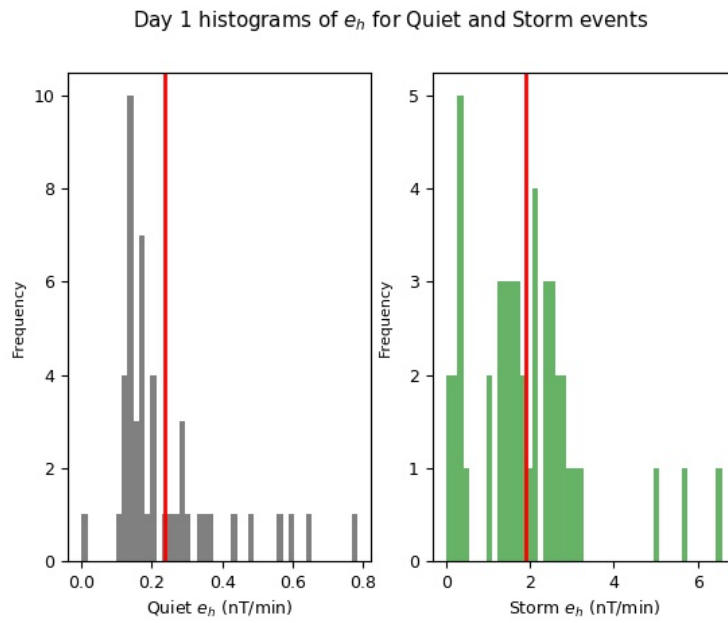


Figure 4.20: Histograms for Day 1 of ‘Quiet’ event during the period 2011-03-14 to 2011-03-19 (left) and storm event e_h against time during the period 2015-03-17 to 2015-03-22 (right). The red line denotes the mean e_h .

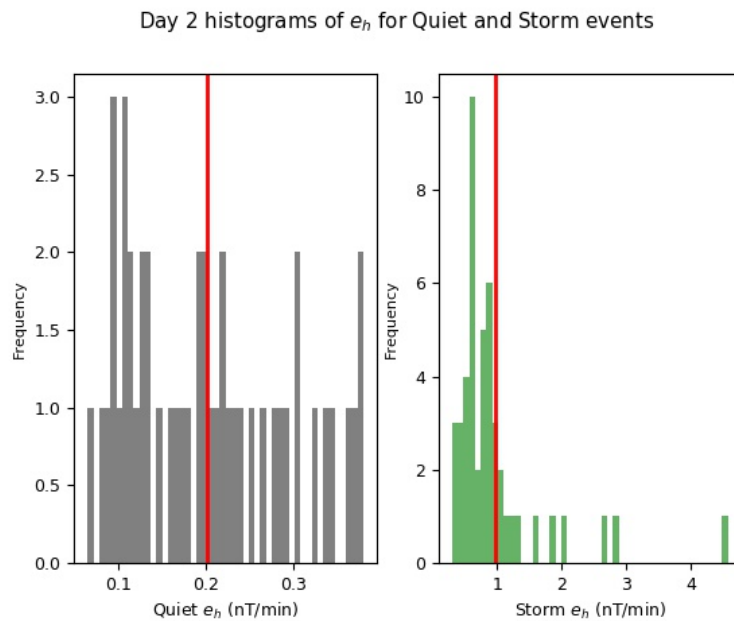


Figure 4.21: Histograms for Day 2 of ‘Quiet’ event during the period 2011-03-14 to 2011-03-19 (left) and storm event e_h against time during the period 2015-03-17 to 2015-03-22 (right). The red line denotes the mean e_h .

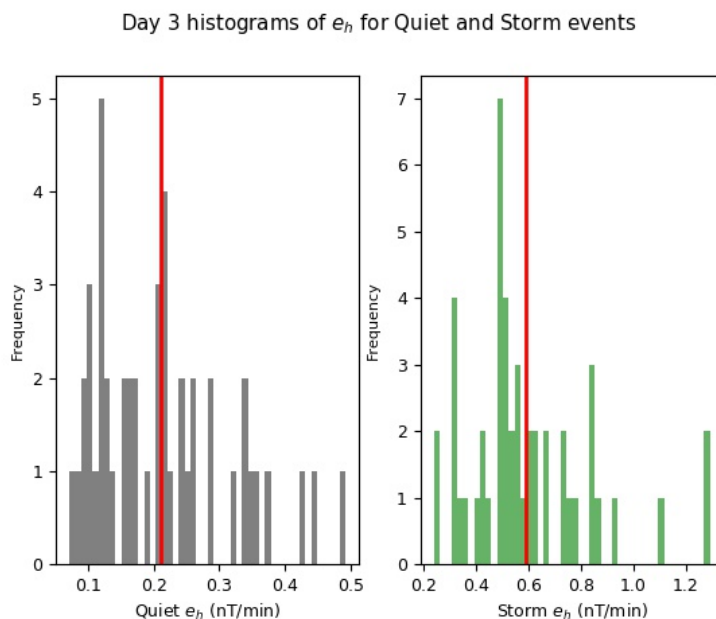


Figure 4.22: Histograms for Day 3 of ‘Quiet’ event during the period 2011-03-14 to 2011-03-19 (left) and storm event e_h against time during the period 2015-03-17 to 2015-03-22 (right). The red line denotes the mean e_h .

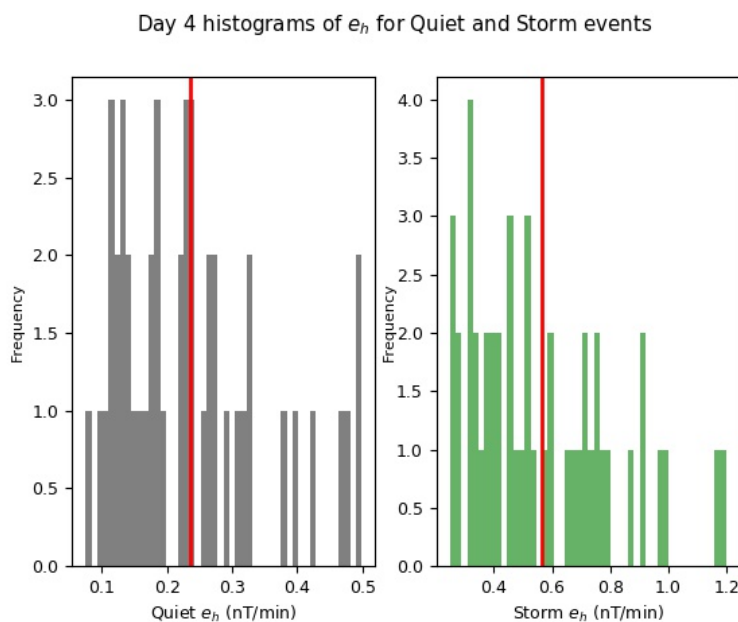


Figure 4.23: Histograms for Day 4 of ‘Quiet’ event during the period 2011-03-14 to 2011-03-19 (left) and storm event e_h against time during the period 2015-03-17 to 2015-03-22 (right). The red line denotes the mean e_h .

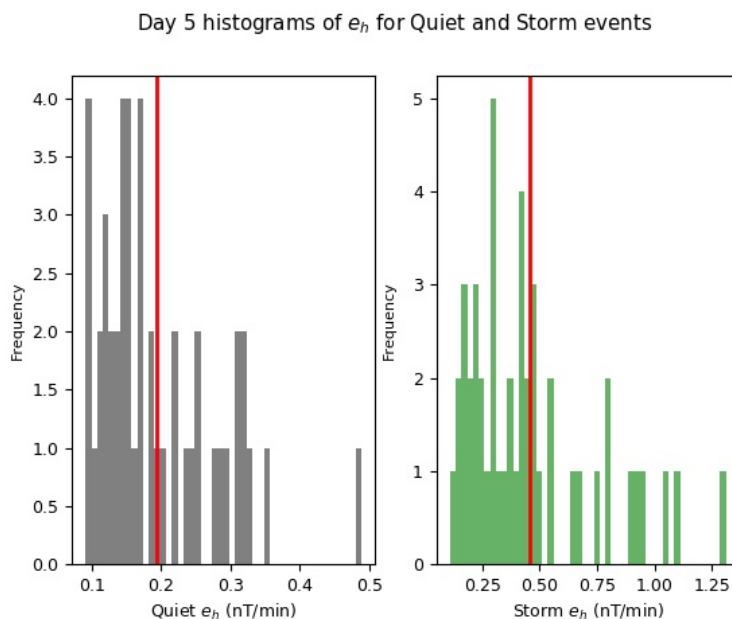


Figure 4.24: Histograms for Day 5 of ‘Quiet’ event during the period 2011-03-14 to 2011-03-19 (left) and storm event e_h against time during the period 2015-03-17 to 2015-03-22 (right). The red line denotes the mean e_h .

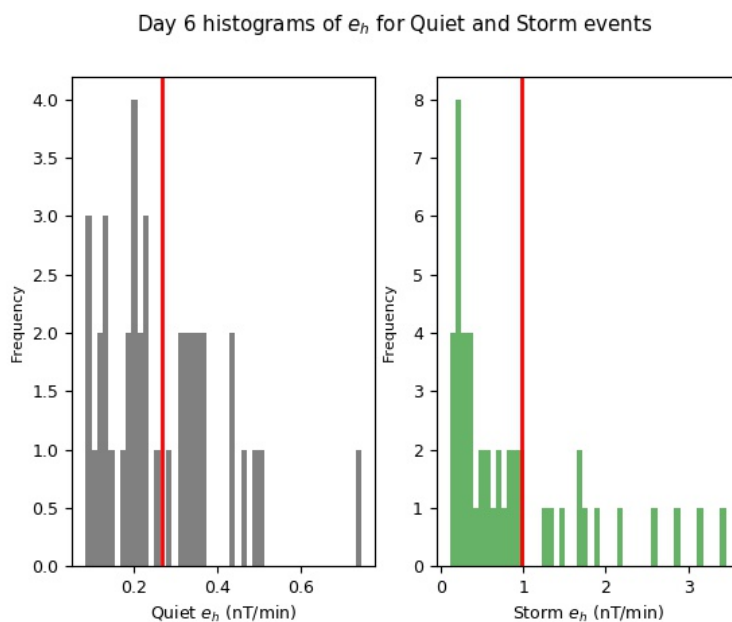


Figure 4.25: Histograms for Day of ‘Quiet’ event during the period 2011-03-14 to 2011-03-19 (left) and storm event e_h against time during the period 2015-03-17 to 2015-03-22 (right). The red line denotes the mean e_h .

The means for each day are given in Table 4.7.

Table 4.7: Mean e_h for each day of the quiet (row 1) and storm (row 2) events plotted in Figures 4.20-4.25 above as well as the percentage of the fraction (row 3) of the quiet day mean to storm day mean for each day i. e. taking the ratio of the value in row 1 over row 2 as a percentage.

Event (nT/min)	Day 1	Day 2	Day 3	Day 4	Day 5	Day 6
Quiet	0.237	0.201	0.210	0.235	0.193	0.266
Storm	1.907	0.967	0.592	0.564	0.457	0.982
% Quiet/Storm	12.43	20.79	35.47	41.67	42.23	27.09

From Table 4.7 it can be established that the ratio (when comparing the daily means of e_h) of storm time to quiet time as percentages, range upwards from about 12%. This indicates how much more the daily mean of e_h during a storm exceeds the daily mean of e_h for a quiet period of the same duration. This method of comparison then establishes a quantifiable manner to assess false warnings for e_h .

4.6.2 Long-term index

To assess false warnings for the cumulative index C , e_h data for the period 2014-03-01 to 2014-12-31 was compressed into a 6 day period by averaging out the e_h values. The derivation of this 6 day period excluded the data set of 21 storm events used in this study and is supposed to represent the e_h activity of a quiet period. A value for C representative of a quiet period lasting 6 days was computed from this period. The C values from Table 4.6 are then used to compute C values that can be used for comparison to this quiet day C value such as the median C value for the median number of days in Table 4.6.

Table 4.8: Cumulative index (C) value categories in the first column, the computed value for C based on its requisite number of computed days in the second column, and the estimated 10-day value for C in the second column adjusted for 10 days, all based on Table 4.6 (columns 6 and 5).

C data category	Computed C (nT/min)/(days)	Estimated 6 day C (nT/min)
Median	71.026/(3.5)	202.931
Median without 3 extremes	70.457/(3.5)	201.306
Mean	107.674/(4.09)	44.0387
Mean without 3 extremes	73.279/(4.05)	295.314
Highest	681.615/(3)	2272.00
Lowest	24.911/(4)	62.273
Quiet	5.449/(6)	9.082

For Table 4.8, the second column has the value of the cumulative index for the requisite number of days e.g. in row 1, the median C value of all the data for a median duration

of 3.5 days has been computed. This value is then adjusted to give what the estimated C value would be for a 10-day event in the third column.

The mean values differ significantly because the law of large numbers in statistics cannot be used. This law states that for sufficiently large data sets, the mean remains relatively unchanged for single values added to the data set that are much bigger or smaller than the average. Thus the average is significantly skewed by the removal of 3 data points.

If the storm events lasted for 10 days, it can be seen that they will differ by a minimum multiplicative factor of about 7 (if looking at the lowest event extrapolated to ten days) from the quiet day period C value, intermediate factors of about 20 to 30 (using the extrapolated 10-day median and means without extremes respectively) and up to a maximum factor of about 250 (when comparing the Halloween storm extrapolated to 10 days) if taking the most extreme event into account. This serves as a good ‘sanity’ check to show that the quiet period C value does not exceed the storm C value.

The data in rows 1 and 2 and 4 (column 3) of Table 4.8 have similar C values but differ considerably from the C values in rows 3 and row 5. All values calculated in column 3 of Table 4.8 overestimate the quiet value computed for the 10-day event.

Comparing the quiet C values in column 3 of Table 4.8 with highest value (Halloween storm), yields an overestimate of 2 orders of magnitude. Comparing the lowest value gives an overestimate of about 7 times the quiet value.

What is also important to note is that the amount of times the threshold was exceeded during the quiet event was 1463 times out of a total of 14688 data points, which gives a percentage of active time to storm duration of about 11 percentage points. The lowest percentage value in the Table 4.6 gives 17.33 percentage points going up to about 99 percentage points of active time to storm duration.

In light of the above information, parameters for assessing false warnings should take into account the duration of the storm, the active time, the percentage of the active time to the duration of storm and the value of C for the event. By these metrics it may be possible for it to be concluded that this 10-day event is in fact a quiet day by comparing it with the levels of activity it could encounter in 10 days ranging from a lower estimate to a higher estimate in column 3 of Table 4.8 above.

In practice, other indicators of storm activity will be used to show that a storm is occurring, and not necessarily the threshold of e_h only.

Perhaps a higher threshold might assist, yet based on the available data, the lowest peak was 1.8 nT/min. There could also be an integrated system used which establishes a threshold based on a specific station based on local characteristics in conjunction with the duration of an event, its active time, and its peak(s) to give a sort of taxonomic classification for accumulated damage.

Chapter 5

Conclusion

5.1 Conclusion

In this study, a near real time short GIC proxy index e_h was developed using an algorithm similar to that outlined by Wintoft et al. [1] (see section 3.1). Thereafter, cumulative index C was developed (see section 3.2) based on a discrete summation of e_h values based on a threshold verified (see subsection 4.5.1) to indicate a moderate level of storm activity. SANSa Space Science magnetometer data (the Hermanus station) from selected storm events spanning 2011 to 2016, as well as the Halloween storm in 2003 (see Table 4.1) were used to check e_h against various indices, as well as $\frac{dB}{dt}$, yielding correlations similar to other indices (see Table 4.2). Furthermore, directly recorded GIC data provided by power utilities for two events at the Matimba station and one event at the Grassridge station were compared with e_h , giving good or better correlations compared to the proxies $\left|\frac{dB_y}{dt}\right|$, $\left|\frac{dB_x}{dt}\right|$ (see Table 4.3). Generally, e_h correlates well with other indices and proxies, although statistically verifiable results cannot be established due to the small size of the data set. e_h is essential in understanding when GICs might occur as a result of geomagnetic storms in as close to real time as possible and will have to be developed eventually to work in real time.

For the cumulative index, a threshold was selected based on the classification for “moderate storm” activity or higher given by Bartels [13]. The threshold, however is biased in its selection due to the fact that all data used is storm data, even though a quiet period of magnetometer data was assessed to verify its choice (see section 4.6). The threshold is also a difficult value to determine given the dearth in the literature on cumulative proxy indices indicative of GIC damage. It must also be mentioned that raising the threshold too high would render half the data in Table 4.6 unusable, while lowering the threshold would introduce more ambiguity in the calculation of the proxy, which may give false warnings for periods that are not considered storms.

Given that it had the cumulative index proxy value higher (see Table 4.6) than all other events under investigation, the Halloween storm may be said to be an intense event, as verified in the literature [43]. It could also be verified that moderate storm events of a

longer duration can cause more or comparable damage to intense storm events of shorter duration, a distinction made by Lotz and Danskin [3] (see Figures 4.15, 4.16, and 4.17). In Figure 4.14, a linear trend was observed between the cumulative proxy C and the period of time that a storm is active, although again statistically verifiable results cannot be obtained due to the small size of the data set available. Furthermore cumulative proxies indicative of GIC related damage are not yet established in the literature.

The cumulative index is a novel, yet retrospective way of looking at an accumulation of damage post event, which, though new, offers valuable insights in the manner in which a storm can cause damage. This definitely needs refining as it is a new way of approaching and approximating cumulative damage although it must be noted that not all accumulated GICs cause damage. As can be seen from Table 4.6 and the results given in the latter part of Chapter 4, the cumulative index can give a better understanding to the accumulated level of GIC since it is based on the short-term index which correlates similarly with the provided GIC data than $\frac{dB}{dt}$ although there were just three cases available for study.

Finally, to check the indices against false warnings (see section 4.6), investigations were carried out to ensure that both proxies do not give ambiguous cases of storm events taking place in the case of e_h and having taken place in the case of C , although the data set needs to be bigger to draw significant conclusions.

5.2 Future work

e_h needs to be assessed for data sets big enough to draw statistically relevant conclusions, and will be developed in more detail and efficiency such as for use as a near real time service at SANSA Space Science, in a similar manner to the system in use at Dourbes developed by Stankov et al. [65] for alerting stakeholders to possible geomagnetic storms (see section 2.10). Furthermore, a data set of statistically significant size apropos direct GIC data will be needed to verify the use of e_h as an index, although in the South African context this is not currently possible since there are not currently any direct GIC recording devices in use.

The threshold selection problem will be investigated further to establish an unambiguous threshold value to carry out the calculation of the cumulative proxy index. The cumulative proxy index will need verification across a data set of statistically significant size in order to draw reliable conclusions.

Reference List

- [1] P. Wintoft, M. Wik, and A. Viljanen, “Solar wind driven empirical forecast models of the time derivative of the ground magnetic field,” *Journal of Space Weather and Space Climate*, vol. 5, p. A7, 2015.
- [2] Y. Yu and A. J. Ridley, “Validation of the space weather modeling framework using ground-based magnetometers,” *Space Weather*, vol. 6, no. 5, 2008.
- [3] S. I. Lotz and D. W. Danskin, “Extreme value analysis of induced geoelectric field in South Africa,” *Space Weather*, vol. 15, no. 10, pp. 1347–1356, 2017.
- [4] M. G. Kivelson and C. T. Russell, *Introduction to space physics*. Cambridge University Press, 1995.
- [5] M. Herbrink and K. D. Kokkotas, “Stability analysis of magnetized neutron stars—a semi-analytic approach,” *Monthly Notices of the Royal Astronomical Society*, vol. 466, no. 2, pp. 1330–1347, 2017.
- [6] D. H. Hathaway, “The solar cycle,” *Living reviews in solar physics*, vol. 12, no. 1, p. 4, 2015.
- [7] M. Aschwanden, *Physics of the solar corona*. Springer Science & Business Media, 2005.
- [8] M. Moldwin, *An introduction to space weather*. Cambridge University Press, 2008, vol. 1.
- [9] T. Howard, *Coronal mass ejections: An introduction*. Springer Science & Business Media, 2011, vol. 376.
- [10] W. P. Olsen, “The geomagnetic field and its extension into space,” *Advances in Space Research*, (2)1, pp. 13–17, 1982.
- [11] SOHO online. <https://sohowww.nascom.nasa.gov/gallery/images/nov00cme.html>. Accessed April 24, 2021.
- [12] W. Gonzalez, J.-A. Joselyn, Y. Kamide, H. W. Kroehl, G. Rostoker, B. Tsurutani, and V. Vasyliunas, “What is a geomagnetic storm?” *Journal of Geophysical Research: Space Physics*, vol. 99, no. A4, pp. 5771–5792, 1994.

- [13] J. Bartels, N. Heck, and H. Johnston, "The three-hour-range index measuring geomagnetic activity," *Terrestrial Magnetism and Atmospheric Electricity*, vol. 44, no. 4, pp. 411–454, 1939.
- [14] H. K. Chisepo, C. T. Gaunt, and L. D. Borrill, "Measurement and FEM analysis of DC/GIC effects on transformer magnetization parameters," in *2019 IEEE Milan PowerTech*. IEEE, 2019, pp. 1–6.
- [15] S. Stankov, K. Stegen, R. Warnant, and U. RMI, "Local Operational Geomagnetic Index K Calculation (K-LOGIC) from digital ground-based magnetic measurements," *Royal Meteorological Institute*, 2010.
- [16] J. G. Kappenman, S. R. Norr, G. A. Sweezy, D. L. Carlson, V. D. Albertson, J. E. Harder, and B. L. Damsky, "GIC mitigation: a neutral blocking/bypass device to prevent the flow of GIC in power systems," *IEEE Transactions on Power Delivery*, vol. 6, no. 3, pp. 1271–1281, 1991.
- [17] C. T. Gaunt, "Calculations leading to voltage stability and transformer assessment in the presence of geomagnetically induced currents," *Cigre Session*, 2020.
- [18] I. P. Zois, "Solar activity and transformer failures in the Greek national electric grid," *Journal of Space Weather and Space Climate*, vol. 3, p. A32, 2013.
- [19] J. Koen and C. T. Gaunt, "Geomagnetically induced currents in the Southern African electricity transmission network," in *2003 IEEE Bologna Power Tech Conference Proceedings*, vol. 1. IEEE, 2003, p. 7.
- [20] A. W. Thomson, C. T. Gaunt, P. Cilliers, J. Wild, B. Opperman, L.-A. McKinnell, P. Kotze, C. M. Ngwira, and S. I. Lotz, "Present day challenges in understanding the geomagnetic hazard to national power grids," *Advances in Space Research*, vol. 45, no. 9, pp. 1182–1190, 2010.
- [21] J. G. Kappenman, "An overview of the impulsive geomagnetic field disturbances and power grid impacts associated with the violent Sun-Earth connection events of 29–31 October 2003 and a comparative evaluation with other contemporary storms," *Space Weather*, vol. 3, no. 8, 2005, Accessed April 24, 2021. [Online]. Available: <http://doi:10.1029/2004SW000128>
- [22] D. N. Baker, E. Daly, I. Daglis, J. G. Kappenman, and M. Panasyuk, "Effects of space weather on technology infrastructure," *Space Weather*, vol. 2, no. 2, 2004.
- [23] E. G. Gibson, *The quiet sun*. National Aeronautics and Space Administration, Scientific and Technical Information Office, U.S. Government Printing Office, 1973, vol. 303.

- [24] K. Schwarzschild, “On the equilibrium of the sun’s atmosphere,” *Nachrichten von der Königlichen Gesellschaft der Wissenschaften zu Göttingen. Math.-phys. Klasse*, vol. 195, pp. 41–53, 1906.
- [25] E. N. Parker, “The Formation of Sunspots from the Solar Toroidal Field.” *The astrophysical journal*, vol. 121, p. 491, 1955.
- [26] N. Oda, “Morphological study of the solar granulation,” *Solar physics*, vol. 93, no. 2, pp. 243–255, 1984.
- [27] M. L. DeRosa and J. Toomre, “Evolution of solar supergranulation,” *The Astrophysical Journal*, vol. 616, no. 2, p. 1242, 2004.
- [28] J. Beckers, “Solar spicules,” *Solar Physics*, vol. 3, no. 3, pp. 367–433, 1968.
- [29] J.-P. Rozelot, *Solar and Heliospheric Origins of Space Weather Phenomena*. Springer, 2006, vol. 699.
- [30] R. M. Skoug, J. T. Gosling, J. T. Steinberg, D. J. McComas, C. W. Smith, N. F. Ness, Q. Hu, and L. F. Burlaga, “Extremely high speed solar wind: 29–30 October 2003,” *Journal of Geophysical Research: Space Physics*, vol. 109, no. A9, 2004.
- [31] B. U. Ö. Sonnerup, “Magnetopause reconnection rate,” *Journal of Geophysical Research*, vol. 79, no. 10, pp. 1546–1549, 1974.
- [32] J. H. Piddington, “The closed model of the earth’s magnetosphere,” *Journal of Geophysical Research: Space Physics*, vol. 84, no. A1, pp. 93–100, 1979.
- [33] D. P. Stern, “A study of the electric field in an open magnetospheric model,” *Journal of Geophysical Research*, vol. 78, no. 31, pp. 7292–7305, 1973.
- [34] A. J. Hundhausen, *Coronal expansion and solar wind*. Springer Science & Business Media, 2012, vol. 5.
- [35] M. Vellante, M. Piersanti, and E. Pietropaolo, “Comparison of equatorial plasma mass densities deduced from field line resonances observed at ground for dipole and igrf models,” *Journal of Geophysical Research: Space Physics*, vol. 119, no. 4, pp. 2623–2633, 2014.
- [36] K. Huttunen, S. Kilpua, A. Pulkkinen, A. Viljanen, and E. Tanskanen, “Solar wind drivers of large geomagnetically induced currents during the solar cycle 23,” *Space Weather*, vol. 6, no. 10, 2008.
- [37] T. W. Speiser, “Particle trajectories in a model current sheet, based on the open model of the magnetosphere, with applications to auroral particles,” *Journal of Geophysical Research*, vol. 70, no. 7, pp. 1717–1728, 1965.

- [38] X. H. Deng and H. Matsumoto, “Rapid magnetic reconnection in the Earth’s magnetosphere mediated by whistler waves,” *Nature*, vol. 410, no. 6828, pp. 557–560, 2001.
- [39] B. U. Ö. Sonnerup, “The reconnecting magnetosphere,” in *Magnetospheric Physics*. Springer, 1974, pp. 23–33.
- [40] P. Cassen and J. Szabo, “The viscous magnetopause,” *Planetary and Space Science*, vol. 18, no. 3, pp. 349–366, 1970.
- [41] J. K. Hargreaves, *The solar-terrestrial environment: an introduction to geospace—the science of the terrestrial upper atmosphere, ionosphere, and magnetosphere*. Cambridge University Press, 1992.
- [42] G. Atkinson, “Energy flow and closure of current systems in the magnetosphere,” *Journal of Geophysical Research: Space Physics*, vol. 83, no. A3, pp. 1089–1103, 1978.
- [43] A. Pulkkinen, S. Lindahl, A. Viljanen, and R. Pirjola, “Geomagnetic storm of 29–31 October 2003: Geomagnetically induced currents and their relation to problems in the Swedish high-voltage power transmission system,” *Space Weather*, vol. 3, no. 8, 2005.
- [44] A. Hady, “Descriptive study of solar activity sudden increase and Halloween storms of 2003,” *Journal of atmospheric and solar-terrestrial physics*, vol. 71, no. 17-18, pp. 1711–1716, 2009.
- [45] P. Perreault and S. Akasofu, “A study of geomagnetic storms,” *Geophysical Journal International*, vol. 54, no. 3, pp. 547–573, 1978.
- [46] A. J. Dessler, W. E. Francis, and E. N. Parker, “Geomagnetic storm sudden-commencement rise times,” *Journal of Geophysical Research*, vol. 65, no. 9, pp. 2715–2719, 1960.
- [47] J. A. Wanliss and K. M. Showalter, “High-resolution global storm index: Dst versus SYM-H,” *Journal of Geophysical Research: Space Physics*, vol. 111, no. A2, 2006.
- [48] P.-N. Mayaud, “The aa indices: A 100-year series characterizing the magnetic activity,” *Journal of Geophysical Research*, vol. 77, no. 34, pp. 6870–6874, 1972.
- [49] J. Curto, T. Araki, and L. Alberca, “Evolution of the concept of sudden storm commencements and their operative identification,” *Earth, planets and space*, vol. 59, no. 11, pp. i–xii, 2007.
- [50] B. T. Tsurutani, W. D. Gonzalez, F. Tang, S. I. Akasofu, and E. J. Smith, “Origin of interplanetary southward magnetic fields responsible for major magnetic storms near solar maximum (1978–1979),” *Journal of Geophysical Research: Space Physics*, vol. 93, no. A8, pp. 8519–8531, 1988.

- [51] R. Fiori, D. H. Boteler, and D. M. Gillies, "Assessment of GIC risk due to geomagnetic sudden commencements and identification of the current systems responsible," *Space Weather*, vol. 12, no. 1, pp. 76–91, 2014.
- [52] J. Kappenman, *Geomagnetic storms and their impacts on the US power grid*. Golete, Metatech, 2010.
- [53] G. N. Du, L. G. Liu, and K. R. Wang, "Study on Relationship between Power Grid GIC (Geomagnetically Induced Currents) and Interplanetary Disturbances," in *Advanced Materials Research*, vol. 732. Trans Tech Publ, 2013, pp. 726–730.
- [54] D. M. Oliveira and C. M. Ngwira, "Geomagnetically induced currents: Principles," *Brazilian Journal of Physics*, vol. 47, no. 5, pp. 552–560, 2017.
- [55] G. Rostoker and C.-G. Fälthammar, "Relationship between changes in the interplanetary magnetic field and variations in the magnetic field at the Earth's surface," *Journal of Geophysical Research*, vol. 72, no. 23, pp. 5853–5863, 1967.
- [56] S. V.-a. Makki, T. Z. Ershadi, and M. S. Abrishamian, "Determining the specific ground conductivity aided by the horizontal electric dipole antenna near the ground surface," *Progress In Electromagnetics Research*, vol. 1, pp. 43–65, 2008.
- [57] J. Weaver, "The electromagnetic field within a discontinuous conductor with reference to geomagnetic micropulsations near a coastline," *Canadian Journal of Physics*, vol. 41, no. 3, pp. 484–495, 1963.
- [58] A. G. Jones, M. R. Muller, R. L. Evans, M. P. Miensopust, D. T. Khoza, and Team, Samtex, "Lithospheric geometries revealed through electromagnetic imaging: SAM-TEX (Southern Africa MagnetoTelluric Experiment) observations and results," in *AGU Fall Meeting Abstracts*, vol. 2011, 2011, pp. T32A–05.
- [59] B. Dong, Z. Wang, D. Boteler, and R. Pirjola, "Review of earth conductivity structure modelling for calculating geo-electric fields," in *2013 IEEE Power & Energy Society General Meeting*. IEEE, 2013, pp. 1–5.
- [60] C. T. Gaunt and G. Coetzee, "Transformer failures in regions incorrectly considered to have low GIC-risk," in *2007 IEEE Lausanne Power Tech*. IEEE, 2007, pp. 807–812.
- [61] D. H. Boteler and R. J. Pirjola, "Modeling geomagnetically induced currents," *Space Weather*, vol. 15, no. 1, pp. 258–276, 2017.
- [62] S. P. Blake, P. T. Gallagher, J. McCauley, A. G. Jones, C. Hogg, J. Campanyà, C. D. Beggan, A. W. P. Thomson, G. S. Kelly, and D. Bell, "Geomagnetically induced currents in the Irish power network during geomagnetic storms," *Space Weather*, vol. 14, no. 12, pp. 1136–1154, 2016.

- [63] R. Tozzi, P. De Michelis, I. Coco, and F. Giannattasio, “A preliminary risk assessment of geomagnetically induced currents over the Italian territory,” *Space Weather*, vol. 17, no. 1, pp. 46–58, 2019.
- [64] J. Uwamahoro and J. B. Habarulema, “Empirical modeling of the storm time geomagnetic indices: a comparison between the local K and global Kp indices,” *Earth, Planets and Space*, vol. 66, no. 1, p. 95, 2014.
- [65] S. Stankov, K. Stegen, and R. Warnant, “K-type geomagnetic index nowcast with data quality control,” *Annals of Geophysics*, vol. 54, no. 3, pp. 285–295, 2011.
- [66] L. M. Winter, J. Gannon, R. Pernak, S. Huston, R. Quinn, E. Pope, A. Ruffenach, P. Bernardara, and N. Crocker, “Spectral scaling technique to determine extreme Carrington-level geomagnetically induced currents effects,” *Space Weather*, vol. 15, no. 5, pp. 713–725, 2017.
- [67] A. V. Vorobev and G. R. Vorobeva, “Approach to assessment of the relative informational efficiency of INTERMAGNET magnetic observatories,” *Geomagnetism and Aeronomy*, vol. 58, no. 5, pp. 625–628, 2018.
- [68] L. Trichtchenko and D. H. Boteler, “Modeling geomagnetically induced currents using geomagnetic indices and data,” *IEEE transactions on plasma science*, vol. 32, no. 4, pp. 1459–1467, 2004.
- [69] M. Sugiura, “Equatorial Dst index 1957-1986,” *IAGA Bulletins*, vol. 40, pp. 17–38, 1991.
- [70] C. Cid, E. Saiz, A. Guerrero, J. Palacios, and Y. Cerrato, “A Carrington-like geomagnetic storm observed in the 21st century,” *Journal of Space Weather and Space Climate*, vol. 5, p. A16, 2015.
- [71] G. Rostoker, “Geomagnetic indices,” *Reviews of Geophysics*, vol. 10, no. 4, pp. 935–950, 1972.
- [72] K. Takahashi, B. A. Toth, and J. V. Olson, “An automated procedure for near-real-time Kp estimates,” *Journal of Geophysical Research: Space Physics*, vol. 106, no. A10, pp. 21 017–21 032, 2001.
- [73] A.-B. Essop, “Development of a GIC proxy index,” *Unpublished Honours Thesis*.
- [74] R. Marshall, C. Waters, and M. Sciffer, “Spectral analysis of pipe-to-soil potentials with variations of the Earth’s magnetic field in the Australian region,” *Space Weather*, vol. 8, no. 5, 2010.
- [75] C. Hill, *Learning scientific programming with Python*. Cambridge University Press, 2020.

- [76] J. Ranjani, A. Sheela, and K. P. Meena, "Combination of Numpy, Scipy and Matplotlib/PyLab-a good alternative methodology to MATLAB-A Comparative analysis," in *2019 1st International Conference on Innovations in Information and Communication Technology (ICIICT)*. IEEE, 2019, pp. 1–5.
- [77] P. Wintoft, "Study of the solar wind coupling to the time difference horizontal geomagnetic field," *Annales Geophysicae, European Geosciences Union*, vol. 23(5), pp. 1949–1957, 2005. [Online]. Available: <https://hal.archives-ouvertes.fr/hal-00317841>
- [78] C. J. Schrijver and S. D. Mitchell, "Disturbances in the US electric grid associated with geomagnetic activity," *Journal of Space Weather and Space Climate*, vol. 3, p. A19, 2013.
- [79] R. S. Weigel, D. Vassiliadis, and A. J. Klimas, "Coupling of the solar wind to temporal fluctuations in ground magnetic fields," *Geophysical Research Letters*, vol. 29, no. 19, pp. 21–1, 2002.
- [80] J. A. Joselyn and B. T. Tsurutani, "Geomagnetic sudden impulses and storm sudden commencements: A note on terminology," *Eos, Transactions American Geophysical Union*, vol. 71, no. 47, pp. 1808–1809, 1990.
- [81] J. A. Wanliss and K. M. Showalter, "High-resolution global storm index: Dst versus SYM-H," *Journal of Geophysical Research: Space Physics*, vol. 111, no. A2, 2006.
- [82] E. Demidenko, "The p-value you can't buy," *The American Statistician*, vol. 70, no. 1, pp. 33–38, 2016.
- [83] M. Heyns, S. Lotz, and C. T. Gaunt, "Probabilistic Analysis of Power Network Susceptibility to GICs," in *2020 International Conference on Probabilistic Methods Applied to Power Systems (PMAPS)*. IEEE, 2020, pp. 1–6.

Appendix A

Appendix: Figure Permissions and Proofreading certificates

The permissions given by publishers for figures used in this study as well as proofreading certificates for both the thesis and the bibliography are given in the following order:

1. Figure 2.1
2. Figure 2.4
3. Figure 2.5
4. Figure 2.6
5. Figure 2.7
6. Figure 2.9
7. Proofreading certificate: Thesis
8. Proofreading certificate: Bibliography



PARTIES:

1. **Cambridge University Press** [CompanyNumber] (Licensor); and
2. **Abu-Bakr Essop** (Licensee).

Thank you for your recent permission request. Some permission requests for use of material published by the Licensor, such as this one, are now being facilitated by PLSclear.

Set out in this licence cover sheet (the **Licence Cover Sheet**) are the principal terms under which Licensor has agreed to license certain Licensed Material (as defined below) to Licensee. The terms in this Licence Cover Sheet are subject to the attached General Terms and Conditions, which together with this Licence Cover Sheet constitute the licence agreement (the **Licence**) between Licensor and Licensee as regards the Licensed Material. The terms set out in this Licence Cover Sheet take precedence over any conflicting provision in the General Terms and Conditions.

Free Of Charge Licence Terms

Licence Date: 09/02/2021
PLSclear Ref No: 47121

The Licensor

Company name: Cambridge University Press
Address: University Printing House
Shaftesbury Road
Cambridge
CB2 8BS
GB

The Licensee

Licensee Contact Name: Abu-Bakr Essop
Licensee Address: Room 208 Juwon Village
Deokjeongdong 164-8
Yangju
11451
Korea, Republic of

Licensed Material

title: Introduction to Space Physics
ISBN: 9780521457149
publisher: Cambridge University Press

Are you requesting permission to reuse the cover of the publication?	No
Figure number & title	3.2
Page numbers	61
Are you requesting permission to reuse your own work?	No
Additional Information	Needed for Masters thesis dissertation

For Use In Licensee's Publication(s)

usage type	Book, Journal, Magazine or Academic Paper-Thesis / Dissertation
Will your dissertation be placed in an online repository?	No
Author	Abu-Bakr Essop
Estimated publication date	2021/06
Language	English
Title of dissertation/thesis	Development of near real time and cumulative GIC proxy indices
University or institution	University of KwaZulu-Natal
Unlimited circulation?	No

Rights Granted

Exclusivity:	Non-Exclusive
Format:	Thesis / Dissertation
Language:	English
Territory:	UK & Commonwealth
Duration:	Lifetime of Licensee's Edition
Maximum Circulation:	1

GENERAL TERMS AND CONDITIONS

1. Definitions and Interpretation

1.1 Capitalised words and expressions in these General Terms and Conditions have the meanings given to them in the Licence Cover Sheet.

1.2 In this Licence any references (express or implied) to statutes or provisions are references to those statutes or provisions as amended or re-enacted from time to time. The term including will be construed as illustrative, without limiting the sense or scope of the words preceding it. A reference to in writing or written includes faxes and email. The singular includes the plural and vice versa.

2. Grant of Rights

2.1 The Licensor grants to Licensee the non-exclusive right to use the Licensed Material as specified in the Licence Cover Sheet.

2.2 The rights licensed to Licensee under this Licence do not include the right to use any third party copyright material incorporated in the Licensed Material. Licensee should check the Licensed Material carefully and seek permission for the use of any such third party copyright material from the relevant copyright owner(s).

2.3 Unless otherwise stated in the Licence Cover Sheet, the Licensed Material may be:

2.3.1 subjected to minor editing, including for the purposes of creating alternative formats to provide access for a beneficiary person (provided that any such editing does not amount to derogatory treatment); and/or

2.3.2 used for incidental promotional use (such as online retail providers' search facilities).

2.4 Save as expressly permitted in this Licence or as otherwise permitted by law, no use or modification of the Licensed Material may be made by Licensee without Licensor's prior written permission.

3. Copyright Notice and Acknowledgement

3.1 Licensee must ensure that the following notices and acknowledgements are reproduced prominently alongside each reproduction by Licensee of the Licensed Material:

3.1.1 the title and author of the Licensed Material;

3.1.2 the copyright notice included in the Licensed Material; and

3.1.3 the statement "Reproduced with permission of The Licensor through PLSclear."

4. Reversion of Rights

4.1 The rights licensed to Licensee under this Licence will terminate immediately and automatically upon the earliest of the following events to occur:

4.1.1 the Licensed Material not being used by Licensee within 18 months of the Licence Date;

4.1.2 expiry of the Licence Duration; or

4.1.3 the Maximum Circulation being reached.

5. Miscellaneous

5.1 By using the Licensed Material, Licensee will be deemed to have accepted all the terms and conditions contained in this Licence.

5.2 This Licence contains the entire understanding and agreement of the parties relating to its subject matter and supersedes in all respects any previous or other existing arrangements, agreements or understandings between the parties whether oral or written in relation to its subject matter.

5.3 Licensee may not assign this Licence or any of its rights or obligations hereunder to any third party without Licensor's prior written consent.

5.4 This Licence is governed by and shall be construed in accordance with the laws of England and Wales and the parties hereby irrevocably submit to the non-exclusive jurisdiction of the Courts of England and Wales as regards any claim, dispute or matter arising under or in relation to this Licence.

Email from Springer:

Dear A. Essop,

Thank you for your e-mail.

The figure has an external reference: courtesy of Yohkoh Team.

Please contact the original copyright holder for permission.

Best regards,

Sara Martínez

Rights Sales Assistant

SpringerNature

Tiergartenstr. 17, 69121 Heidelberg, Germany
sara.martinezgarcia@springernature.com

<http://www.nature.com>

<http://www.springer.com>

<http://www.palgrave.com>

Yohkoh Website:

http://ylstone.physics.montana.edu/ylegacy/sxt_obsrpt/new_data_policy.txt

* Yohkoh Data Becomes Available Without Any Delay

Yohkoh Data Becomes Available Without Any Delay

>From Takeo Kosugi <kosugi@laputa2.solar.isas.ac.jp>
>27 Feb 2001

A new decision has been made in the international Yohkoh team that all the Yohkoh data be immediately opened to the world science community without any delay except for a short time for reformatting the data. This new policy will become effective when this announcement is circulated.

For more than nine years since launch on 30 August 1991, the Yohkoh team has opened a full set of data, together with a software package for data analysis, after one year had elapsed since acquisition. The one-year interval for privileged data use by Yohkoh team members was introduced as a reward to those who worked hard for instruments buildings as well as to those who contribute to daily satellite operations by sacrificing their own time to do science. On the other hand, the one-year interval might not be idealistic for the quickest and widest data use by the world science community. After evaluating such positive and negative aspects, we have reached a consensus that the reasoning for holding the privileged data use interval is now drastically reduced thanks to longevity of Yohkoh. Thus, with concurrence by ISAS, we here announce a new policy that all the Yohkoh data be opened immediately after acquisition.

We hope the world science community in solar physics and solar-terrestrial physics will analyze Yohkoh data as actively as but more quickly than before. Those who are not familiar with how to make use of the Yohkoh data, please contact the Solar Data Analysis Center, NASA/GSFC (yohkoh_sdac@solar.stanford.edu), the UK Yohkoh team at the Mullard Space Science Laboratory (J. Len Culhane; jlc@mssl.ucl.ac.uk), or the ISAS Yohkoh Analysis (Takeo Kosugi; kosugi@solar.isas.ac.jp).



PARTIES:

1. **Cambridge University Press** [CompanyNumber] (Licensor); and
2. **Abu-Bakr Essop** (Licensee).

Thank you for your recent permission request. Some permission requests for use of material published by the Licensor, such as this one, are now being facilitated by PLSclear.

Set out in this licence cover sheet (the **Licence Cover Sheet**) are the principal terms under which Licensor has agreed to license certain Licensed Material (as defined below) to Licensee. The terms in this Licence Cover Sheet are subject to the attached General Terms and Conditions, which together with this Licence Cover Sheet constitute the licence agreement (the **Licence**) between Licensor and Licensee as regards the Licensed Material. The terms set out in this Licence Cover Sheet take precedence over any conflicting provision in the General Terms and Conditions.

Free Of Charge Licence Terms

Licence Date: 17/02/2021
PLSclear Ref No: 47353

The Licensor

Company name: Cambridge University Press
Address: University Printing House
Shaftesbury Road
Cambridge
CB2 8BS
GB

The Licensee

Licensee Contact Name: Abu-Bakr Essop
Licensee Address: Room 208 Juwon Village
Deokjeongdong 164-8
Yangju
11451
Korea, Republic of

Licensed Material

title: An Introduction to Space Weather
ISBN: 9780521861496
publisher: Cambridge University Press

Are you requesting permission to reuse the cover of the publication?	No
Figure number & title	4.2 A noon–midnight cross section of Earth’s magnetosphere. Note the dipole shape of the inner magnetosphere. The Sun (hence noon) is to the left and north is up
Page numbers	52
Name of illustrator	None provided
Are you requesting permission to reuse your own work?	No
Additional Information	Permission for MSc. Thesis

For Use In Licensee's Publication(s)

usage type	Book, Journal, Magazine or Academic Paper-Thesis / Dissertation
Will your dissertation be placed in an online repository?	Yes
Author	Abu-Bakr Essop
Estimated publication date	May 2021
Language	English
Title of dissertation/thesis	Development of near real time and cumulative GIC proxy indices
University or institution	UKZN
Unlimited circulation?	No

Rights Granted

Exclusivity:	Non-Exclusive
Format:	Thesis / Dissertation
Language:	English
Territory:	UK & Commonwealth
Duration:	Lifetime of Licensee's Edition
Maximum Circulation:	1

GENERAL TERMS AND CONDITIONS

1. Definitions and Interpretation

1.1 Capitalised words and expressions in these General Terms and Conditions have the meanings given to them in the Licence Cover Sheet.

1.2 In this Licence any references (express or implied) to statutes or provisions are references to those statutes or provisions as amended or re-enacted from time to time. The term including will be construed as illustrative, without limiting the sense or scope of the words preceding it. A reference to in writing or written includes faxes and email. The singular includes the plural and vice versa.

2. Grant of Rights

2.1 The Licensor grants to Licensee the non-exclusive right to use the Licensed Material as specified in the Licence Cover Sheet.

2.2 The rights licensed to Licensee under this Licence do not include the right to use any third party copyright material incorporated in the Licensed Material. Licensee should check the Licensed Material carefully and seek permission for the use of any such third party copyright material from the relevant copyright owner(s).

2.3 Unless otherwise stated in the Licence Cover Sheet, the Licensed Material may be:

2.3.1 subjected to minor editing, including for the purposes of creating alternative formats to provide access for a beneficiary person (provided that any such editing does not amount to derogatory treatment); and/or

2.3.2 used for incidental promotional use (such as online retail providers' search facilities).

2.4 Save as expressly permitted in this Licence or as otherwise permitted by law, no use or modification of the Licensed Material may be made by Licensee without Licensor's prior written permission.

3. Copyright Notice and Acknowledgement

3.1 Licensee must ensure that the following notices and acknowledgements are reproduced prominently alongside each reproduction by Licensee of the Licensed Material:

3.1.1 the title and author of the Licensed Material;

3.1.2 the copyright notice included in the Licensed Material; and

3.1.3 the statement "Reproduced with permission of The Licensor through PLSclear."

4. Reversion of Rights

4.1 The rights licensed to Licensee under this Licence will terminate immediately and automatically upon the earliest of the following events to occur:

4.1.1 the Licensed Material not being used by Licensee within 18 months of the Licence Date;

4.1.2 expiry of the Licence Duration; or

4.1.3 the Maximum Circulation being reached.

5. Miscellaneous

5.1 By using the Licensed Material, Licensee will be deemed to have accepted all the terms and conditions contained in this Licence.

5.2 This Licence contains the entire understanding and agreement of the parties relating to its subject matter and supersedes in all respects any previous or other existing arrangements, agreements or understandings between the parties whether oral or written in relation to its subject matter.

5.3 Licensee may not assign this Licence or any of its rights or obligations hereunder to any third party without Licensor's prior written consent.

5.4 This Licence is governed by and shall be construed in accordance with the laws of England and Wales and the parties hereby irrevocably submit to the non-exclusive jurisdiction of the Courts of England and Wales as regards any claim, dispute or matter arising under or in relation to this Licence.

SPRINGER NATURE LICENSE
TERMS AND CONDITIONS

Feb 26, 2021

This Agreement between UKZN -- Abu-Bakr Essop ("You") and Springer Nature ("Springer Nature") consists of your license details and the terms and conditions provided by Springer Nature and Copyright Clearance Center.

License Number

5016811118105

License date

Feb 26, 2021

Licensed Content Publisher

Springer Nature

Licensed Content Publication

Springer eBook

Licensed Content Title

Interaction With the Earth and Other Planets: Contribution to Space Weather

Licensed Content Author

Timothy Howard

Licensed Content Date

Jan 1, 2011

Type of Use

Thesis/Dissertation

Requestor type

academic/university or research institute

Format

print and electronic

Portion

figures/tables/illustrations

Number of figures/tables/illustrations

1

Will you be translating?

no

Circulation/distribution

1 - 29

Author of this Springer Nature content

no

Title

Abu-Bakr Essop

Institution name

UKZN

Expected presentation date

May 2021

Order reference number

1

Portions

Figure 10.4: (b) A close-up view of the Earth's magnetosphere...

Requestor Location

UKZN
Deokjeong dong 164-8
Yangju
Gyeonggido
Yangju, Gyeonggi 11451
Korea, Republic Of
Attn: Masters

Customer VAT ID

KR9311105520024

Total

0.00 USD

Terms and Conditions

Springer Nature Customer Service Centre GmbH
Terms and Conditions

This agreement sets out the terms and conditions of the licence (the Licence) between you and Springer Nature Customer Service Centre GmbH (the Licensor). By clicking 'accept' and completing the transaction for the material (Licensed Material), you also confirm your acceptance of these terms and conditions.

Grant of License

The Licensor grants you a personal, non-exclusive, non-transferable, world-wide licence to reproduce the Licensed Material for the purpose specified in your order only. Licences are granted for the specific use requested in the order and for no other use, subject to the conditions below.

The Licensor warrants that it has, to the best of its knowledge, the rights to license reuse of the Licensed Material. However, you should ensure that the material you are requesting is original to the Licensor and does not carry the copyright of another entity (as credited in the published version).

If the credit line on any part of the material you have requested indicates that it was reprinted or adapted with permission from another source, then you should also seek permission from that source to reuse the material.

Scope of Licence

You may only use the Licensed Content in the manner and to the extent permitted by these Ts&Cs and any applicable laws.

A separate licence may be required for any additional use of the Licensed Material, e.g. where a licence has been purchased for print only use, separate permission must be obtained for electronic re-use. Similarly, a licence is only valid in the language selected and does not apply for editions in other languages unless additional translation rights have been granted separately in the licence. Any content owned by third parties are expressly excluded from the licence.

Similarly, rights for additional components such as custom editions and derivatives require additional permission and may be subject to an additional fee. Please apply to Journalpermissions@springernature.com/bookpermissions@springernature.com for these rights.

Where permission has been granted free of charge for material in print, permission may also be granted for any electronic version of that work, provided that the material is incidental to your work as a whole and that the electronic version is essentially equivalent to, or substitutes for, the print version.

An alternative scope of licence may apply to signatories of the STM Permissions Guidelines, as amended from time to time.

Duration of Licence

A licence for is valid from the date of purchase ('Licence Date') at the end of the relevant period in the below table :

Scope of Licence	Duration of Licence
Post on a website	12 months
Presentations	12 months
Books and journals	Lifetime of the edition in the language purchased

Acknowledgement

The Licensor's permission must be acknowledged next to the Licenced Material in print. In electronic form, this acknowledgement must be visible at the same time as the figures/tables/illustrations or abstract, and must be hyperlinked to the journal/book's homepage. Our required acknowledgement format is in the Appendix below.

Restrictions on use

Use of the Licensed Material may be permitted for incidental promotional use and minor editing privileges e.g. minor adaptations of single figures, changes of format, colour and/or style where the adaptation is credited as set out in Appendix 1 below. Any other changes including but not limited to, cropping, adapting, omitting material that affect the meaning, intention or moral rights of the author are strictly prohibited.

You must not use any Licensed Material as part of any design or trademark.

Licensed Material may be used in Open Access Publications (OAP) before publication by Springer Nature, but any Licensed Material must be removed from OAP sites prior to final publication.

Ownership of Rights

Licensed Material remains the property of either Licensor or the relevant third party and any rights not explicitly granted herein are expressly reserved.

Warranty

IN NO EVENT SHALL LICENSOR BE LIABLE TO YOU OR ANY OTHER PARTY OR ANY OTHER PERSON OR FOR ANY SPECIAL, CONSEQUENTIAL, INCIDENTAL OR INDIRECT DAMAGES, HOWEVER CAUSED, ARISING OUT OF OR IN CONNECTION WITH THE DOWNLOADING, VIEWING OR USE OF THE MATERIALS REGARDLESS OF THE FORM OF ACTION, WHETHER FOR BREACH OF CONTRACT, BREACH OF WARRANTY, TORT, NEGLIGENCE, INFRINGEMENT OR OTHERWISE (INCLUDING, WITHOUT L

IMITATION, DAMAGES BASED ON LOSS OF PROFITS, DATA, FILES, USE, BUSINESS OPPORTUNITY OR CLAIMS OF THIRD PARTIES), AND WHETHER OR NOT THE PARTY HAS BEEN ADVISED OF THE POSSIBILITY OF SUCH DAMAGES. THIS LIMITATION SHALL APPLY NOTWITHSTANDING ANY FAILURE OF ESSENTIAL PURPOSE OF ANY LIMITED REMEDY PROVIDED HEREIN.

Limitations

BOOKS ONLY: Where 'reuse in a dissertation/thesis' has been selected the following terms apply: Print rights of the final author's accepted manuscript (for clarity, NOT the published version) for up to 100 copies, electronic rights for use only on a personal website or institutional repository as defined by the Sherpa guideline (www.sherpa.ac.uk/romeo/).

For content reuse requests that qualify for permission under the STM Permissions Guidelines, which may be updated from time to time, the STM Permissions Guidelines supersede the terms and conditions contained in this licence.

Termination and Cancellation

Licences will expire after the period shown in Clause 3 (above).

Licensee reserves the right to terminate the Licence in the event that payment is not received in full or if there has been a breach of this agreement by you.

Appendix 1 — Acknowledgements:

For Journal Content:

Reprinted by permission from [the Licensor]: [Journal Publisher (e.g. Nature/Springer/Palgrave)] [JOURNAL NAME] [REFERENCE CITATION (Article name, Author(s) Name), [COPYRIGHT] (year of publication)]

For Advance Online Publication papers:

Reprinted by permission from [the Licensor]: [Journal Publisher (e.g. Nature/Springer/Palgrave)] [JOURNAL NAME] [REFERENCE CITATION (Article name, Author(s) Name), [COPYRIGHT] (year of publication), advance on line publication, day month year (doi: 10.1038/sj.[JOURNAL ACRONYM].)]

For Adaptations/Translations:

Adapted/Translated by permission from [the Licensor]: [Journal Publisher (e.g. Nature/Springer/Palgrave)] [JOURNAL NAME] [REFERENCE CITATION (Article name, Author(s) Name), [COPYRIGHT] (year of publication)]

Note: For any republication from the British Journal of Cancer, the following credit line style applies:

Reprinted/adapted/translated by permission from [the Licensor]: on behalf of Cancer Research UK: [Journal Publisher (e.g. Nature/Springer/Palgrave)] [JOURNAL NAME] [REFERENCE CITATION (Article name, Author(s) Name), [COPYRIGHT] (year of publication)]

For Advance Online Publication papers:

Reprinted by permission from The [the Licensor]: on behalf of Cancer Research UK: [Journal Publisher (e.g. Nature/Springer/Palgrave)] [JOURNAL NAME] [REFERENCE CITATION (Article name, Author(s) Name), [COPYRIGHT] (year of publication), advance online publication, day month year (doi: 10.1038/sj.[JOURNAL ACRONYM].)]

For Book content:

Reprinted/adapted by permission from [the Licensor]: [Book Publisher (e.g. Palgrave Macmillan, Springer etc)] [B

ook Title] by [Book author(s)] [COPYRIGHT] (year of publication)

Other Conditions:

Version 1.3

Questions? customercare@copyright.com or +1-855-239-3415 (toll free in the US) or +1-978-646-2777.

ELSEVIER LICENSE
TERMS AND CONDITIONS

Feb 18, 2021

This Agreement between UKZN -- Abu-Bakr Essop ("You") and Elsevier ("Elsevier") consists of your license details and the terms and conditions provided by Elsevier and Copyright Clearance Center.

License Number

5011760644055

License date

Feb 18, 2021

Licensed Content Publisher

Elsevier

Licensed Content Publication

Advances in Space Research

Licensed Content Title

The geomagnetic field and its extension into space

Licensed Content Author

W.P. Olsen

Licensed Content Date

Jan 1, 1982

Licensed Content Volume

2

Licensed Content Issue

1

Licensed Content Pages

5

Start Page

13

End Page

17

Type of Use

reuse in a thesis/dissertation

Portion

figures/tables/illustrations

Number of figures/tables/illustrations

1

Format

both print and electronic

Are you the author of this Elsevier article?

No

Will you be translating?

No

Title

Abu-Bakr Essop

Institution name

UKZN

Expected presentation date

May 2021

Order reference number

None

Portions

Current topologies of three separate currents.

Requestor Location

UKZN
Deokjeong dong 164-8
Yangju
Gyeonggido
Yangju, Gyeonggi 11451
Korea, Republic Of
Attn: Masters

Publisher Tax ID

GB 494 6272 12

Customer VAT ID

KR9311105520024

Total

0.00 USD

Terms and Conditions

INTRODUCTION

1. The publisher for this copyrighted material is Elsevier. By clicking "accept" in connection with completing this licensing transaction, you agree that the following terms and conditions apply to this transaction (along with the Billing and Payment terms and conditions established by Copyright Clearance Center, Inc. ("CCC"), at the time that you opened your Rightslink account and that are available at any time at <http://myaccount.copyright.com>).

GENERAL TERMS

2. Elsevier hereby grants you permission to reproduce the aforementioned material subject to the terms and conditions indicated.

3. Acknowledgement: If any part of the material to be used (for example, figures) has appeared in our publication with credit or acknowledgement to another source, permission must also be sought from that source. If such permission is not obtained then that material may not be included in your publication/copies. Suitable acknowledgement to the source must be made, either as a footnote or in a reference list at the end of your publication, as follows:

"Reprinted from Publication title, Vol /edition number, Author(s), Title of article / title of chapter, Pages No., Copyright (Year), with permission from Elsevier [OR APPLICABLE SOCIETY COPYRIGHT OWNER]." Also Lancet special credit - "Reprinted from

The Lancet, Vol. number, Author(s), Title of article, Pages No., Copyright (Year), with permission from Elsevier."

4. Reproduction of this material is confined to the purpose and/or media for which permission is hereby given.

5. Altering/Modifying Material: Not Permitted. However figures and illustrations may be altered/adapted minimally to serve your work. Any other abbreviations, additions, deletions and/or any other alterations shall be made only with prior written authorization of Elsevier Ltd. (Please contact Elsevier's permissions helpdesk here). No modifications can be made to any Lancet figures/tables and they must be reproduced in full.

6. If the permission fee for the requested use of our material is waived in this instance, please be advised that your future requests for Elsevier materials may attract a fee.

7. Reservation of Rights: Publisher reserves all rights not specifically granted in the combination of (i) the license details provided by you and accepted in the course of this licensing transaction, (ii) these terms and conditions and (iii) CCC's Billing and Payment terms and conditions.

8. License Contingent Upon Payment: While you may exercise the rights licensed immediately upon issuance of the license at the end of the licensing process for the transaction, provided that you have disclosed complete and accurate details of your proposed use, no license is finally effective unless and until full payment is received from you (either by publisher or by CCC) as provided in CCC's Billing and Payment terms and conditions. If full payment is not received on a timely basis, then any license preliminarily granted shall be deemed automatically revoked and shall be void as if never granted. Further, in the event that you breach any of these terms and conditions or any of CCC's Billing and Payment terms and conditions, the license is automatically revoked and shall be void as if never granted. Use of materials as described in a revoked license, as well as any use of the materials beyond the scope of an unrevoked license, may constitute copyright infringement and publisher reserves the right to take any and all action to protect its copyright in the materials.

9. Warranties: Publisher makes no representations or warranties with respect to the licensed material.

10. Indemnity: You hereby indemnify and agree to hold harmless publisher and CCC, and their respective officers, directors, employees and agents, from and against any and all claims arising out of your use of the licensed material other than as specifically authorized pursuant to this license.

11. No Transfer of License: This license is personal to you and may not be sublicensed, assigned, or transferred by you to any other person without publisher's written permission.

12. No Amendment Except in Writing: This license may not be amended except in a writing signed by both parties (or, in the case of publisher, by CCC on publisher's behalf).

13. Objection to Contrary Terms: Publisher hereby objects to any terms contained in any purchase order, acknowledgment, check endorsement or other writing prepared by you, which terms are inconsistent with these terms and conditions or CCC's Billing and Payment terms and conditions. These terms and conditions, together with CCC's Billing and Payment terms and conditions (which are incorporated herein), comprise the entire agreement between you and publisher (and CCC) concerning this licensing

transaction. In the event of any conflict between your obligations established by these terms and conditions and those established by CCC's Billing and Payment terms and conditions, these terms and conditions shall control.

14. Revocation: Elsevier or Copyright Clearance Center may deny the permissions described in this License at their sole discretion, for any reason or no reason, with a full refund payable to you. Notice of such denial will be made using the contact information provided by you. Failure to receive such notice will not alter or invalidate the denial. In no event will Elsevier or Copyright Clearance Center be responsible or liable for any costs, expenses or damage incurred by you as a result of a denial of your permission request, other than a refund of the amount(s) paid by you to Elsevier and/or Copyright Clearance Center for denied permissions.

LIMITED LICENSE

The following terms and conditions apply only to specific license types:

15. Translation: This permission is granted for non-exclusive world English rights only unless your license was granted for translation rights. If you licensed translation rights you may only translate this content into the languages you requested. A professional translator must perform all translations and reproduce the content word for word preserving the integrity of the article.

16. Posting licensed content on any Website: The following terms and conditions apply as follows: Licensing material from an Elsevier journal: All content posted to the web site must maintain the copyright information line on the bottom of each image; A hyper-text must be included to the Homepage of the journal from which you are licensing at <http://www.sciencedirect.com/science/journal/xxxxx> or the Elsevier homepage for books at <http://www.elsevier.com>; Central Storage: This license does not include permission for a scanned version of the material to be stored in a central repository such as that provided by Heron/XanEdu.

Licensing material from an Elsevier book: A hyper-text link must be included to the Elsevier homepage at <http://www.elsevier.com> . All content posted to the web site must maintain the copyright information line on the bottom of each image.

Posting licensed content on Electronic reserve: In addition to the above the following clauses are applicable: The web site must be password-protected and made available only to bona fide students registered on a relevant course. This permission is granted for 1 year only. You may obtain a new license for future website posting.

17. For journal authors: the following clauses are applicable in addition to the above:

Preprints:

A preprint is an author's own write-up of research results and analysis, it has not been peer-reviewed, nor has it had any other value added to it by a publisher (such as formatting, copyright, technical enhancement etc.).

Authors can share their preprints anywhere at any time. Preprints should not be added to or enhanced in any way in order to appear more like, or to substitute for, the final versions of articles however authors can update their preprints on arXiv or RePEc with their Accepted Author Manuscript (see below).

If accepted for publication, we encourage authors to link from the preprint to their formal publication via its DOI. Millions of researchers have access to the

formal publications on ScienceDirect, and so links will help users to find, access, cite and use the best available version. Please note that Cell Press, The Lancet and some society-owned have different preprint policies. Information on these policies is available on the journal homepage.

Accepted Author Manuscripts: An accepted author manuscript is the manuscript of an article that has been accepted for publication and which typically includes author-incorporated changes suggested during submission, peer review and editor-author communications.

Authors can share their accepted author manuscript:

- immediately
 - via their non-commercial person homepage or blog
 - by updating a preprint in arXiv or RePEc with the accepted manuscript
 - via their research institute or institutional repository for internal institutional uses or as part of an invitation-only research collaboration work-group
- directly by providing copies to their students or to research collaborators for their personal use
 - for private scholarly sharing as part of an invitation-only work group on commercial sites with which Elsevier has an agreement
- After the embargo period
 - via non-commercial hosting platforms such as their institutional repository
 - via commercial sites with which Elsevier has an agreement

In all cases accepted manuscripts should:

- link to the formal publication via its DOI
- bear a CC-BY-NC-ND license - this is easy to do
- if aggregated with other manuscripts, for example in a repository or other site, be shared in alignment with our hosting policy not be added to or enhanced in any way to appear more like, or to substitute for, the published journal article.

Published journal article (JPA): A published journal article (PJA) is the definitive final record of published research that appears or will appear in the journal and embodies all value-adding publishing activities including peer review co-ordination, copy-editing, formatting, (if relevant) pagination and online enrichment.

Policies for sharing publishing journal articles differ for subscription and gold open access articles:

Subscription Articles: If you are an author, please share a link to your article rather than the full-text. Millions of researchers have access to the formal publications on ScienceDirect, and so links will help your users to find, access, cite, and use the best available version.

Theses and dissertations which contain embedded PJAs as part of the formal submission can be posted publicly by the awarding institution with DOI links back to the formal publications on ScienceDirect.

If you are affiliated with a library that subscribes to ScienceDirect you have additional private sharing rights for others' research accessed under that agreement. This includes use for classroom teaching and internal training at the institution (including use in course packs and courseware programs), and inclusion of the article for grant funding purposes.

Gold Open Access Articles: May be shared according to the author-selected end-user

license and should contain a CrossMark logo, the end user license, and a DOI link to the formal publication on ScienceDirect.

Please refer to Elsevier's posting policy for further information.

18. For book authors the following clauses are applicable in addition to the above: Authors are permitted to place a brief summary of their work online only. You are not allowed to download and post the published electronic version of your chapter, nor may you scan the printed edition to create an electronic version. Posting to a repository: Authors are permitted to post a summary of their chapter only in their institution's repository.

19. Thesis/Dissertation: If your license is for use in a thesis/dissertation your thesis may be submitted to your institution in either print or electronic form. Should your thesis be published commercially, please reapply for permission. These requirements include permission for the Library and Archives of Canada to supply single copies, on demand, of the complete thesis and include permission for Proquest/UMI to supply single copies, on demand, of the complete thesis. Should your thesis be published commercially, please reapply for permission. Theses and dissertations which contain embedded PJAs as part of the formal submission can be posted publicly by the awarding institution with DOI links back to the formal publications on ScienceDirect.

Elsevier Open Access Terms and Conditions

You can publish open access with Elsevier in hundreds of open access journals or in nearly 2000 established subscription journals that support open access publishing. Permitted third party re-use of these open access articles is defined by the author's choice of Creative Commons user license. See our open access license policy for more information.

Terms & Conditions applicable to all Open Access articles published with Elsevier:

Any reuse of the article must not represent the author as endorsing the adaptation of the article nor should the article be modified in such a way as to damage the author's honour or reputation. If any changes have been made, such changes must be clearly indicated.

The author(s) must be appropriately credited and we ask that you include the end user license and a DOI link to the formal publication on ScienceDirect.

If any part of the material to be used (for example, figures) has appeared in our publication with credit or acknowledgement to another source it is the responsibility of the user to ensure their reuse complies with the terms and conditions determined by the rights holder.

Additional Terms & Conditions applicable to each Creative Commons user license:

CC BY: The CC-BY license allows users to copy, to create extracts, abstracts and new works from the Article, to alter and revise the Article and to make commercial use of the Article (including reuse and/or resale of the Article by commercial entities), provided the user gives appropriate credit (with a link to the formal publication through the relevant DOI), provides a link to the license, indicates if changes were made and the licensor is not represented as endorsing the use made of the work. The full details of the license are available at <http://creativecommons.org/licenses/by/4.0>.

CC BY NC SA: The CC BY-NC-SA license allows users to copy, to create extracts, abstracts and new works from the Article, to alter and revise the Article, provided this is not done for commercial purposes, and that the user gives appropriate credit (with a link to the formal publication through the relevant DOI), provides a link to the license, indicates if changes were made and the licensor is not represented as endorsing the use made of the work. Further, any new works must be made available on the same conditions. The full details of the license are available at <http://creativecommons.org/licenses/by-nc-sa/4.0>.

CC BY NC ND: The CC BY-NC-ND license allows users to copy and distribute the Article, provided this is not done for commercial purposes and further does not permit distribution of the Article if it is changed or edited in any way, and provided the user gives appropriate credit (with a link to the formal publication through the relevant DOI), provides a link to the license, and that the licensor is not represented as endorsing the use made of the work. The full details of the license are available at <http://creativecommons.org/licenses/by-nc-nd/4.0>. Any commercial reuse of Open Access articles published with a CC BY NC SA or CC BY NC ND license requires permission from Elsevier and will be subject to a fee.

Commercial reuse includes:

- Associating advertising with the full text of the Article
- Charging fees for document delivery or access
- Article aggregation
- Systematic distribution via e-mail lists or share buttons

Posting or linking by commercial companies for use by customers of those companies.

20. Other Conditions:

v1.10

Questions? customer care@copyright.com or +1-855-239-3415 (toll free in the US) or +1-978-646-2777.



PARTIES:

1. **Cambridge University Press** [CompanyNumber] (Licensor); and
2. **Abu-Bakr Essop** (Licensee).

Thank you for your recent permission request. Some permission requests for use of material published by the Licensor, such as this one, are now being facilitated by PLSclear.

Set out in this licence cover sheet (the **Licence Cover Sheet**) are the principal terms under which Licensor has agreed to license certain Licensed Material (as defined below) to Licensee. The terms in this Licence Cover Sheet are subject to the attached General Terms and Conditions, which together with this Licence Cover Sheet constitute the licence agreement (the **Licence**) between Licensor and Licensee as regards the Licensed Material. The terms set out in this Licence Cover Sheet take precedence over any conflicting provision in the General Terms and Conditions.

Free Of Charge Licence Terms

Licence Date: 17/02/2021
PLSclear Ref No: 47357

The Licensor

Company name: Cambridge University Press
Address: University Printing House
Shaftesbury Road
Cambridge
CB2 8BS
GB

The Licensee

Licensee Contact Name: Abu-Bakr Essop
Licensee Address: Room 208 Juwon Village
Deokjeongdong 164-8
Yangju
11451
Korea, Republic of

Licensed Material

title: An Introduction to Space Weather
ISBN: 9780521861496
publisher: Cambridge University Press

Are you requesting permission to reuse the cover of the publication?	No
Figure number & title	Figure 4.6 The Disturbed Storm Time (Dst) index over a ten day interval showing the characteristic phases of a geomagnetic storm.
Page numbers	59
Name of illustrator	None
Are you requesting permission to reuse your own work?	No
Additional Information	Needed for MSc. thesis

For Use In Licensee's Publication(s)

usage type	Book, Journal, Magazine or Academic Paper-Thesis / Dissertation
Will your dissertation be placed in an online repository?	Yes
Author	Abu-Bakr Essop
Estimated publication date	May 2021
Language	English
Title of dissertation/thesis	Development of near real time and cumulative GIC proxy indices.
University or institution	UKZN
Unlimited circulation?	No

Rights Granted

Exclusivity:	Non-Exclusive
Format:	Thesis / Dissertation
Language:	English
Territory:	UK & Commonwealth
Duration:	Lifetime of Licensee's Edition
Maximum Circulation:	1

GENERAL TERMS AND CONDITIONS

1. Definitions and Interpretation

1.1 Capitalised words and expressions in these General Terms and Conditions have the meanings given to them in the Licence Cover Sheet.

1.2 In this Licence any references (express or implied) to statutes or provisions are references to those statutes or provisions as amended or re-enacted from time to time. The term including will be construed as illustrative, without limiting the sense or scope of the words preceding it. A reference to in writing or written includes faxes and email. The singular includes the plural and vice versa.

2. Grant of Rights

2.1 The Licensor grants to Licensee the non-exclusive right to use the Licensed Material as specified in the Licence Cover Sheet.

2.2 The rights licensed to Licensee under this Licence do not include the right to use any third party copyright material incorporated in the Licensed Material. Licensee should check the Licensed Material carefully and seek permission for the use of any such third party copyright material from the relevant copyright owner(s).

2.3 Unless otherwise stated in the Licence Cover Sheet, the Licensed Material may be:

2.3.1 subjected to minor editing, including for the purposes of creating alternative formats to provide access for a beneficiary person (provided that any such editing does not amount to derogatory treatment); and/or

2.3.2 used for incidental promotional use (such as online retail providers' search facilities).

2.4 Save as expressly permitted in this Licence or as otherwise permitted by law, no use or modification of the Licensed Material may be made by Licensee without Licensor's prior written permission.

3. Copyright Notice and Acknowledgement

3.1 Licensee must ensure that the following notices and acknowledgements are reproduced prominently alongside each reproduction by Licensee of the Licensed Material:

3.1.1 the title and author of the Licensed Material;

3.1.2 the copyright notice included in the Licensed Material; and

3.1.3 the statement "Reproduced with permission of The Licensor through PLSclear."

4. Reversion of Rights

4.1 The rights licensed to Licensee under this Licence will terminate immediately and automatically upon the earliest of the following events to occur:

4.1.1 the Licensed Material not being used by Licensee within 18 months of the Licence Date;

4.1.2 expiry of the Licence Duration; or

4.1.3 the Maximum Circulation being reached.

5. Miscellaneous

5.1 By using the Licensed Material, Licensee will be deemed to have accepted all the terms and conditions contained in this Licence.

5.2 This Licence contains the entire understanding and agreement of the parties relating to its subject matter and supersedes in all respects any previous or other existing arrangements, agreements or understandings between the parties whether oral or written in relation to its subject matter.

5.3 Licensee may not assign this Licence or any of its rights or obligations hereunder to any third party without Licensor's prior written consent.

5.4 This Licence is governed by and shall be construed in accordance with the laws of England and Wales and the parties hereby irrevocably submit to the non-exclusive jurisdiction of the Courts of England and Wales as regards any claim, dispute or matter arising under or in relation to this Licence.



Declaration of Professional Editing

16 April 2021

This letter serves to confirm that Abu-Bakr Essop submitted a dissertation to myself for editing. The dissertation is entitled, '**DEVELOPMENT OF NEAR REAL TIME AND CUMULATIVE GIC PROXY INDICES**'.

The following aspects were edited:

- Spelling
- Grammar
- In-text reference formatting only (Reference checking involves proofreading and perhaps some editing with regards to the simple formatting of the references into the referencing style required i.e. changing the order of the elements - author, date, title, series, place, publisher, journal, volume, issue, pagination etc.)

Only the following sections were edited at the request of the student:

- Abstract
- Chapter 1
- Chapter 2
- Chapter 3
- Chapter 4
- Chapter 5

My involvement was restricted to language use and spelling, and referencing formatting (in-text). I did no structural re-writing of the content and did not influence the academic content in any way. The content and formatting of the final document submitted for examination remains the responsibility of the student.

Should you have any further queries, please do not hesitate to contact me.

Kind regards,



Kim Smit

● Tel: +27 (0)78 493 6554

● Email: kimnsmit@gmail.com

Member of the Freelance panel for the University of South Africa

Member of the Freelance panel for the University of Pretoria

Full Member of the Professional Editor's Guild

HILTON RATCLIFFE, PROFESSIONAL EDITOR cell 082 650 8313
Email hiltongratcliffe@gmail.com

EDITING CERTIFICATE

I hereby confirm that I have reviewed the
Reference List of the
Thesis to be submitted to the

UNIVERSITY of KWAZULU-NATAL

by

Abu-Bakr Essop

entitled

**Development of Near Real Time and
Cumulative GIC Proxy Indices**

I hereby certify that the list meets the requirements laid down by the IEEE.

Signed: 

Date: 23 April 2021

Hilton Ratcliffe, Professional Text Editor
PhD (Celestial Mechanics) University of Texas, USA

Professional EDITORS Guild	Hilton Ratcliffe PhD email: hiltongratcliffe@gmail.com cell: 27 82 650 8313
	language and technical editing text and layout formatting proofreading academic style formatting transcription from audio to text
Associate Member	
www.editors.org.co.za	www.hiltonratcliffe.com